Russian Original Vol. 34, No. 4, April, 1973

October, 1973

SATEAZ 34(4) 305-416 (1973)

SOVIET ATOMIC ENERGY

АТОМНАЯ ЭНЕРГИЯ
(ATOMNAYA ÉNERGIYA)

TRANSLATED FROM RUSSIAN

CONSULTANTS BUREAU, NEW YORK

SOVIET ATOMIC ENERGY

Soviet Atomic Energy is a cover-to-cover translation of *Atomnaya Énergiya*, a publication of the Academy of Sciences of the USSR.

An arrangement with Mezhdunarodnaya Kniga, the Soviet book export agency, makes available both advance copies of the Russian journal and original glossy photographs and artwork. This serves to decrease the necessary time lag between publication of the original and publication of the translation and helps to improve the quality of the latter. The translation began with the first issue of the Russian journal.

Consultants Bureau journals appear about six months after the publication of the original Russian issue. For bibliographic accuracy, the English issue published by Consultants Bureau carries the same number and date as the original Russian from which it was translated. For example, a Russian issue published in December will appear in a Consultants Bureau English translation about the following June, but the translation issue will carry the December date. When ordering any volume or particular issue of a Consultants Bureau journal, please specify the date and, where applicable, the volume and issue numbers of the original Russian. The material you will receive will be a translation of that Russian volume or issue.

Subscription
$80 per volume (6 issues)
2 volumes per year
(Add $5 for orders outside the United States and Canada.)

Single Issue: $30
Single Article: $15

CONSULTANTS BUREAU, NEW YORK AND LONDON

227 West 17th Street
New York, New York 10011

Davis House
8 Scrubs Lane
Harlesden, NW10 6SE
England

Published monthly. Second-class postage paid at Jamaica, New York 11431.

SOVIET ATOMIC ENERGY

A translation of *Atomnaya Énergiya*
October, 1973

Volume 34, Number 4 April, 1973

CONTENTS

CONTENTS

(continued)

The Russian press date (podpisano k pechati) of this issue was 3/28/1973. Publication therefore did not occur prior to this date, but must be assumed to have taken place reasonably soon thereafter.

L'VA ANDREEVICH ARTSIMOVICH

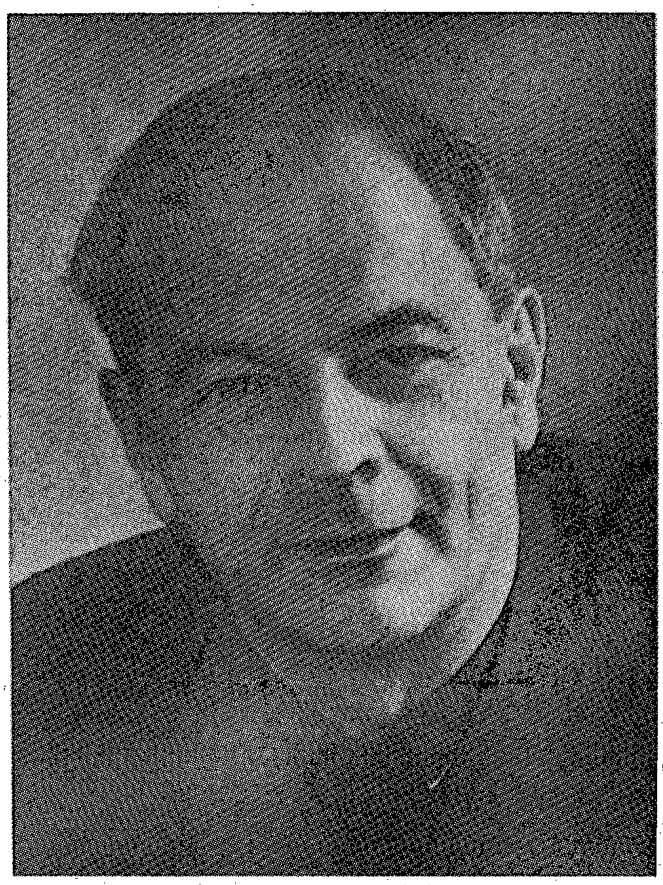

On March 1, 1973, L. A. Artsimovich died; he was in his sixty-fifth year. The editorial board of the journal "Atomnaya Energiya" wish to express their sorrow on the occasion of the death of this outstanding organizer of science and public-spirited person.

L. A. Artsimovich was a great man, as is evinced by the titles he held and the positions of responsibility he occupied: Academician-Secretary of the Department of Physics and Astronomy and member of the Presidium of the Academy of Sciences of the USSR; Scientific Director of the I. V. Kurchatov Institute of Atomic Energy, Academy of Sciences of the USSR; Chairman of the National Committee of Soviet Physicists; Hero of Socialist Labor; Lenin Prize Laureate; and winner of the Academic State Prize of the USSR.

The death of L. A. Artsimovich is mourned by all relations, friends, and pupils of this outstanding man of science.

Translated from Atomnaya Energiya, Vol. 34, No. 4, April, 1973.

HYDRAULIC RESISTANCE AND VELOCITY FIELDS IN TUBES WITH ARTIFICIAL WALL ROUGHNESS

M. D. Millionshchikov, V. I. Subbotin,
M. Kh. Ibragimov, G. S. Taranov,
and L. L. Kobzar'

UDC 532.542.4

Modern technology is frequently concerned with channels containing projections of various kinds on their surfaces, being either necessitated by structural considerations or provided in order to intensify heat transfer. Such projections may validly be classed as surface roughness; however, the theoretical and experimental study of flow in rough-walled channels has lagged seriously behind that of flow in smooth channels and is inadequate to meet practical requirements. The problem is complicated by the great variety of geometrical characteristics encountered in practice with rough surfaces.

A considerable amount of experimental material has now been gathered together in relation to this problem. A high proportion of the data relates to flow in tubes with annular and spiral linings [1-3], single-threaded surfaces [4, 5], sand roughness [6-9], and flow in tubes with natural roughness [8]. Different types of rough surfaces have been studied for flow in a plane channel [10-12]. The experiments have shown that the effect of roughness on flow hydrodynamics cannot be characterized simply by the relative height of the elements of roughness, as would follow, for example, from the laws derived in [6]. The shape of the elements and their mutual disposition also has an effect.

Existing experimental data relating to flow in rough tubes is insufficient for a complete elucidation of flow structure in the presence of a rough wall. Witness to this is the absence of any universal approach to the problem under consideration based on the geometrical characteristics of the rough surface.

Attempts have been made to describe flow in tubes with different kinds of roughness by using a single parameter – the height of the projections, k. However, this single quantity cannot embrace all possible types of roughness. Further, comparison between different experiments involving sand roughness [6, 7] shows that this parameter does not always facilitate correlation of experimental data, even for roughness of one particular type. Thus, in the experiments of [7], sand with a grain size of 1.35 mm caused a resistance which in the experiments of [6] would correspond to sand with a grain size of 2.22 mm.

The use of an equivalent roughness parameter k_{eq} as a surface characteristic fails to solve the problem, since it cannot reflect the complicated manner in which the resistance coefficient varies with the Reynolds number Re for various forms of roughness.

There is at present a pressing need for the development of universal computing relationships reflecting the connection between the hydrodynamic flow characteristics and the geometrical characteristics of the rough surface; this necessitates studying flow in channels with rough walls in which the shape, size, density distribution over the surface, and mutual disposition of the roughness elements are all known.

In the present investigation we studied turbulent flow in round tubes with a regular artificial wall roughness. The experiments were carried out in air ($Re = 4 \cdot 10^3$-$2 \cdot 10^5$) and water ($Re = 7 \cdot 10^4$-10^6) testbeds.

The vertical working section of the air system was connected at its upper end to the suction line of a fan through a damping tank. At the entrance into the working section, a filter, a honeycomb, a nozzle, and a turbulizing ring were arranged along the path of the air. The ring was needed because of the low turbulence

Translated from Atomnaya Énergiya, Vol. 34, No. 4, pp. 235-245, April, 1973. Original article submitted January 8, 1973.

of the flow after passing the nozzle, as a result of which the development of flow in the inlet section was delayed (for example, in the case of a smooth tube the laminar mode of flow existed over a considerable proportion of the tube right up to $Re = 5 \cdot 10^4$). The air test-bed was used for measuring the hydraulic resistance and velocity profiles.

In the experiments with air, small drops in static pressure for low Re numbers (4000-20,000) were determined by means of a bell-type balance micromanometer based on an analytical laboratory balance (the VLA-200G-M). This micromanometer measured pressure differences of 0.05 mm water to an error of no greater than 1%. The static pressure drops for $Re = 15 \cdot 10^3$-$2 \cdot 10^5$ and the velocity profiles were measured with an inclined liquid micromanometer having a minimal scale coefficient of 0.03. The maximum error in determining velocity close to the tube wall when measuring the dynamic head with an inclined differential manometer could be as high as 2%.

The water test-bed was made of Kh18N10T stainless steel. The working section was arranged horizontally. Distilled water was used as working medium. We used the water system solely for determining resistance coefficients. To this end we employed U-type differential manometers containing carbon tetrachloride and mercury.

The velocity profiles were measured in the exit cross section of the working parts, using a Pitot tube with an external diameter of 0.86 mm and a wall thickness of 0.18 mm; the tip of the tube had a spherical trim and passed 5 mm into the tube. The static pressure was taken from a measuring cabinet containing the end of the working section. The Pitot tube was moved by means of a locating system with a micrometer screw. The instant at which the sensor touched the tube wall was established by reference to an electrical contact, using an ohmmeter.

In measuring the hydraulic resistance the static pressure was selected by means of probes. The section in which the measurements were made amounted to 20 bore diameter; it was preceded by an inlet section 90 diameters long. In the air experiments the pressure drop was measured between the take-off point in the measuring chamber at the tube outlet and a static pressure probe placed in the working section. The probe constituted a tube with an external diameter of 1.8 mm and a wall thickness of 0.3 mm; the tip of the tube was sealed and rounded; at a distance of 10 mm from it four apertures 0.3 mm in diameter were drilled uniformly around a circle. In the water experiments we used two static pressure probes made of a tube 3×0.3 mm in diameter with six receiver apertures 0.3 mm in diameter. The static pressure sensors were placed at a distance from the tube wall equal to half its radius. The additional resistance due to the first sensor (counting along the path of the working medium) was determined in experiments with a smooth tube by comparing the static pressure drops measured in the same section of a tube 20 diameters long by wall sampling in the presence and absence of the sensors, respectively. The resistance coefficients of the sensors were independent of the Re number. The pressure loss due to the sensor was approximately 7% of the measured pressure in a smooth tube at $Re = 10^6$ (this proportion naturally diminished with decreasing Re number).

As flow meter in the air test-bed we used a nozzle placed at the entrance into the working section. The nozzle was calibrated by integration of the velocity profiles measured at the exit cross section of the smooth tube. For small flow rates corresponding to Re numbers of under $2 \cdot 10^4$ the flow-meter nozzle was calibrated by reference to the velocity profile measured in an auxiliary nozzle placed at the outlet from the tube, creating a contraction of the flow equal to a multiple of 9. This increased the accuracy of flow rate measurement. In the experiments in the air test-bed we used flow-meter discs calibrated by a volumetric method. For determining the temperature of the working medium we used mercury thermometers with a scale division of 0.1°C.

The local mean flow velocity was determined from the equation

$$u = \sqrt{\frac{2\Delta P}{\rho \xi_1 \xi_2}},$$

where ΔP is the reading of the differential manometer; ξ_1 and ξ_2 are the corrections for the compressibility and viscosity of the air. The density of the air was determined with due allowance for its humidity by using the equation of state for ideal gases. The correction for the compressibility of the air was calculated in the same way as in [13]. In order to calculate the correction for the viscosity we used the data provided in [14] in the form of the dependence of the coefficient ξ_2 on the Re number calculated from the internal diameter of the receiving aperture of the Pitot tube and the local velocity.

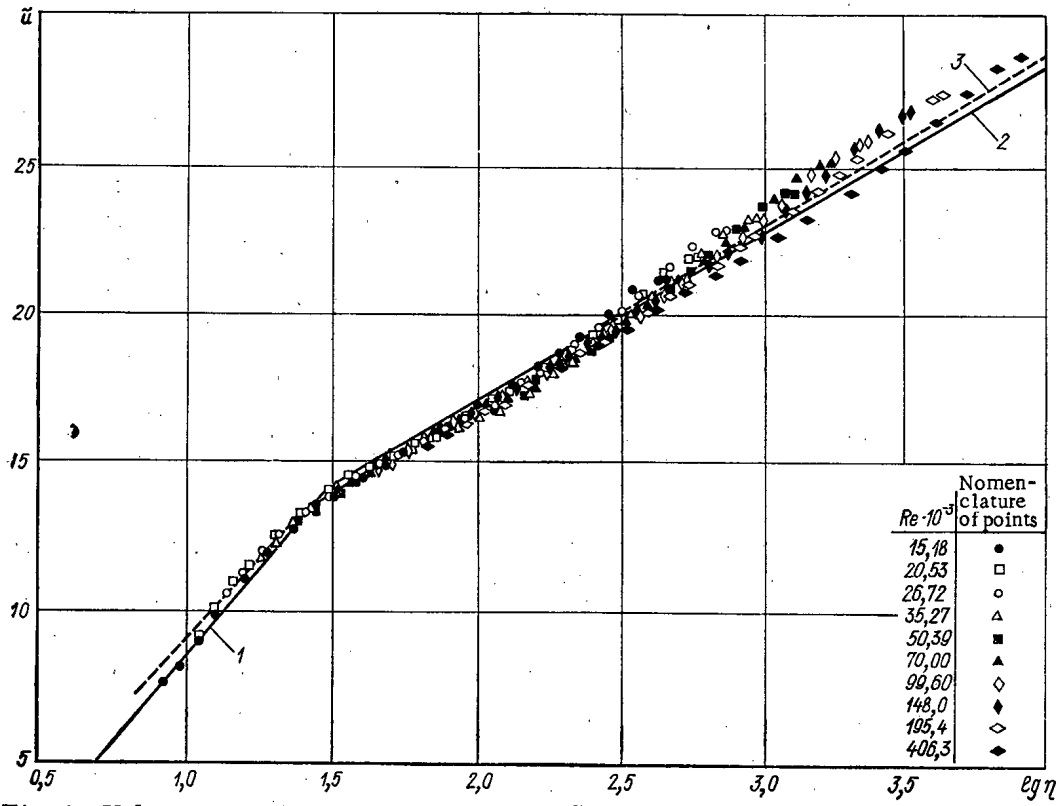

Fig. 1. Velocity profiles in a smooth tube ($\tilde{u} = u/u^*$ is the dimensionless velocity, where u^* is the dynamic velocity; $\eta = yu^*/\nu$ is the dimensionless distance from the wall, where ν is the viscosity of the liquid).

In determining the velocities we also introduced a correction for the displacement of the "effective" center of the Pitot tube in the direction of higher velocities. On the basis of the recommendations made in [15] the velocity calculated with due allowance for the foregoing corrections was referred not to the coordinate y (distance from the wall to the center of the Pitot tube) but to the coordinate y + 0.15 d, where d is the external diameter of the Pitot tube.

The loss of static pressure in friction during the flow of the air was determined by introducing into the measured pressure drop a correction for the additional resistance due to the static head sensor, and for the change in the mean dynamic head along the tube due to the change in air density. In addition to this, a correction was introduced into the readings of the micromanometer to allow for the change in the density of the alcohol arising from the difference in room temperature between the experimental and calibration periods.

As effective tube size we used the reduced diameter $D_r = \sqrt{4V/\pi L}$, where V is the internal volume and L is the length of the tube.

The first stage of the investigations was carried out in smooth tubes with internal diameters of 59 and 113 mm. The tube diameter 59 mm had a length of 114.3 diameters and consisted of eleven sections joined together by close-fitting sleeves. The fitting dimensions and the internal diameter of all the sections were made to second-class accuracy. In the most unfavorable case there might be a step 0.03 mm high at the join between two sections. The material of the first four sections along the path of the working medium was Duralumin D16T; the remaining seven sections were made of Kh18N10T stainless steel. For taking the static pressure, four holes 0.5 mm in diameter were drilled uniformly around a circle in fifteen cross sections of the tube wall.

The tube 113 mm in diameter consisted of seven sections with a total length of 61 diameters made of Kh18N10T steel to second-class accuracy. The apertures for taking the static pressure, situated in nine tube cross sections, had a diameter of 1 mm.

TABLE 1. Versions of Rough Tubes Studied

Form of roughness No.	Height of projection No.	1	2	3	4	5
	k	0,06	0,19	0,5	1,0	2,0
	$D_{av}/2k$	492	155	59	~30	~15
1	Single triangular thread	△ 1-1 S=0,25	△ 1-2 S=0,5 b=0,11 α=75°	▲ 1-3 S=1 b=0,05; α=40°	▽ 1-4 S=2 b=0,27 α=60°	▼ 1-5 S=4 b=0,54; α=60°
2	Single rectangular thread					□ 2-5 S=4 b=1,7
3	Single rounded thread					● 3-5 S=4 r_1=0,75; r_2=1,25
4	Multiple crossed triangular thread			◇ 4-3 S=1 N_1=80 ◆ 4-3-B S=2 N_1=40 ◇ 4-3-D S=2 N_1=40		◆ 4-5-1 S=4 N_1=20 ◇ 4-5-2 S=4 N_1=44 ◆ 4-5-3 S=8 N_1=22 ◇ 4-5-4 S=16 N_1=11
5	Annular grooves			◻ 5-3-1 S=30 b=29 ■ 5-3-2 S=30 b=20 ■ 5-3-3 S=30 b=10		
6	Hemispherical projections					◇ 6-5-1 a S=32 N_2=6 ◆ 6-5-2 b S=32 N_2=11 ◆ 6-5-3 a S=16 N_2=11 ◆ 6-5-4 b S=16 N_2=22 ◇ 6-5-5 a S=8 N_2=22 ◇ 6-5-6 b S=8 N_2=44

Note. The shape of the projections of version 1-1 was similar to that of a trapezium with rounded corners ($\alpha \approx 90°$, $b \approx 0.11$); s is the screw pitch or the distance between roughness projections in the axial direction; N_1 is the number of turns of the thread; N_2 is the number of roughness projections on the perimeter of the tube.

The resistance coefficients for the smooth tubes are shown in Fig. 3a; they agree closely with the experimental data of [16] for a smooth tube (curve 2) in the range Re $= 10^4$-$25 \cdot 10^4$. On moving away from the boundaries of this range in either direction we found a systematic monotonically increasing difference, reaching approximately 4% at the limits of the range of Re numbers studied. Also shown in Fig. 3a is the theoretical curve for a smooth tube calculated from the equation of [17].

Using coordinates of $\tilde{u} - \log\eta$, Fig. 1 shows velocity profiles measured at the exit cross section of smooth tubes 59 and 113 mm in diameter. For $y/R < 0.2$ (R = tube radius) all the experimental points lie on a single, almost straight line (with a slight scatter); for $y/R > 0.2$ the velocity profiles corresponding to different Re numbers fall into layers. This layer formation reflects a regular deviation of the velocity profile from the logarithmic law in the center of the flow [18]. The experimental data are compared with the Prandtl–Karman velocity distribution (curves 1 and 2) and the calculated relationship

$$\tilde{u} = \frac{1}{0.39} \ln [1 + 0.39 (\eta - 7.8)] + 7.8,$$

corresponding to the velocity profile for flow in a boundary layer [17]. This relationship (curve 3) is the same both for the transient layer and for the turbulent core; it describes the whole set of experimental data with the minimum scatter.

Table 1 shows all versions of the rough tubes studied (23 versions). Each line in the table corresponds to one form of roughness, each column to one height of the projections on the rough surface. All versions are denoted digitally. The first digit characterizes the form of roughness, the second the height of the projections, the third indicates different versions with one particular form with the same height of the projections. For each version of roughness the table gives the symbol used for the experimental points in the figures; the dimensions are given in millimeters. The average diameter of the tubes for the first five forms of roughness is 59 mm, for the sixth it is 58 mm; the ratios $D_{av}/2k$ (where D_{av} is the diameter of the circle drawn through the middle of the roughness projections) are similar to those in the experiments of Nikuradse with sand roughness.

The roughness of the first five forms was created by cutting single and multiple crossed threads and annular grooves on the inner surface of the tubes; the tube material was Duralumin D16T. The hemispherical projections of the sixth form were obtained by stamping in a special attachment giving a high accuracy of the dimensions of the projections and their arrangement on the tube surface. For the working sections of this form of roughness we used tubes made from ductile Duralumin.

The single threads were cut with special screw taps. Five versions were made with a single triangular thread: 1-1; 1-2; 1-3; 1-4; 1-5; the roughness projections differed in respect of size. In the case of rectangular and rounded single threads only one version was made (2-5 and 3-5). Versions 1-5, 2-5, and 3-5 had the same screw pitches, projection heights, and reduced diameters D_r; they differed in the shape of the projections.

The multiple crossed threads were made thus: first all the right-handed turns of the thread were made in turn with the cutter, then all the left-handed ones; this gave truncated small pyramids arranged in a checkered disposition. Seven versions of roughness were made with crossed multiple threads. Versions 4-3 and 4-5-1 had geometrically similar pyramids, differing only in dimensions. In versions 4-5-1 and 4-5-2 there was the same density of pyramids in the axial direction, but there were more pyramids in

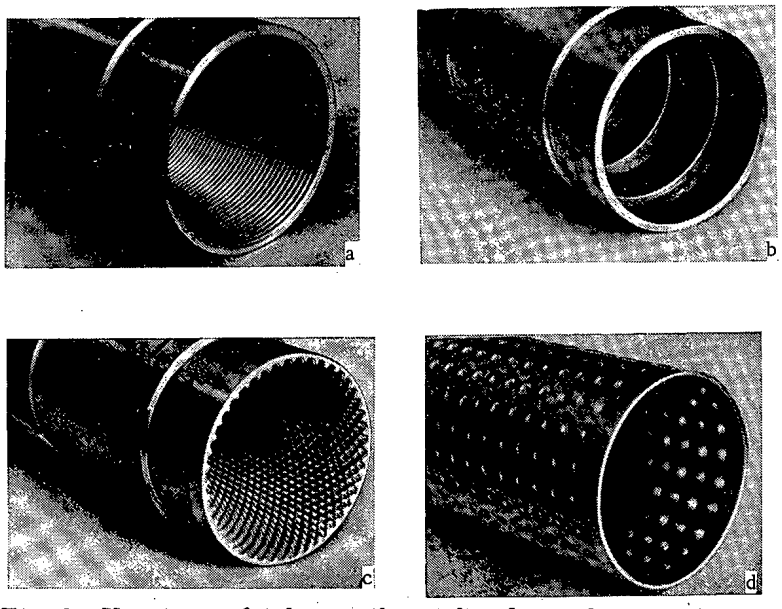

Fig. 2. Versions of tubes with artificial roughness: a) 1-4; b) 5-3-2; c) 4-5-2; d) 6-5-5.

the tangential direction in version 4-5-2 (in proportion to the number of turns). The shape of the pyramids in these versions was of course different. Version 4-5-3 was obtained from 4-5-2 by cutting away every second turn of the right- and left-handed threads as far as the base of the pyramids. Version 4-5-4 was obtained from 4-5-3 in the same way.

In order to study the way in which the dispersion of the heights of the projections affected the hydrodynamic characteristics of the flow, we also made versions 4-3-B and 4-3-D. The elements of roughness (projections) of these versions were made by cutting a crossed 40-fold thread with a length of 80 mm. The projections of version 4-3-B were truncated pyramids of the same height, 0.5 mm. Those of version 4-3-D had the same pyramid base as 4-3-B, but the heights varied from 0 to 1 mm with an arithmetic mean height of 0.5 mm. The number of pyramids of each height (nine heights) was determined from the condition that the histogram of their distribution should, on smoothing, obey a normal distribution law.

The annular grooves (fifth form of roughness) were produced with a cutter. We made three versions of tubes differing in the width of the grooves (5-3-1; 5-3-2; 5-3-3). The depth of the grooves and the cutting pitch was the same for all these versions.

The versions of the sixth form of roughness were obtained by successively doubling the thickness of the hemispherical projections; thus corridor-like and checkered dispositions of the projections alternated. Version 6-5-6 had the same thickness as 4-5-3, while version 6-5-4 corresponded to 4-5-4. These two pairs of versions were only distinguished by the shape of the projections.

The technology used for producing the cuts on the tubes ensured that the height of the projections should remain constant along the length of the channel to within 0.03 mm. This was achieved as follows. In the case of the first five forms of roughness, before cutting the projections the internal diameter of the tubes was finished to second-class accuracy. The cutting parts of the screw taps used for producing the single threads were finished to the same class of accuracy. In cutting the projections in the tubes with multiple crossed threads and annular grooves, the transverse feed of the cutter was started from the point at which the cutter touched the inner surface of the tube, using an indicator with a scale division of 0.01 mm. For the sixth form of roughness the accuracy with which the hemispherical projections were prepared was lower, their height being maintained to an accuracy of 0.15 mm; the accuracy of disposition of the projections over the surface of the tube was 0.2 mm. The final dimensions of the projections (Table 1) were determined from photographs of microsections. The microsections enabled us to refine the dimensions of the projections of versions 1-1, 1-2, and 1-3 given in [19]. Figure 2 shows several versions of the rough tubes studied.

The rough tubes were 30 diameters long and consisted of individual sleeve-interlinked sections 10 or 5 diameters long. In carrying out the experiments the working part was set up as follows: moving along

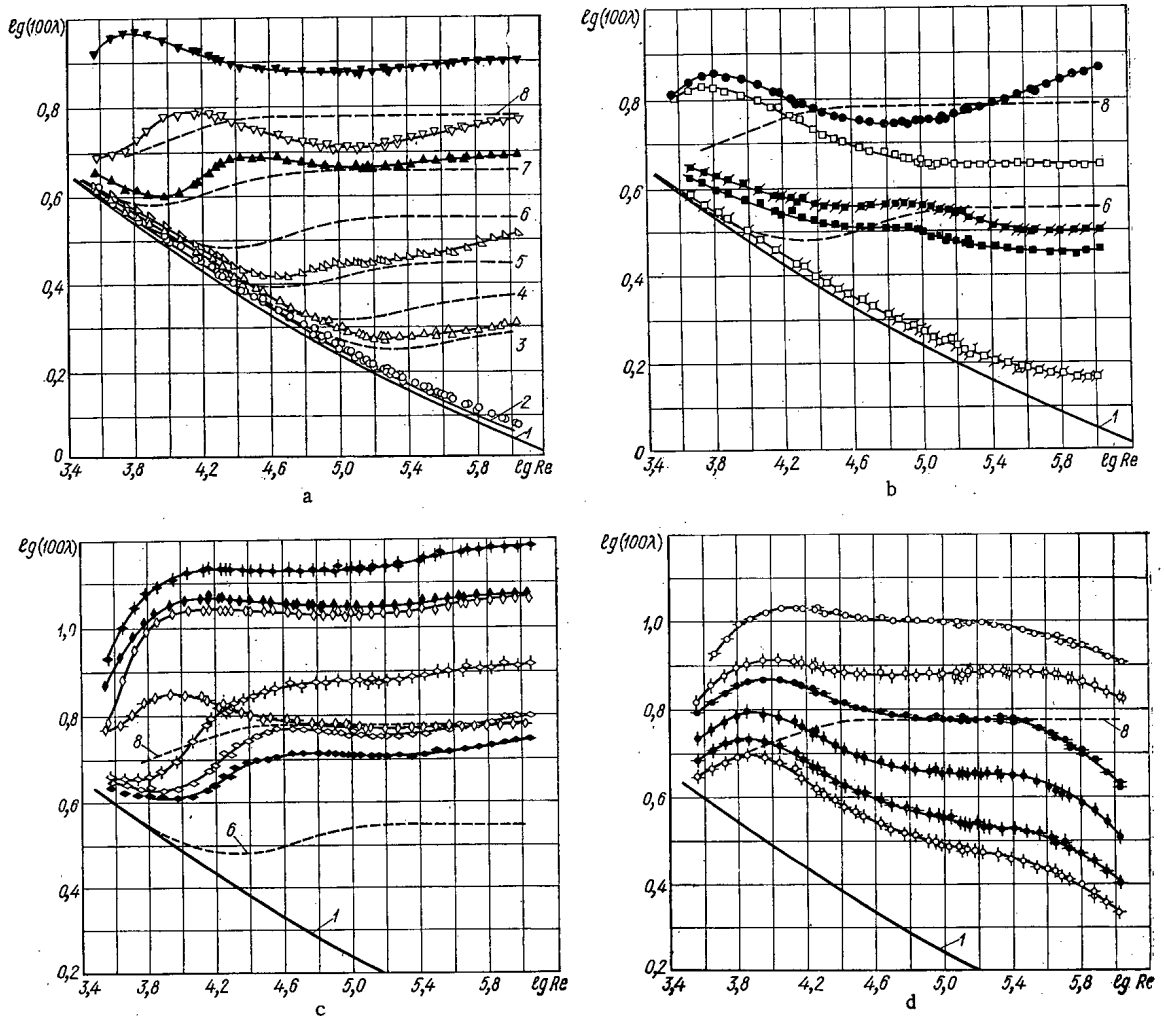

Fig. 3. Coefficients of hydraulic resistance λ of the rough tubes (here and subsequently ○ denotes the authors' experimental results for a smooth tube): 1) theoretical curve for a smooth tube [17]; 2) averaging line of the experimental results for a smooth tube [16]; 3-8) for rough tubes [6] with a ratio $D_{av}/2k$ of 507, 252, 126, 60, 30.6, and 15, respectively. (The remaining nomenclature employed here and in Figs. 4 and 5 may be found in Table 1.)

the path of the working medium, first there was a smooth section 50 diameters long, then followed the entrance section 30 diameters long with a roughness similar to that being studied, and finally the section with the roughness under consideration, 30 diameters long. The fall in static pressure was measured in the last 20 diameters of the working section, and the velocity profile at the outlet. A determination of the velocity profiles at the beginning and end of the measuring section 20 diameters long for several types of rough tubes showed that the flow was hydrodynamically stabilized along the whole length of this section.

Figure 3 shows the relations between the resistance coefficients and the Re numbers so obtained (where $Re = \bar{u}D_r/\nu$). The experimental data are divided into four groups (a, b, c, d). This division is continued in Figs. 4 and 5. The resistance coefficients in different ranges of Re numbers were measured in different test-beds (distinguished by the medium) and different times. The individual ranges of Re numbers corresponding to the different experimental conditions overlapped. The scatter in the experimental data at the points at which these intervals merged was no greater than 3%.

In Fig. 3a the resistance coefficients for single triangular threads are shown. Here the broken line indicates the averaged lines of the experimental points in [6]. It is of course a little arbitrary to compare our present experimental data with those of [6], since two different forms of roughness were involved.

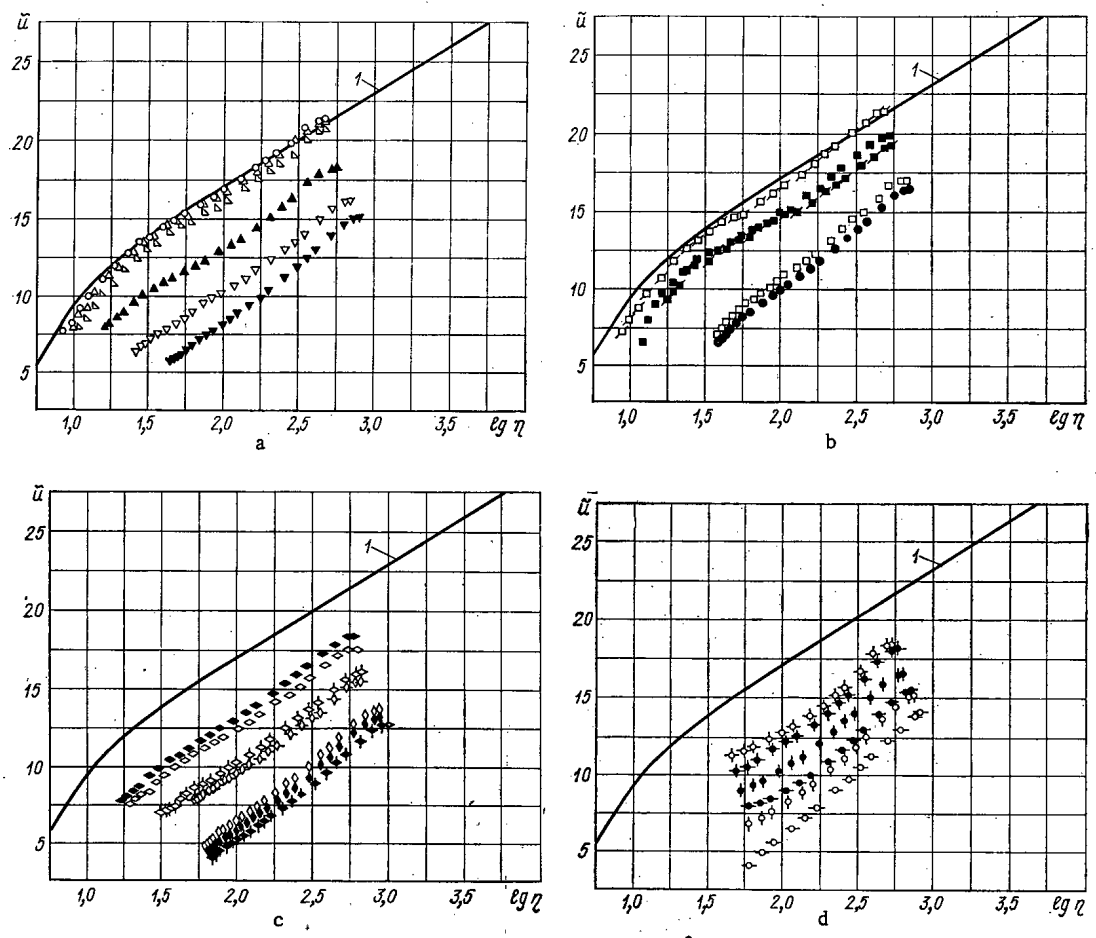

Fig. 4. Velocity profiles in rough tubes at Re = $15 \cdot 10^3$: 1) theoretical velocity profile for a boundary layer at a smooth wall [17].

The λ(Re) relationships for tubes with a triangular thread and $D_{av}/2k$ equal to 492 and 155 (versions 1-1 and 1-2) are reminiscent in form of the relationships obtained in [6], except for the fact that the resistance coefficients for version 1-2 still have a pronounced tendency to increase as Re → 10^6. With increasing height of the projections the difference between our λ(Re) curves and those of Nikuradse becomes greater. The hydrodynamic effects of roughness set in much earlier than in Nikuradse's experiments; then with increasing Re number there is a rapid increase in the resistance coefficient. On further increasing the Re number the experimental curves pass through a maximum and a minimum, and then tend to rise right up to the upper limit of the Re range studied. For high projections the separation of the λ(Re) curves from the relationship for the smooth tube occurs very early and in a sharp manner, while the resistance maxima have a very pronounced character. With diminishing height of the projections the maxima move in the direction of high Re numbers and degenerate. In absolute magnitude the resistance coefficients for tubes with threads and sand roughness are similar to one another for $D_{av}/2k = 492$. For smaller values of this parameter the resistance coefficients of tubes with a thread exceed those of tubes with sand roughness by up to 60%.

The λ(Re) relationships for tubes with single rectangular and rounded threads and with annular grooves are extremely peculiar (Fig. 3b). The λ(Re) curve for a tube with a rounded thread reproduces the form of the λ(Re) relationship for a tube with a triangular thread (Fig. 3a), but the tendency for the resistance coefficient to increase at high Re numbers appears far more sharply in the case of 3-5 than in that of 1-5. For a tube with a rectangular thread (version 2-5) there is an automodel region at high Re numbers. For equal heights of the projections the greatest resistance occurs in a tube with a triangular thread and the least in one with a rectangular thread.

In tubes with wide annular grooves (versions 5-3-2 and 5-3-3) the roughness starts manifesting itself very early; however, the subsequent deviation of the resistance coefficient from the law corresponding to a smooth tube takes place slowly. The maxima of the λ(Re) relationship are weakly expressed and are

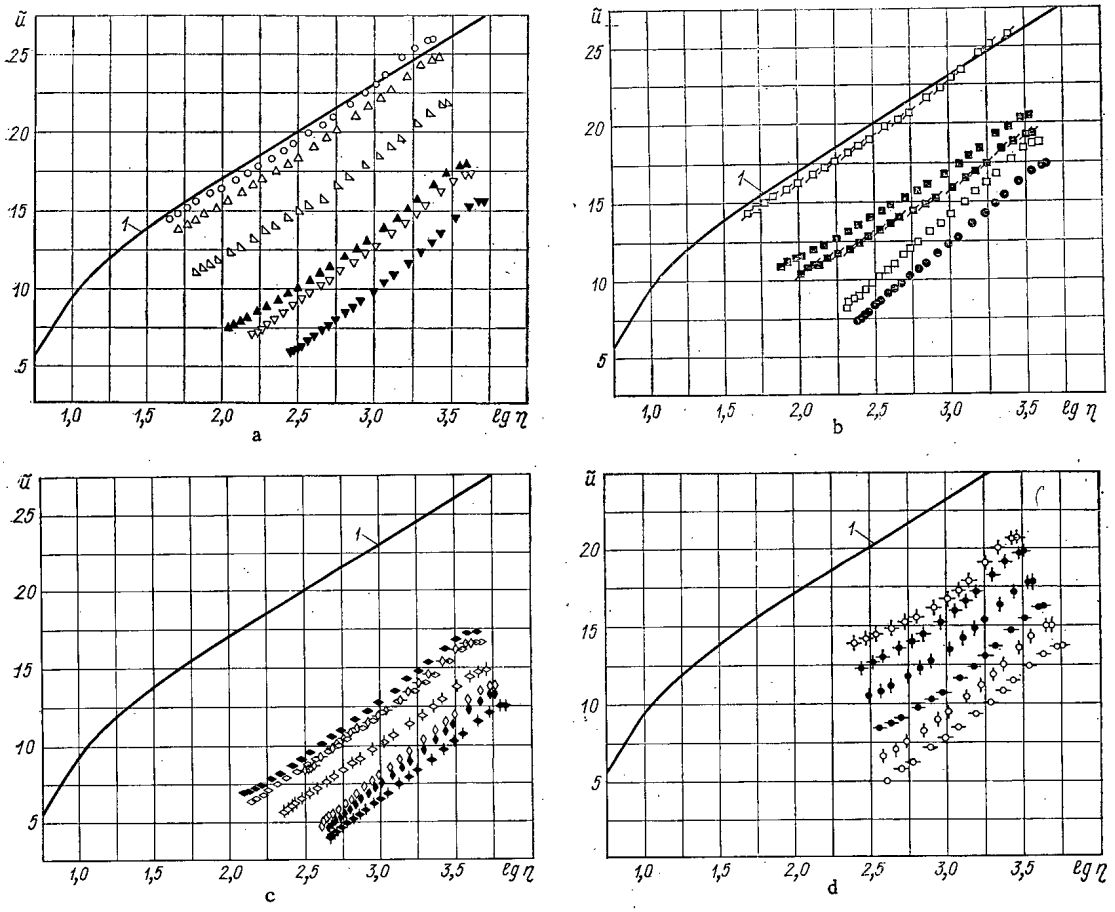

Fig. 5. Velocity profiles in rough tubes for Re = 10^5: 1) see Fig. 4.

displaced in the direction of larger Re numbers than other forms of roughness with the same height of the projections. For a tube with narrow grooves (5-3-1) λ coincides over a wide range of Re numbers with the resistance coefficient for a smooth tube; the effect of the grooves only starts appearing markedly for Re $> 10^5$.

The resistance coefficients of tubes with a multiple crossed thread are shown in Fig. 3c. In this case comparison with Nikuradse's data for tubes with sand roughness would appear the most competent. The resistance coefficients obtained for a tube with sand roughness and $D_{av}/2k = 15$ (curve 8) might be expected to resemble those relating to one of our experimental tubes with an equal value of $D_{av}/2k$ and a close disposition of the pyramids (4-5-1, 4-5-2, 4-5-3); however, the resistance coefficients of these tubes are in fact 2-2.5 times greater than those of tubes with sand roughness. Agreement with Nikuradse's data for $D_{av}/2k = 15$ is close in the case of version 4-5-4 for large Re numbers; however, the low density of the pyramids in this version does not, of course, correspond to the density of the projections in sand roughness – the coincidence is a matter of chance. This difference in the resistance coefficients for tubes with multiple crossed threads and sand roughness respectively even appears for $D_{av}/2k = 59$.

It is interesting to compare the results obtained for versions 4-5-2, 4-5-3, and 4-5-4. For the first reduction in the number of projections in this series, viz., by a factor of four (4-5-3 version), the resistance coefficients increased; on further reducing it by a factor of four (4-5-4 version) they fell sharply. For small Re numbers a maximum of the resistance coefficient appeared. An analogous result was obtained in [1, 2] when studying the influence of the distance between rings inserted into a tube on the hydrodynamic resistance. According to the experimental data presented in these papers we may conclude that the maximum of the resistance coefficient corresponded to a relative distance of s/k = 8-10 between the rings. It follows from Fig. 3c that in the case of a multiple crossed thread a value of s/k equal to four corresponds to the maximum in the resistance coefficient. A reduction in the resistance coefficient for a denser disposition of the projections also appears on comparing cases 4-5-1 and 4-5-2.

An analysis of the experimental data obtained for 4-3-B and 4-3-D shows that any dispersion (spread) of the height of the projections (keeping the mean height constant) causes an increase in the resistance coefficient over the whole range of Re numbers studied (for $Re = 10^5$ the resistance coefficient for 4-3-D is 60% greater than for 4-3-B), and an earlier appearance of the effects of roughness (this confirms the views expressed in [17]).

For tubes with a multiple crossed thread and a close-packed disposition of the pyramids, the $\lambda(Re)$ relationship approaches the relationships corresponding to tubes with sand roughness more closely that in the case of tubes with a single triangular thread. There is no sharp maximum for small Re numbers. However, the tendency for the resistance coefficient to increase at high Re numbers remains intact.

The resistance coefficients for tubes with hemispherical projections are shown in Fig. 3d. All the curves have a maximum for small Re numbers and fall for $Re > 2 \cdot 10^5$. With increasing density of the projections the hydraulic resistance increases up to $s/k = 4$ (6-5-6). On further increasing the density one might expect a fall in λ; however, it proved technically impossible to increase the number of projections on the tube surface. Up to a number of $Re = 10^5$ the form of the $\lambda(Re)$ relationships coincides for tubes with hemispherical projections and multiple crossed threads; furthermore, for the same density of the projections the resistance coefficients for the forms of roughness under comparison are extremely close (see 6-5-6 and 4-5-3, and also 6-5-4 and 4-5-4). However, in tubes with hemispherical projections the resistance coefficients start falling for large Re numbers, whereas in tubes with small pyramids there is a tendency for the resistance coefficient to rise.

The velocity profiles are shown in Figs. 4 and 5 in coordinates of $\tilde{u} - \log\eta$ for Re numbers of $15 \cdot 10^3$ and 10^5. At the same (small) distance from the surface, corresponding to the diameter through the tips of the projections, the rate of flow depends on whether the point of measurement is disposed over a projection or over a depression. Special measurements showed that the influence of local geometrical singularities of the surface on the velocity field extended over only a short distance. On moving away from the tip of the projection by a distance of 0.4-0.5 mm (first measuring point) the average local velocity was practically equal to the rate of flow over a depression.

For the majority of tube versions the velocity profiles in Figs. 4 and 5 are satisfactorily described by a straight line with a slope usually exceeding the slope of the straight line obtained for the smooth tube. The greatest slope occurs for the smoothing line corresponding to the velocity profile of version 2-5, for $Re = 100 \cdot 10^3$ (Fig. 5b). The tangent of the slope angle of the graph plotted in coordinates of $\tilde{u} - \log\eta$ is almost 1.4 times that corresponding to the velocity profile in a smooth tube. The displacement of the velocity profile of the rough tube along the vertical axis relative to the profile of the smooth tube depends on the coefficient of hydraulic resistance: the greater the coefficient, the greater is the downward displacement of the velocity profile.

Peculiar velocity profiles are obtained in the case of roughnesses in the form of hemispherical projections (Figs. 4d and 5d): at the tube walls the profile is more gradually slanting, and in the center sharper, than for the other versions of tubes; this is particularly characteristic of low-density projections.

In coordinates $u/u_{max} - y/R$ (where u_{max} is the velocity in the center of the tube) the shape of the velocity profile is determined by the resistance coefficient; the greater the resistance coefficient, the sharper is the velocity profile.

The experimental data presented in Figs. 3, 4, and 5 are hard to explain from the point of view of existing theoretical constructions relating to flow in rough tubes. The hydraulic effects of roughness are observed earlier than would follow from the theoretical models. In the majority of cases this effect is felt for $ku^*/\nu < 3$. In the range of Re numbers up to 10^6 there is hardly any interval in which the square law of resistance might act (apart from case 2-5).

The experiments of Nikuradse give a sharp separation of the λ curves into layers with respect to the parameter $D_{av}/2k$. A similar separation is found in the data here presented if the roughness elements possess geometric similarity and there is a constant distance between the projections. On changing the shape and step of the projections the resistance coefficient changes considerably, independently of whether the quantity $D_{av}/2k$ remains constant. Thus for $D_{av}/2k = 15$ the coefficient λ corresponding to $Re = 10^6$ takes values of 0.022 (6-5-1) to 0.15 (4-5-1), whereas in [6] it was equal to ~0.06.

The agreement between the resistance coefficients of tubes with pyramids and hemispherical projections for the same density of the elements of roughness (versions 4-5-3 and 6-5-6, 4-5-4 and 6-5-4) is evidently a matter of chance. For tubes with hemispherical projections the resistance coefficient should (one would have thought) be lower than for tubes with pyramids, owing to the fact that flow around a sphere is easier. However, in the present case the frontal resistance of the sphere (smaller than that of a pyramid) is compensated by its greater frontal cross section.

For the same height of the projections and an equal distance between them in the axial direction, the greatest resistance is obtained for roughnesses in the form of pyramids and spherical projections. If the elements of roughness are close together, the mutual screening of the projections starts playing a major part. This may, in particular, explain the fact that the resistance coefficient of 4-5-2 is smaller than that of 4-5-3.

The manner in which the flow passes around individual roughness projections has a great influence on the hydrodynamic characteristics of the flow in rough tubes. For bodies of spherical shape, of course, the coefficient of frontal resistance changes with changing Re number owing to the changing circumfluence pattern. Correspondingly the most complicated $\lambda(\mathrm{Re})$ relationships obtained in the present experiments were those relating to tubes with hemispherical projections. We should therefore expect that the resistance coefficients of rough tubes with projections giving poor circumfluence (pyramids) should depend less on the Re number than the resistance coefficients of tubes with projections giving good circumfluence, other geometrical characteristics being equal. This is confirmed by comparing versions 1-5 and 3-5 and also tubes of the fourth and sixth forms of roughness.

The resultant experimental data obtained for 23 versions of rough tubes indicate the fairly complicated nature of the flow along rough walls. Further investigations are in hand in order to elucidate the mechanism underlying the interaction of a turbulent flow with elements of roughness, to obtain generalizing relationships, and to set up computing techniques.

LITERATURE CITED

1. H. Möbius, Phys. Z., No. 7, 202 (1940).
2. W. Nunner, VDI-Forschungsh., No. 455 (1956).
3. N. F. Novozhilov and V. K. Migai, Teploenergetika, No. 9, 60 (1964).
4. L. Schiller, Z. Angew. Math. und Mech., 3, 2 (1923).
5. B. M. Teverovskii, Izv. VUZ. Energetika, No. 7 (1958).
6. J. Nikuradse, VDI-Forschungsh., No. 361 (1933).
7. H. Schlichting, Ingr.-Arch., 7, No. 1 (1936).
8. F. A. Shevelev, Study of the Principal Hydraulic Laws of Turbulent Motion in Tubes [in Russian], Gosstroiizdat, Moscow (1953).
9. R. S. Tyul'panov, Inzh.-Fiz. Zh., No. 6, 40 (1964).
10. H. Schlichting, Theory of the Boundary Layer [Russian translation], Nauka, Moscow (1969).
11. K. Fromm, Z. Angew. Math. und Mech., 3, 339 (1923).
12. W. Fritsch, ibid., 8, 199 (1928).
13. N. A. Sachs, Fundamentals of Experimental Aerodynamics [Russian translation], Oborongiz, Moscow (1953).
14. F. Macmillan, J. Roy. Aeronaut. Soc., 58, 570 (1954).
15. Yu. D. Boltoev et al., "Method of measuring velocities by total head tubes in the boundary region of a flow," Preprint FEI, No. 320 (1972).
16. J. Nikuradse, VDI-Forschungsh., No. 356 (1932).
17. M. D. Millionshchikov, At. Energ., 28, 207 (1970).
18. P. O. Khinze, Turbulence [in Russian], Fizmatgiz, Moscow (1963).
19. M. D. Millionshchikov et al., Dokl. Akad. Nauk SSSR, 207, 1292 (1972).

INVESTIGATION OF SWELLING OF STRUCTURAL STEELS IN CARBIDE ZONE OF THE BR-5 FAST REACTOR

V. N. Bykov, A. G. Vakhtin,
V. D. Dmitriev, Yu. V. Konobeev,
L. G. Kostromin, and V. F. Reutov

UDC 621.039.5.053

Recent investigations of materials irradiated by high-level integrated fast flux have shown that radiation-induced porosity typified by some specific patterns and regularities [1] shows up in pure metals and structural steels. The formation of radiation porosity is accompanied by a macroscopic increase in the volume of the metals, and must be taken into account in the development and operation of reactors. Results of the investigations reveal the presence of numerous factors affecting swelling of metals and alloys. Securing further information on the principal regularities underlying the formation and evolution of radiation-induced pores is a paramount problem in solid state physics, and is of great practical importance.

This paper presents some results of an electron-microscopic investigation of radiation-induced porosity in materials of hexagonal cladding and fuel-element envelopes, and working bundles in the carbide zone of the BR-5 fast reactor (steel grades 18-8, 16-15, with integrated flux to $3.6 \cdot 10^{22}$ neutrons/cm^2).

Table 1 shows results of measurements of radiation-induced pore volume under different conditions of irradiation of steel grades 0Kh18N19T and 00Kh16N15M3B, the cladding materials in this instance. A slight spread in the data for individual cladding systems for the same grade of steel seems to be traceable to the contrasting structural states of the original material in those instances.

We also conducted an investigation of the distribution of radiation-induced pores over the perimeter of the cladding in six cross sections throughout the length of the fuel element, being careful to take into account the known irradiation conditions and the unevenness in the ambient temperature in the case of peripherally placed fuel elements. Our findings were that the pore density and pore size in the different cross sections of the centrally located fuel elements correlate closely with changes in temperature and in integrated flux over the core height. Investigation of specimens taken from cross sections of the cladding

TABLE 1. Irradiation Conditions and Variations in Volume of Cladding Materials

Material	Irradiation dose, $\cdot 10^{22}$ neutrons/cm^2	Temperature of irradiation, °C (± 30°C)	$\frac{\Delta V}{V}$, %
0Kh18N9T	0,9	430	0,05
"	1,6	430	0,2
"	1,8	430	1,0
"	1,7	450	0,4
"	2,9	460	0,6
"	3,6	460	3,1
"	0,9	510	0,2
00Kh16N15M3B	1,5	430	0,3
"	3,0	460	2,2

TABLE 2. Behavior of Mean Pore Size ⟨d⟩, Pore Concentration N_V, and Relative Volume Change in Annealing of 0Kh18N9T Steel

Irradiation conditions	1.8 · 10^{22} neutrons/cm^2, T_{irr} = 430°C			3.6 · 10^{22} neutrons/cm^2, T_{irr} = 460°C		
	⟨d⟩, Å	N_V, $\times 10^{14}$ cm^{-3}	$\frac{\Delta V}{V}$, %	⟨d⟩, Å	N_V, $\times 10^{14}$ cm^{-3}	$\frac{\Delta V}{V}$, %
After irradiation	290±20	4,6	1,1	525±20	5,6	5,0
Annealing						
600°C, 100 h	310±20	5,5	1,7	—	—	—
800°C, 100 h	235±20	8,6	0,9	550±20	3,2	2,2
800°C, 1 h	—	—	—	570±20	2,3	4,8
800°C, 10 h	—	—	—	460±20	2,54	1,5

Translated from Atomnaya Énergiya, Vol. 34, No. 4, pp. 247-250, April, 1973. Original article submitted April 10, 1972.

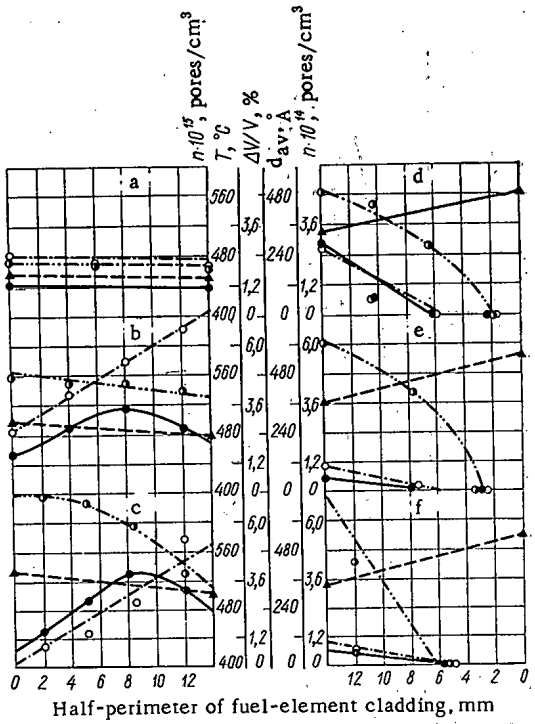

Fig. 1. Graphs showing variation in irradiation temperature (– – –; ▲), in mean diameter (– · · –; ◑), in concentration (– · – · –; ○), and in total volume of voids (——; ●) over perimeter of cladding of fuel element made from 0Kh18N9T steel, plotted for different integrated flux levels in neutrons/cm^2: a) $1.8 \cdot 10^{22}$; b) $2.4 \cdot 10^{22}$; c) $2.95 \cdot 10^{22}$; d) $2.8 \cdot 10^{22}$; e) $2.12 \cdot 10^{22}$; f) $0.97 \cdot 10^{22}$.

on peripherally positioned fuel elements made it possible to discern the temperature dependence of the formation of pores directly, since each cross section of the cladding corresponded to a definite integrated flux level at a different temperature of the perimeter. The experimental results, together with the exposure conditions for the six cross sections through the cladding of a fuel element made of 0Kh18N9T steel, are plotted in Fig. 1, from which it may be seen that a rise in the temperature at which the steel was irradiated means a decline in the concentration of porous voids, while the mean dimension increases, in agreement with observations made by other authors [1]. The observed nonuniformity in the distribution of radiation-induced pores over the perimeter of the cladding, in different cross sections through the fuel elements,

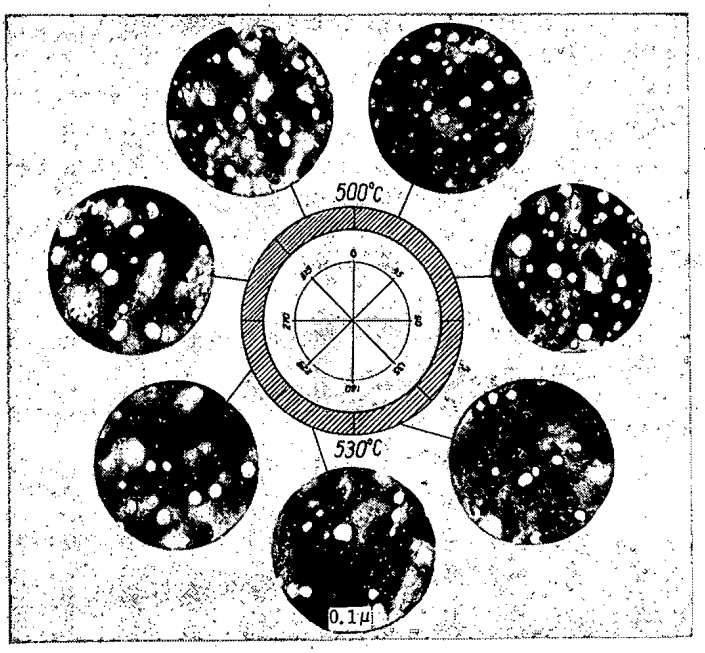

Fig. 2. Peripheral nonuniformity of radiation-induced porosity over perimeter of cladding of peripherally positioned fuel element.

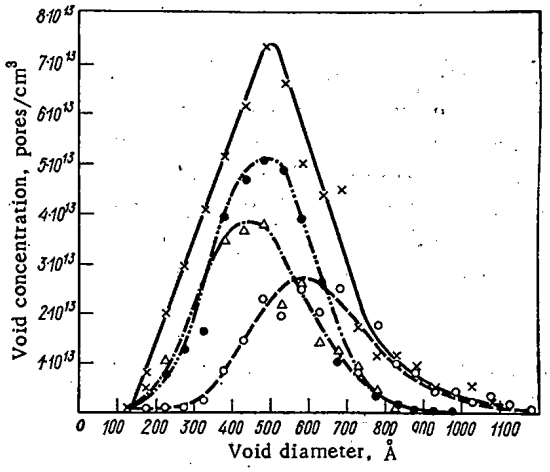

Fig. 3

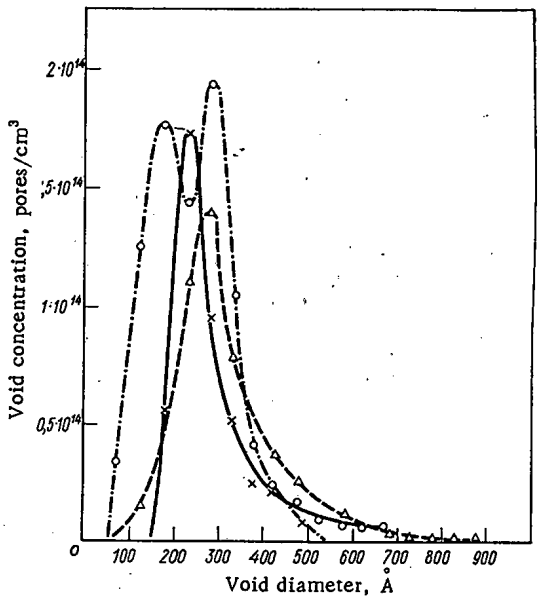

Fig. 4

Fig. 3. Spectrum of void sizes in 0Kh18N9T steel at integrated flux $3.6 \cdot 10^{22}$ neutrons/cm^2, T_{irr} = 460°C in the case of unannealed coupons (——) and coupons annealed at 800°C for 1 h (– – –), 10 h (–·–), and 100 h (–···–).

Fig. 4. Void size distribution in 0Kh18N9T steel at integrated flux $1.8 \cdot 10^{22}$ neutrons/cm^2, T_{irr} = 430°C for unannealed coupons and those annealed at 600°C (– – –) and at 800°C (–·–), for 100 h.

corresponds to the peripheral unevenness of the temperature. The marked nonuniformity in radiation porosity over the perimeter of the fuel-element cladding in one of the cross sections is evident in Fig. 2.

A similar investigation of radiation-induced porosity in the cladding of a fuel element made of 0Kh16N15M3B steel revealed a lesser proclivity to swelling in that steel, as compared to the behavior of steel grades 0Kh18N9T and 00Kh16N15M3B; this might be due to the greater stability of the steel tested, and to the presence of finely dispersed precipitations in that steel.

Annealing Behavior of Radiation-Induced Pores. Coupons cut from cladding were annealed at 600° and 800°C for 100 h, at 800°C for 1, 10, and 100 h, and at 1000°C for 1 h. The evolution of the pore size distribution in the case of 0Kh18N9T steel is shown as a function of irradiation and annealing conditions in Table 2 and Figs. 3 and 4. The microstructure of the 0Kh18N9T steel coupon after irradiation and annealing for 1 h at 800°C is shown in Fig. 5a, b. Annealing for 1 h at 1000°C brings about a complete disappearance of porosity.

The behavior of the radiation-induced pores when coupons of these steels are annealed indicates that the processes by which the pores form and subsequently evolve are of some complexity. The dynamics of the development of voids and their redistribution on annealing depends on the structural state, and also on the temperature and duration of the annealing.

DISCUSSION

The growth of a vacancy pore takes place as a result of a diffusional flow of vacancies greater in magnitude than the flow of interstitial atoms. The concentrations of these imperfections some distance from the pore are C_V and C_I. These values are reached as a result of competition between the processes of point defect formation by the neutron flux and the processes of their disappearance through mutual recombination, and also through the capture of sinks either existing or created as a result of the irradiation (dislocations, dislocation loops, grain boundaries, particles of phase separations, etc.). If we assume that each defect contributes (in the case of a vacancy) or takes away (in the case of an interstitial atom) the same

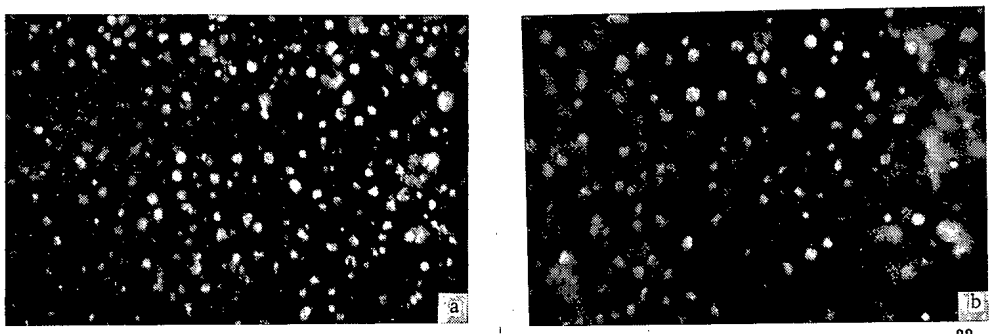

Fig. 5. Pores in 0Kh18N9T steel after irradiation in integrated flux $3.6 \cdot 10^{22}$ neutrons/cm^2, T_{irr} = 460°, ×68,000 (a), and after annealing for 1 h at 800°C, ×68,000 (b).

volume Ω in the void, then the rate of change of the radius r of a spherical pore will be, under steady-state conditions,

$$\frac{dr}{dt} = \frac{1}{r}[D_V C_V - D_I C_I] - \frac{D_S}{r} e^{\frac{2\gamma\Omega}{rkT}}, \quad (1)$$

where D_V and D_I are the diffusion coefficients of vacancies and interstitial atoms; D_S is the self-diffusion coefficient; γ is the surface energy density; k is the Boltzmann constant; T is the absolute temperature. In the absence of irradiation $C_V = C_{V0}$, $C_I = 0$, and Eq. (1) throws light on the annealing of a radiation-induced pore. The growth of a pore at irradiation temperatures at which the last term in Eq. (1) can be safely neglected is possible when $D_V C_V > D_I C_I$. This last constraint is satisfied only in the case where there exist in the metal sinks capable of trapping atoms in interstices more often than in vacancies. At the present time, the assumption is that these sinks are dislocations [2, 3]. According to that assumption, vacancy dislocation loops must not grow during the time of irradiation; this is contradicted by observations [5].

The formation of vacancy voids in the metals studied to date (including those studied in the present work) occurs within a comparative narrow range of irradiation temperatures. The pores appear at temperatures ~0.3 T_m (T_m being the melting point in °K) and do not form at temperatures higher than 0.5 T_m. Within that temperature range, swelling attains a maximum in the neighborhood of 0.4 T_m. In the theoretical explanation of the temperature dependence of swelling, it is commonly assumed [2, 3] that the absence of pores in the range $T_{irr} < 0.3\ T_m$ is due to recombination of point defects. Evidently it should also be noted that the temperature at which the formation of radiation-induced porosity begins coincides with the temperature of the V stage of annealing-out of radiation-induced imperfections, as detected in the electrical resistivity, microhardness, and lattice constant in annealing [4]. The upper limit of radiation-induced porosity coincides with the VI stage of annealing, when the annealing rate is characterized by the activation energy of self-diffusion. We can therefore infer that the growth of voids at temperatures starting with 0.3 T_m takes place as a result of competition between capture of vacancies by pores and by other sinks (e.g., by vacancy dislocation loops), growth of which does not eventuate in any substantial change in the geometrical dimensions of the specimen. As the temperature is increased, these clusters of imperfections become increasingly unstable, and the vacancies induced by irradiation are capable of condensing only into three-dimensional voids.

The variation in void distribution in annealing which we investigated shows that gaseous atoms play a role in void formation. That is indicated by the fact that fine voids at first disappear from the field of vision in the electron microscope upon annealing, but their number picks up again later on, apparently because of diffusion of gas into fine gas pores, which persist to the end without collapsing because of the gas present in them.

We can infer from the void size distribution in Figs. 3 and 4 that:

a) annealing for 1 h brings about a sharp decrease in the number of voids of sizes up to 750 Å; this is in agreement with Eq. (1), according to which annealing-out of voids of large size will take place more slowly than annealing-out of fine voids;

b) annealing for 10 h at 800°C led to an increase in the density of voids of sizes up to 550 Å compared to annealing for 1 h, whilst the concentration of coarse voids decreased;

c) annealing for 100 h at 800°C brought about a still further increase in the number of fine voids and a concomitant decrease in the number of coarse voids.

We should draw attention to the disappearance of coarse voids in annealing, as evidence of their vacancy derivation. The appearance of fine voids in long-term annealing supports the assumption that gas present in the irradiated steels stimulates the formation of fine gas voids.

The authors are deeply indebted to N. P. Agapova and V. V. Orlov, for their kind and persistent attention and interest, and for helpful discussion of the results, and also to V. A. Kuznetsov for much-appreciated support and invaluable counsel.

LITERATURE CITED

1. K. Bagley, J. Bramman, and C. Cawthorne, Proc. BNES European Conference, Paper 1, March (1971).
2. S. Harkness, J. Tesk, and Li Che-Yu, Nucl. Appl. Techn., 9, July (1970).
3. R. Bullongh and R. Perrin, Proc. BNES European Conference, Paper 8, March (1971).
4. L. Keys and J. Moteff, J. Appl. Phys., 40, 3866 (1969).
5. K. Urban, Proc. BNES European Conference, Paper 24, March (1971).

THERMOKINETIC ANALYSIS OF HELIUM EVOLUTION FROM IRRADIATED MATERIALS

V. S. Karasev, V. S. Kislik,
G. F. Shved, and R. V. Grebennikov

UDC 621.039.548.343

The effect of helium and other inert gases produced by nuclear reactions on the properties of reactor materials has attracted much interest [1-4].

Owing to the low solubility of helium, even after small neutron doses a supersaturated solid solution is formed and the crystal lattice is markedly distorted. Therefore diffusion of helium in materials is accompanied by an effective interaction of the helium atoms with other defects, principally vacancies and their accumulations.

Evolution of helium during annealing may therefore be controlled by various mechanisms: migration via interstices [5] and vacancies [6-8], diffusion of mobile helium–vacancy and helium–divacancy complexes [7, 8], movement of gas-filled pores [9-11], etc.

In investigating these mechanisms of diffusional evolution of helium, as is necessary in order to determine the effect of helium on the properties of reactor material during irradiation, the experimental analysis methods used must enable different evolution stages with similar activation energies to be clearly distinguished and must facilitate the determination of the energy and frequency parameters of diffusion.

The characteristic annealing temperature is determined most accurately by investigating the differential dependence of the change in some property [12]; we therefore used mass-spectrometric measurement of the helium flux, proportional to the rate of helium evolution from irradiated specimens during linear heating (a similar procedure is used in geochemistry [4]).

The helium flux was measured by means of an analyzer (Fig. 1), based on a PTI-7 leak detector; its design and measuring circuit were modified and supplemented so as to ensure heightened sensitivity, higher stability, an increase in its range, and automatic measurement. The specimens were heated at a constant rate in a low-inertia annealing chamber with a tantalum heater. To ensure that reproducible results were obtained, particular attention was devoted to maintaining a constant "geometry" of the experiment and to ensuring the accuracy of temperature measurements.

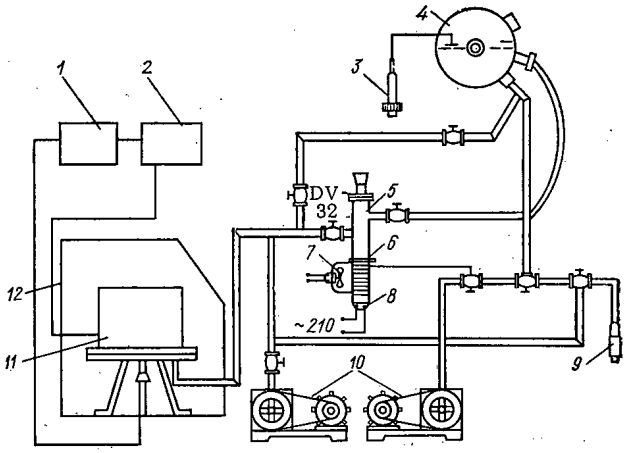

Fig. 1. Block diagram of the analyzer of the rate of helium evolution from irradiated material: 1) selecting and recording unit; 2) supply unit for furnace; 3) remote electrometric stage; 4) mass-spectrometer chamber; 5) freeze trap; 6) steam-jet pump; 7) fan; 8) heater; 9) LT-4M thermomanometer; 10) VN-461M pumps; 11) furnace; 12) chamber.

Translated from Atomnaya Énergiya, Vol. 34, No. 4, pp 251-254, April, 1973. Original article submitted May 15, 1972.

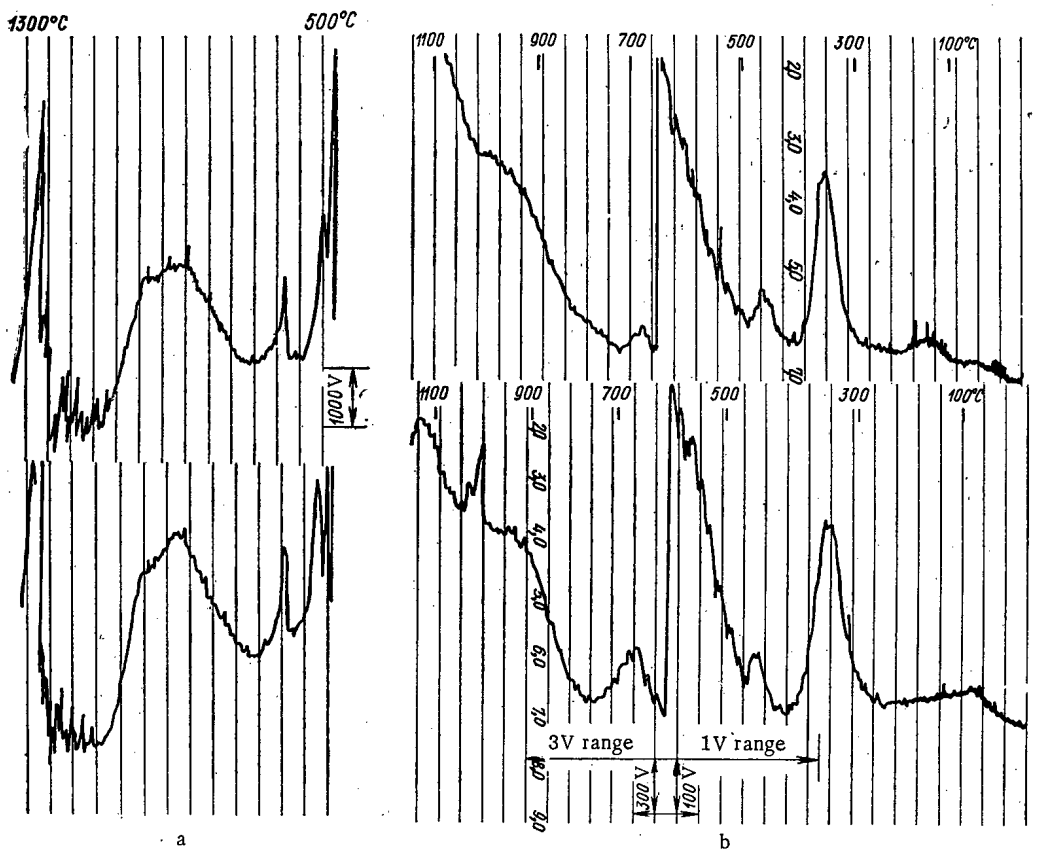

Fig. 2. Reproducibility of measurements of the rate of evolution of helium from specimens (heating rate 1/3 deg · sec^{-1}): a) Al + B_4C (15 wt.%), t_{irr} = 80°C; b) 0Kh16N15M3B austenitic steel, t_{irr} = 700°C.

At a constant rate of evacuation of the annealing chamber, corresponding to a pressure of $2 \cdot 10^{-4}$ mm in the latter, the analyzer sensitivity was 10^{-8} mV for one helium atom per liter of chamber volume. This sensitivity ensured better resolution of the peak due to evolution of ~0.001 of the total amount of helium, which was $\sim 10^{15}$ atoms. This amount of helium is formed in 1 g of austenitic steel when subjected to a dose rate of 10 MW for 100 h in a VVR-M reactor, owing to fast-neutron (n, α) reactions ($E \geq 3$ MeV), or when irradiated for 3 h with thermal neutrons (if the steel contains 10^{-3} wt.% B^{10}).

It will be seen from Fig. 2 that if we take account of the variation in weight of the specimens (up to 20%), the reproducibility of the results of the two experiments on annealing of irradiated specimens (steel 0Kh16N15M3B and dispersed boron carbide in aluminum) is very satisfactory. The reproducibility of the temperature of the maxima (peaks) of the rate of evolution of helium in all the experiments on annealing of equivalent specimens at the same heating rate was ±3% of the measured value.

Figure 3 shows the temperature dependence of the helium flux through the analyzer chamber during evolution of helium from a specimen (0.3 g) of 0Kh16N15M3B austenitic steel, irradiated by a neutron flux of $5 \cdot 10^{19}$ neutrons · cm^{-2} ($E \geq 3$ MeV) at 600°C in helium at a pressure of 0.7 atm. Curve 1 has eight well-resolved peaks (denoted by Roman numerals), enabling one to determine with sufficient accuracy the characteristic temperature of the corresponding stage of helium evolution. Figure 3 also shows the temperature dependence of the analyzer background (curve 2) obtained when the furnace is heated without a specimen in the annealing chamber.

The results of the experiments, given in Figs. 2 and 3, confirm the presence of several stages in helium evolution from irradiated materials. To classify these mechanisms we must establish the relation between the experimentally-determined characteristic temperature of the peaks, T_i (see Fig. 3) and the diffusion parameters of helium in the i-th stage.

The diffusion model of inert gases taking account of their interaction with traps [5] enabled us to derive a differential equation representing helium evolution from a specimen in the i-th stage:

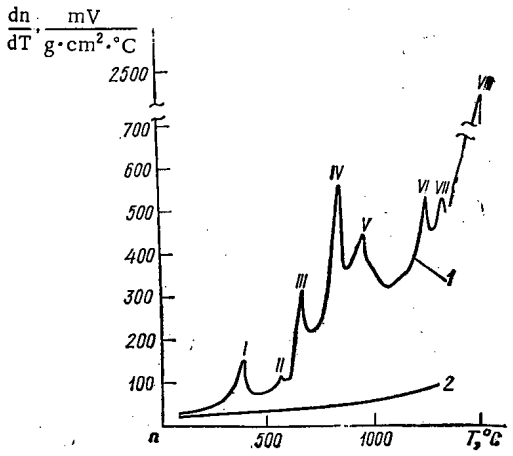

Fig. 3

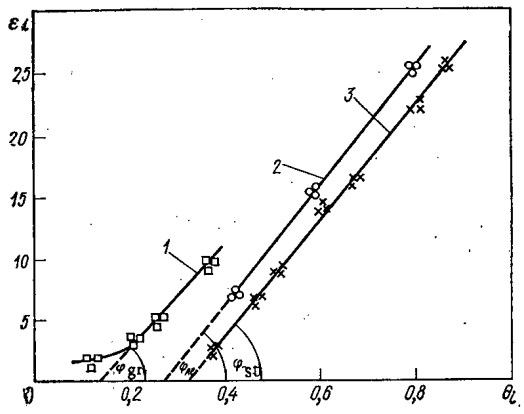

Fig. 4

Fig. 3. Differential curve of helium evolution from a specimen of 0Kh16N15M3B austenitic steel (heating rate 1/3 deg · sec^{-1}): 1) rate of evolution of helium; 2) analyzer background.

Fig. 4. Temperature dependence of the activation energy of helium evolution in different stages of annealing of specimens: 1) graphite with dispersion of B_4C ≈ 80°C, $\tan\varphi_{gr}$ = 41.2; 2) aluminum with dispersion of B_4C, t_{irr} ≈ 80°C, $\tan\varphi_{Al}$ = 48.7; 3) 0Kh16N15M3B austenitic steel, t_{irr} = 600°C, $\tan\varphi_{st}$ = 44.2.

$$\frac{d(1-n)}{dT} = \frac{K_0}{\alpha} n \frac{\exp(-E_i/kT)}{1+A_i \exp(B_i/kT)}. \quad (1)$$

Here (1−n) is the relative amount of helium evolved in a time τ (sec); n is the helium concentration in the specimen; T is the variable annealing temperature in °K; $\alpha = (T-T_0)/\tau$ is the linear heating rate; T_0 is the initial annealing temperature ($\tau = 0$), in °K; A_i is the product obtained by multiplying the concentration of the helium traps by the combined entropy factor; E_i is the activation energy of helium migration, in eV; B_i is the energy of the bond between helium and the trap, in eV; k is Boltzmann's constant, in eV/deg; K_0 is the kinetic coefficient, in sec^{-1}; $K_0 = z\beta D_0$, where z is the coordination number, β is the concentration of surface helium sinks, in cm^2; and D_0 is the preexponential factor of the diffusion coefficient, in cm^2/sec. The values of E_i and B_i are determined by the helium migration mechanisms in the i-th stage and depend markedly on the size, shape, and other characteristics of the point defect accumulations, determined by the irradiation conditions of the specimens (temperature, time, intensity, etc.) and by the properties of the material (for example, the packing defect energy).

From the solution to Eq. (1) for the point $T = T_i$, where $d^2(1-n)/dT^2 = 0$, we obtained the equation:

$$\frac{E_i}{kT_i} = \ln \frac{K_0\tau_i}{1+(1+\omega_i)A_i \exp(B_i/kT_i)} - 2\ln\frac{E_i}{kT_i}, \quad (2)$$

where $\tau_i = E_i/k\alpha$; $\omega_i = B_i/E_i$.

When the value of $(1+\omega_i) \times A_i \exp(B_i/kT_i)$ differs markedly from unity, the dependence of the activation energy of helium evolution on T_i is practically linear:

$$\frac{E_i}{kT_i} \approx \ln(K_0\tau_i) - 2\ln\frac{E_i}{kT_i} \approx \ln(K_0\tau_i) \quad (3)^*$$

when

$$1 \gg (1+\omega_i)A_i \exp(B_i/kT_i);$$
$$\frac{E_i+B_i}{kT_i} = \ln\frac{K_0\tau_i}{(1+\omega_i)A_i} - 2\ln\frac{E_i}{kT_i} \simeq \ln\frac{K_0\tau_i}{(1+\omega_i)A_i} \quad (4)$$

* Equation (3) coincides with the solution of the kinetic equation for annealing of defects without allowing for the effect of the traps [13-15].

when

$$1 \ll (1+\omega_i)\, A_i \exp(B_i/kT_i);$$

$$\frac{E_i+B_i-H_i}{kT_i} = \ln \frac{K_0\tau_i}{(1+\omega_i')\,A_{0i}} - 2\ln\frac{E_i}{kT_i} \simeq \ln \frac{K_0\tau_i}{(1+\omega_i')\,A_{0i}} \tag{5}$$

when

$$1 \ll (1+\omega_i)\, A_i \exp(B_i/kT_i),$$

$$A_i = A_{0i}\exp(-H_i/kT_i), \quad \omega_i' \frac{B_i-H_i}{E_i}.$$

Equation (5) corresponds to the case of thermally activated formation of traps with activation energy H_i [12]. From Eqs. (3)-(5) we can readily find an equation for determining the activation energy of helium evolution in the i-th stage, U_i, from the experimental values of T_{i1} and T_{i2}, obtained in experiments with different heating rates α_1 and α_2:

$$U_i = \left.\begin{cases} E_i & \text{for the conditions of the solution to} \\ E_i+B_i & \text{for the conditions of the solution to} \\ E_i+B_i-H_i & \text{for the conditions of the solution to} \end{cases}\right\} = k\frac{T_{i1}\times T_{i2}}{T_{i2}-T_{i1}} \ln\left[\frac{\alpha_2}{\alpha_1}\left(\frac{T_{i1}}{T_{i2}}\right)^2\right]. \tag{6}$$

The values of U_i are determined by the helium evolution mechanism in the i-th stage and may vary widely: from $U_i < 0.1$ eV (migration via interstices) to $U_i \geq 4$ eV (migration of pores with helium).

Figure 4 plots in dimensionless coordinates ($\varepsilon_i = U_i/kT_m$, $\theta_i = T_i/T_m$) the temperature dependences of the activation energies, determined from experiments with different heating rates ($\alpha_1 = 1/3$ deg · sec^{-1} and $\alpha_2 = 1/6$ deg · sec^{-1}) in different stages of helium evolution from irradiated specimens of austenitic steel, aluminum with dispersion of B_4C (15 wt.%) (see curve 2), graphite with dispersion of B_4C (18 wt.%), sintered at 1200°C [16]; it will be seen that the dependences are satisfactorily approximated by a straight line with slope φ, corresponding to the following values of $K_0\tau/(1+\omega)A_0 = e^{\tan\varphi}$; for graphite ~$10^{18}$; for steel ~$10^{19}$; and for aluminum ~$10^{21}$.

Note that when the data of Nichoul [17] for the III-V stages of annealing of pure metals with bcc (Mo and W), fcc (Al, Ag, Au, Cu, Ni, and Pt), and hcp (Zn, Mg, and Re) lattices were processed, the slope of the straight line ($K_0\tau$) was approximately 10^{17}.

It may be inferred from the data that thermokinetic analysis of helium evolution from irradiated specimens is a highly sensitive method of determining the diffusion characteristics of helium, enabling one to obtain information on the interaction of helium with radiation defects during annealing.

LITERATURE CITED

1. D. Harries et al., Radiation Damage in Reactor Materials, Vol. 2, IAEA-SM-120/G-5, Vienna (1969), p. 357.
2. R. Barnes, Nature, 206, No. 4991, 1307 (1965).
3. A. Rowcliffe, J. Nucl. Materials, 18, No. 1, 60 (1966).
4. L. K. Levskii, Geokhimiya, 6, 544 (1963).
5. M. Norgett and A. Lidiard, Radiation Damage in Reactor Materials, Vol. 1, IAEA-SM-120/A-4, Vienna (1969), p. 61.
6. R. Barnes et al., Phys. Mas., 3, No. 25, 97 (1958).
7. B. Russel and J. Hastings, J. Nucl. Materials, 17, 30 (1965).
8. P. Vela and B. Russel, ibid., 19, 312 (1966).
9. E. Ruedl and R. Kelly, ibid., 16, 39 (1965).
10. R. Kelly and E. Ruedl, Phys. Stat. Sol., 13, 55 (1966).
11. M. Gulder, J. Nucl. Materials, 23, 30 (1967).
12. A. Damask and J. Deans, Point Defects in Metals [Russian translation], Mir, Moscow (1966).
13. J. Deans and J. Vinyard, Radiation Defects in Solids [Russian translation], IL, Moscow (1960).
14. S. T. Konobeevskii, Effect of Irradiation on Materials [in Russian], Izd-vo AN SSSR, Moscow (1967).
15. B. Kelly, Radiation Damage in Solid Bodies [Russian translation], Izd-vo AN SSSR, Moscow (1970).
16. I. Ya. Emel'yanov et al., At. Energ., 31, 3, 213 (1971).
17. J. Nichoul, Radiation Damage in Reactor Materials, Vol. 1, IAEA-SM-120/A-1, Vienna (1969), p. 3.

NEUTRON EXPOSURE DURING STUDIES OF RADIATION DAMAGE TO MATERIALS IN NUCLEAR REACTORS

E. A. Kramer-Ageev, S. S. Ogorodnik, V. D. Popov, and Yu. L. Tsoglin

UDC 621.039.531

The problem of determining neutron exposure reduces to the description of the irradiation conditions, using such parameters which take account of the influence of both the flux and the form of the neutron spectrum on the formation of radiation damage in materials.

The use of the procedures proposed earlier for finding neutron exposure is limited either by the laborious work to determine the form of the neutron spectrum at the irradiation site [1-4] or by the use [5, 6] of the strongly disturbing Hurst wide-range detector. The present paper is devoted to overcoming these limitations.

According to contemporary conceptions, radiation damage is determined first of all by the number of Frenkel pairs generated. Their rate of generation n_d can be described by the following equation:

$$n_d = \frac{dN_d}{dt} = \int_{E_d/\alpha}^{\infty} dE_n \int_{E_{nuc}}^{E_{nuc}^{max}} \varphi(E_n) \frac{d\sigma(E_n, E_{nuc})}{dE_{nuc}} \times n_{nuc} \nu(E_{nuc})\, dE_{nuc}, \quad (1)$$

where N_d is the number of Frenkel defects; t is the time; $\varphi(E_n)$ is the differential neutron flux; $d\sigma(E_n, E_{nuc})/dE_{nuc}$ is the differential scattering cross section for neutrons with energy E_n; $\nu(E_{nuc})$ is the average

TABLE 1. Values of the Ratio n_d/w_H

Material	Model	Reactor										
		BR-1	SV	MR	VVR	BR-5, B-3	UGR	IRT, VEK-10	VVR-M	ITR, VEK-10		IRT, GEK-2
		(0,45)	(0,87)	(0,940)	(0,96)	(1,15)	(1,21)	(1,23)	(1,30)	(1,61)	(2,11)	(2,40)
Al	Rossin [2]	0,814	0,907	0,941	0,887	0,903	0,952	0,984	0,951	1,001	1,000	1,027
	[9]	0,970	0,986	0,992	0,996	0,996	0,995	1,005	0,989	1,009	1,000	1,018
	Kinchin and Pease [7]	1,705	1,362	1,225	1,506	1,427	1,184	1,092	1,168	1,043	1,000	0,941
Si	Rossin [3]	0,833	0,910	0,934	0,906	0,926	0,954	0,961	0,951	0,981	1,000	1,008
	[9]	0,973	0,982	0,978	1,014	1,020	0,990	0,975	0,986	0,987	1,000	0,994
	Lindhardt [10]	0,936	0,966	0,975	0,982	0,996	0,984	0,970	0,990	0,977	1,000	0,986
	Kinchin and Pease [7]	1,580	1,286	1,163	1,482	1,429	1,147	1,033	1,135	1,008	1,000	0,931
W	[2, 7, 9]	0,744	0,872	0,923	0,828	0,848	0,936	0,993	0,934	1,014	1,000	1,051

Note. For convenience, the comparisons of the values of n_d/w_H are given in relative units. In brackets we give the average neutron energy $\overline{E_n}$ of typical spectra for the indicated reactors, expressed in MeV.

Translated from Atomnaya Énergiya, Vol. 34, No. 4, pp. 255-258, April, 1973. Original article submitted April 30, 1972; revision submitted November 23, 1972.

TABLE 2. Values of the Coefficients for Various Substances*

Substance	$w_i/w_H = k_{iH}$		$n_d/w_H = c_0$		$n_d/w_H = c_1 + c_2 \frac{w_{fU^8}}{w_H}$			$n_d/w_H = c_1' + c_2' \frac{A_S}{w_H}$		
	$k_{iH} \times 10^4$	δ, %†	c_0	δ, %	c_1	c_2	δ, %	c_1'	c_2'	δ, %
Be	269,0	6,4	2,83	4,30	2,28	1200	1,41	2,52	402	1,20
C	151,0	8,8	1,63	6,10	1,18	980	1,70	1,37	328	1,45
Mg	41,6	3,5	0,52	4,30	0,61	—205	2,00	0,561	—58,5	2,73
Al	34,4	7,3	0,430	1,40	0,407	51,1	0,70	0,416	18,3	0,53
Si	30,6	5,6	1,09	1,70	1,600	108	1,40	1,06	29,1	1,5
Ti	13,1	11,3	0,17	5,40	0,130	85,4	2,4	0,147	28,2	2,5
V	13,8	10,6	0,211	4,48	0,170	89,6	1,8	0,187	30,0	1,7
Cr	8,47	5,7	0,135	2,07	0,135	1,66	2,1	0,137	—1,79	2,0
Fe	10,1	13,0	0,160	7,6	0,103	126	0,90	0,129	41	1,6
Ni	9,0	7,9	0,148	2,3	0,13	34,7	0,60	0,139	11,6	0,50
Cu	8,68	10,6	0,165	5,4	0,124	89,9	1,2	0,142	29,6	1,20
Ge	—	—	0,176	6,21	2,26	—1120	1,0	2,04	—368	1,0
Zr	5,56	6,9	0,106	4,9	0,082	51,6	1,4	0,093	16,8	1,6
Nb	5,39	6,7	0,103	4,8	0,080	48,6	1,4	0,090	15,8	1,6
Mo	5,16	8,2	0,066	6,2	0,047	41,8	1,2	0,056	13,6	1,5
Ta	1,8	11,3	0,036	11,0	0,017	41,4	1,7	0,025	13,7	2,0
W	1,7	11,0	0,024	11,0	0,012	27,5	1,8	0,017	9,11	1,6
Pb	1,34	11,8	0,027	12,0	0,12	32,5	1,7	0,018	10,8	1,6
Bi	1,32	12,4	0,026	12,0	0,011	33,3	2,0	0,018	11,1	1,4

*Coefficients are given which link the power of the absorbed neutron dose in the materials w_i (MeV/g·sec) with the dose power in hydrogen w_H (MeV/g·sec) and the rate of generation of Frenkel defects n_d (dislocations/g·sec) with w_H and with the spectral parameters $P_{fH} = w_{fU^8}/w_H$ and $P_{SH} = A_S/W_H$; W_{fU^8} (fissions/g·sec) is the fission rate for U^{238}; A_S (disintergrations/g·sec) is the activity of sulfur in saturation.

†The rms errors are according to the spectra shown in Table 1.

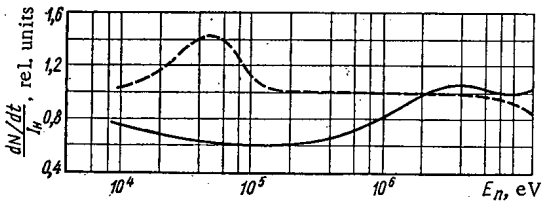

Fig. 1. Ratio of the generation rate of Frenkel pairs [10] to the dose power in hydrogen for silicon (– – –) and germanium (——).

number of defects produced by a recoil nucleus with energy E_{nuc}; E_d is the threshold energy for defect formation; $\alpha = E_{nuc}/E_n$ is the energy-transfer coefficient from a neutron to a recoil nucleus; n_{nuc} is the number of nuclei per gram of material.

The function $\nu(E_{nuc})$ can be expanded into a power series:

$$\nu(E_{nuc}) = a_1 E_{nuc} + a_2 E_{nuc}^2 + \dots \quad (2)$$

Taking into account information on the form of the function $\nu(E_{nuc})$ [3, 7-11] we can presume that the coefficient a_1 will be the largest.

Substituting Eq. (2) into Eq. (1), we obtain

$$n_d = n_{nuc} a_1 \left[\int_{E_d/\alpha}^{\infty} \varphi(E_n)\,\sigma(E_n)\,\alpha E_n\,dE_n \int_{E_d/\alpha}^{\infty} \varphi(E_n)\,dE_n \int_{E_d}^{E_{nuc}^{max}} \frac{d\sigma(E_n, E_{nuc})}{dE_{nuc}} \frac{a_2}{a_1} E_{nuc}^2\,dE_{nuc} \dots \right] \approx a_1 w_i, \quad (3)$$

in which to the first approximation we can disregard all terms besides the first, which differs from the expression for calculating the power of absorbed neutron energy in the given material w_i only by constant factor a_1 and the lower limit of integration (E_d/α rather than zero). According to calculations made for actual neutron spectra in nuclear reactors, the error due to changing the integration limits is less than 1%.

It is not possible to measure w_i directly in all materials, except for hydrogen, against the background of the accompanying reactor γ-radiation. However, as we saw from calculations we made for 22 materials ($4 \le z \le 83$), and 11 different neutron spectra (their average energies are given in Table 1), w_i can be determined from the measured dose power produced by recoil protons in hydrogenous materials w_H, using the coefficient $k_{iH} = w_i/w_H$, which is constant for all spectra (the allowable errors are shown in Table 2).*

*In the calculations, we took into account the contribution from inelastic scattering and the anisotropy of elastic scattering.

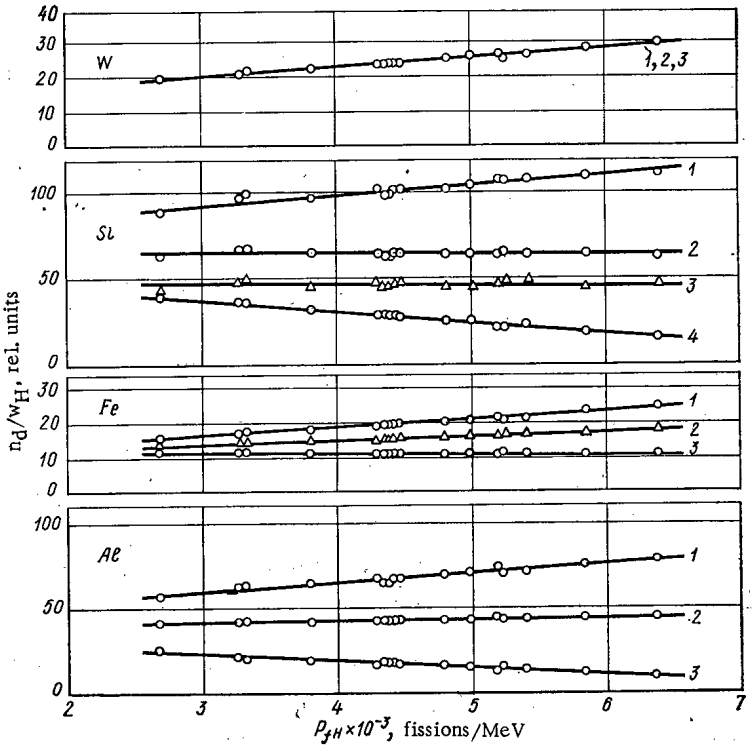

Fig. 2. Dependence of the ratio n_d/w_H in various materials on the spectral parameter $p_{fH} = w_{fU^8}/w_H$: 1) the function $\nu(E)$ calculated without taking ionization losses into account, according to [2]; 2) the same, taking ionization losses into account, according to [9]; 3) the same, according to [7]; 4) the same, according to [8].

Therefore, as the quantity to define neutron exposure, we propose choosing the power of the absorbed neutron dose in hydrogen.

To confirm this choice, we calculated the generation rates for Frenkel defects in 19 materials and the power of the absorbed dose in hydrogen for 11 typical neutron spectra. The results of the calculations reduced to a unit neutron flux are shown in Table 1 for aluminum, silicon, and wolfram. The calculations showed that for the investigated neutron spectra the ratio n_d/w_H is constant with an rms deviation $\leq 13\%$ if $\nu(E_{nuc})$ is calculated according to [2, 8, 9] and is ~30% when one uses the results of [7]. The dependence n_d/w_H for monoenergetic neutrons is shown in Fig. 1.

Further reduction of the monitoring error can be attained through the use of two detectors having different sensitivities depending on the neutron energy. The effect of introducing two or more detectors is analogous to the presentation of the observed radiation effect $\Delta R(T, \tau)$ by an expansion in which the base functions are the detector sensitivities:

$$\Delta R(T, \tau) = F(T, \tau)\, n_{nuc} \int_{E_{d/\alpha}}^{\infty} \varphi(E_n)\, \sigma(E_n)\, \Delta\rho(E_n)\, dE_n = F(T, \tau)\, n_{nuc} \int_{E_{d/\alpha}}^{\infty} \varphi(E_n) \left[\sum_{j=1}^{l} \sigma_j(E_n)\, \psi_j(E_n) \right] dE_n. \quad (4)$$

Here $\Delta\rho(E_n)$ is the average contribution to the observed radiation effect from one neutron with energy E_n; $F(T, \tau)$ is a function taking into account the cessation of the radiation effect; T is the irradiation temperature; $\sigma_j(E_n)$ is the interaction cross section of the j-th detector with neutrons; $\psi_j(E_n)$ is a weight function; l is the number of detectors. Let $l = 2$, $\sigma_1(E_n)$ be the scattering cross section of neutrons by hydrogen, $\sigma_2(E_n)$ be the $U^{238}(n, f)$ reaction cross section, and let us take the weight functions in the form $\psi_1(E_n) = c_1 E_n$ and $\psi_2(E_n) = c_2$. Then, Eq. (4) can be written in the form

$$\frac{\Delta R(T, \tau)}{w_H} = (c_1 + c_2 p_{fH})\, F(T, \tau), \quad (5)$$

where $p_{fH} = w_{fU^8}/w_H$ is the spectral parameter; w_{fU^8} is the fission-reaction rate in U^{238}.

Figure 2 shows the ratios of the generation rate for Frenkel pairs, calculated according to the Kinchin–Pease, Rossin, and Lindhardt models, to the neutron dose power in hydrogen as a function of the spectral parameter. The linear nature of this dependence is preserved for all the models and materials we studied.

Table 2 shows the results of the proposed monitoring by two detectors. It is clear that using two detectors allows one to monitor the formation of Frenkel defects with an rms error less than 3%.

As the calculations showed, a traditional threshold sulfur detector can be used as the second detector.

The indicated methods for determining neutron exposure take into account the flux density as well as the form of the neutron spectrum; here it is not necessary to know the spectrum at the irradiation site. The instruments used as hydrogen and uranium detectors can be calorimeters or ionization chambers. This also assures the possibility of comparing the results of experiments conducted in different nuclear reactors with sufficient accuracy and without laborious spectral measurements.

We should note that the coefficients given in Tables 1 and 2 can vary depending on the model of material damage. The basic consequence of Eq. (5) still holds. This consists of the fact that the radiation effect per unit dose power must be investigated not only as a function of temperature and time, but also as a function of the spectral parameter. Moreover, the experimentally determined values of the coefficients c_1 and c_2 may allow us to choose among various mechanisms of radiation damage in materials.

LITERATURE CITED

1. N. N. Ponomarev-Stepnoi, At. Energ., 11, No. 2, 184 (1961).
2. A. Rossin, Nucl. Sci. Eng., 9, 137 (1961).
3. A. Rossin, IEEE Trans. Nucl. Sci., 5, No. 1, 5 (1964).
4. R. Dahl and H. Yoshikawa, Nucl. Sci. Eng., 21, 312 (1965).
5. N. A. Ukhin and A. V. Khrustalev, Preprint IAE-1880 (1969).
6. A. Kantz, J. Appl. Phys., 34, No. 7, 1944 (1963).
7. J. Kinchin and R. Pease, Usp. Fiz. Nauk, 40, No. 4, 590 (1956).
8. J. Lindhardt and M. Scharff, Mat.-Fys. Medd. Dan. Yid. Selsk., 27, No. 15 (1953); 28, No. 8 (1954).
9. S. S. Ogorodnik et al., in: Metrology of Neutron Radiation [in Russian], Atomizdat, Moscow (1972).
10. E. A. Kramer-Ageev et al., in: Problems of Dosimetry and Radiation Shielding [in Russian], No. 9, Atomizdat, Moscow (1969), p. 39.
11. C. Erginsoy et al., Phys. Rev., 139, No. 1A (1965).

HOW TO CALCULATE AND ESTIMATE INTEGRAL CHARACTERISTICS OF IDEAL TWO-COMPONENT STAGES WITH ARBITRARY ENRICHMENTS PER STEP

N. A. Kolokol'tsov, N. I. Laguntsov, and G. A. Sulaberidze

UDC 621.039.3

The possibility, in principle, of constructing ideal cascades, symmetrical as well as asymmetrical, with arbitrary enrichments per step $\delta^+ = c^+ - c - f(c, \Theta)$, has been demonstrated [1, 2]. The feasibility of introducing a separation potential which would in turn make it possible to obtain formulas useful in estimating the effectiveness of stages is considered in this article, for the specific form of the function $f(c, \Theta)$.

We begin by considering the separation conditions on a separatory stage in the general case, where the difference $\alpha_0 - 1$ (where α_0 is the static separation factor), is not small. We shall assume that a stream L with a concentration of light product c enters the separatory step and, upon passing along a certain channel, becomes separated into an enriched stream ΘL of concentration c^+ and a depleted stream $(1-\Theta)L$ of concentration c^- (see Fig. 1).

Let the stream be G, and its concentration σ, at some point x along the channel. Within the interval dx, the flowrate throughout the boundary of the channel will be dG with the increased concentration $\sigma + \Delta\sigma$, and the concentration increment $\Delta\sigma$ is here expressed in terms of the separation factor α_0 in the familiar formula

$$\Delta\sigma = \frac{(\alpha_0 - 1)\,\sigma\,(1-\sigma)}{(\alpha_0 - 1)\,\sigma + 1}. \tag{1}$$

Denoting a slight change in concentration along dx by $d\sigma$, and neglecting second-order infinitesimals, we obtain from the balance of streams over the elementary interval singled out here:

$$\Delta\sigma\, dG = G\, d\sigma. \tag{2}$$

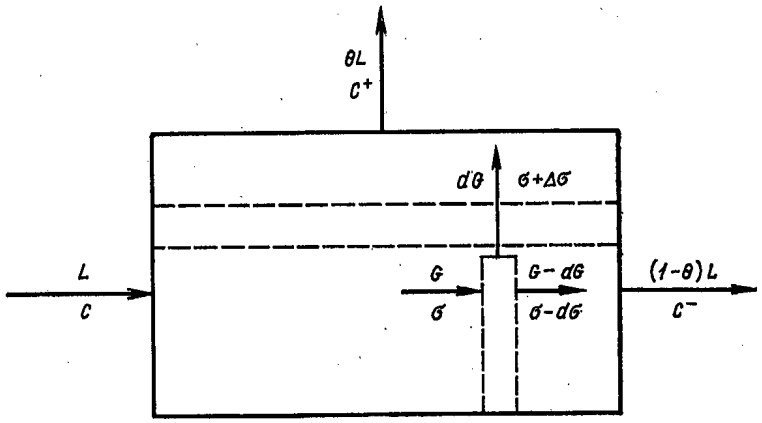

Fig. 1. Scheme of streams in separatory step.

Translated from Atomnaya Énergiya, Vol. 34, No. 4, pp. 259-263, April, 1973. Original article submitted October 2, 1972.

TABLE 1. Values of the Ratio $\bar{\delta}^- = \delta^-/[(\alpha_0-1)c(1-c)\ln 1/(1-\Theta)]$

Θ	c = 0,1				c = 0,3				c = 0,5				c = 0,7				c = 0,9			
	$\bar{\delta}^-$	Δ, %			$\bar{\delta}^-$	Δ, %			$\bar{\delta}^-$	Δ, %			$\bar{\delta}^-$	Δ, %			$\bar{\delta}^-$	Δ, %		
		(6)	(7)	(8)		(6)	(7)	(8)		(6)	(7)	(8)		(6)	(7)	(8)		(6)	(7)	(8)
0,1	0,93	0	0,7	1,9	0,86	0,1	0,3	0,7	0,80	0,3	0,2	−0,2	0,75	0,5	0,05	−0,9	0,70	0,8	0	−1,5
0,3	0,89	0,05	2,2	6,7	0,85	0,4	1,2	2,6	0,80	1,0	0,5	−0,6	0,76	1,7	0,2	−3,0	0,73	2,6	0	−5,0
0,5	0,84	0,1	4,4	13,4	0,82	0,7	2,4	5,5	0,81	1,8	1,1	−0,7	0,78	3,3	0,4	−5,6	0,76	5,2	0,05	−9,5
0,7	0,76	0,1	7,7	24,6	0,79	0,9	4,6	10,5	0,80	2,6	2,2	−0,5	0,81	5,3	0,8	−9,1	0,82	9,2	0,1	−15,9
0,9	0,63	0,1	14,9	52,0	0,7	1,0	10,0	24,5	0,80	3,4	5,6	2,6	0,87	8,3	2,2	−14,6	0,96	17,6	0,3	−28,0

TABLE 2. Values of γ and β for Different c

c	γ	β
$c \ll 1$ (6)	$1-(1-\Theta)^{\alpha_0-1}$	$\alpha_0(1-\Theta)^{\alpha_0-1}-1$
$c(1-C)=$ = const	$(\alpha_0-1)\ln\frac{1}{1-\Theta}$	α_0-1
$1-c \ll 1$	$\left[1-(1-\Theta)^{\frac{\alpha_0-1}{\alpha_0}}\right]\alpha_0$	$\alpha_0(1-\Theta)^{\frac{\alpha_0-1}{\alpha_0}}-1$

Upon integrating Eq. (2) over the length of the entire channel,

$$\int_L^{(1-\Theta)L}\frac{dG}{G}=\int_c^{c^-}\frac{1+(\alpha_0-1)\sigma}{(\alpha_0-1)\sigma(1-\sigma)}\,d\sigma, \tag{3}$$

we get

$$(1-\Theta)^{\alpha_0-1}\left(1+\frac{\delta^-}{1-c}\right)^{\alpha_0}=\left(1-\frac{\delta^-}{c}\right), \tag{4}$$

where

$$c-c^-=\delta^-=\frac{\Theta}{1-\Theta}\delta^+. \tag{5}$$

Equation (4) is an implicit expression for the enrichment function f(c, Θ) for arbitrary enrichments at the step. This expression, in slightly altered form, was derived in the analysis of a distillation process [3, 4]. In explicit form, the formulas for f(c, Θ) can be derived in the limiting cases such that $c \ll 1$ or $1-c \ll 1$, and under the assumption $c(1-c) \approx$ const.

It is clear from physical considerations that $\delta^- \leq c$ consistently, so that the expression $[1+\delta^-/(1-c)]^{\alpha_0}$ can be expanded into a series when $c \ll 1$ and, by neglecting second-order infinitesimals for the entire range of separation factors of the streams $0 < \Theta < 1$, Eq. (4) will be representable in the form

$$\delta^-=\frac{[1-(1-\Theta)^{\alpha_0-1}]\,c(1-c)}{[\alpha_0(1-\Theta)^{\alpha_0-1}-1]\,c+1}. \tag{6}$$

At large concentrations c, when $1-c \ll 1$, we can expand the expression $(1-\delta^-/c)^{1/\alpha_0}$ into a series. Clearly, then, $\delta^+ < 1-c$, so that $\delta^-/c = \Theta/(1-\Theta)\cdot\delta^+/c$ is a small quantity for all values of Θ except those very close to unity. In that case, Eq. (4) admits of representation in the form

$$\delta^-=\frac{[1-(1-\Theta)^{\frac{\alpha_0-1}{\alpha_0}}]\,\alpha_0 c(1-c)}{[\alpha_0(1-\Theta)^{\frac{\alpha_0-1}{\alpha_0}}-1]\,c+1}. \tag{7}$$

According to the above, Eq. (7) is valid, when $1-c \ll 1$, for all Θ values except for those very close to unity, which are in general of no practical interest other than in certain isolated instances.

While $c(1-c) \approx$ const can be approximated over the range of concentrations studied, from Eq. (3) we obtain, in place of Eq. (4),

$$\delta^-=\frac{(\alpha_0-1)\,c(1-c)\ln\frac{1}{1-\Theta}}{1+(\alpha_0-1)\left(c-\frac{\delta^-}{2}\right)}\approx\frac{(\alpha_0-1)\,c(1-c)\ln\frac{1}{1-\Theta}}{1+(\alpha_0-1)\,c}. \tag{8}$$

In the particular case of separation of isotopes, when $\alpha_0-1=\varepsilon_0 \ll 1$, the familiar result

$$\delta^-=\varepsilon_0 c(1-c)\ln\frac{1}{1-\Theta} \tag{9}$$

is obtained directly from Eq. (4) for any concentrations. Here it is worth stressing that the series expansion of Eq. (9), like the expansion of Eq. (7), is suitable only when Θ is not very close to unity. When Θ = 1, we get the limiting value $\delta^- = c$ from Eq. (4).

Table 1 lists the true values of the ratio $\delta^-[(\alpha_0-1)c(1-c)\ln 1/(1-\Theta)]$ calculated on the basis of Eq. (4) at $\alpha_0 = 1.5$, and deviations from those values (in percentages) corresponding to Eqs. (6)-(8). Similar calculations performed for other α_0 values ($\alpha_0 = 2$, 2.5) showed that the accuracy of the calculations depends weakly on α_0. It is clear from Table 1 that Eq. (8) yields deviations, even in its typical c = 0.5 range, comparable to the deviations obtained with Eqs. (6) and (7). It is further evident that the accuracy of all of the approximate formulas suffers with increasing Θ. Equations (6) and (7) provide adequate accuracy over a broad range of variation of the parameters. When $\Theta < 0.8$, the error in calculations of δ^- based on Eq. (6) for small c (down to 0.5) and on Eq. (7) for large c (starting with 0.5) is not greater than 2-3%. The mean deviations are far smaller.

The difference between the true δ^- values and the values calculated on the basis of Eq. (9) for $\varepsilon_0 = \alpha_0 - 1$ can be quite large, and reach the level 30% even at $\alpha_0 = 1.5$.

The formulas derived show that concentration increments depend sensitively on the separation factor Θ of the streams for both small and large enrichments per stage.

All three formulas (6)-(8) can be written in the general form

$$\frac{1-\Theta}{\Theta}\delta^- = \delta^+ = \frac{1-\Theta}{\Theta}\cdot\frac{\gamma c(1-c)}{\beta c+1} \tag{10}$$

(values of γ and β are entered in Table 2).

A theory of ideal symmetrical stages with large enrichments per step has been constructed [3] under the assumption that the step separation factor $\bar{\alpha} = [c^+/(1-c^+)]/[c^-/(1-c^-)]$ remains constant and independent of both c and Θ, and that Eq. (1), where α_0 is replaced by $\bar{\alpha}$, can be applied to the entire step as a whole. From the condition for ideal behavior, we see that the coefficient $\bar{\beta} = [c/(1-c)]/[c^-/(1-c^-)]$ must be equal to $\bar{\alpha}$, and then we derive the formula

$$\Theta = \frac{c(\bar{\alpha}-1)+1}{\bar{\alpha}+1}, \tag{11}$$

which must govern the separation of streams in such a stream. Here we encounter the contradiction that values of $\bar{\alpha}$, and later of β, must remain constant given a certain set of values $\Theta \neq 1/2$, and outside of the context of a real separation process. The author of [3] drew attention to this contradiction, and noted that his equation "will not be universally applicable" at reasonably small values of $\bar{\alpha}-1$. These contradictions become aggravated in [5], as well as in subsequent contributions [6, 7] generalizing the Cohen theory [3] in application to asymmetrical stages. Accordingly, only a limited application can have expressions for separation potentials at high enrichments obtained in [4-6]. From those expressions, in particular, it is not possible in principle to determine the most suitable degree of asymmetry in high-enrichment stages.

Let us attempt to construct an approximate theory for the separation potential that would be free of those contradictions. We assume that the specific value of a mixture of concentration c is determined by some function V(c). Then the separatory work done by the stage is estimated on the basis of the formula

$$\delta U = \Theta LV(c+\delta^+) + (1-\Theta)\,LV(c-\delta^-) - LV(c). \tag{12}$$

If the value of α_0 remains within reasonable limits (note that, at $\alpha_0 > 2$ to 2.5, the number of steps is small and the concept of a stage loses its significance), then δ^- and δ^+ are small in absolute magnitude, and the expressions $V(c+\delta^+)$ and $V(c-\delta^-)$ can be expanded in series about c. Retaining second-order terms, we restate Eq. (12) in the form

$$\delta U = \frac{d^2V}{dc^2}L\left[\Theta\frac{\delta^{+2}}{2} + (1-\Theta)\frac{\delta^{-2}}{2}\right] = \frac{L}{2}\cdot\frac{\Theta}{1-\Theta}\delta^{+2}\frac{d^2V}{dc^2}. \tag{13}$$

Substituting δ^+ according to the general formula (10), we get

$$\delta U = \frac{d^2V}{dc^2}\cdot\frac{L}{2}\cdot\frac{1-\Theta}{\Theta}\left[\frac{\gamma c(1-c)}{\beta c+1}\right]^2. \tag{14}$$

The work of separation δU done by the step must be independent of the concentration. This requires that the condition

$$\frac{d^2V}{dc^2} = \left(\frac{\beta c+1}{c(1-c)}\right)^2, \tag{15}$$

which is a differential equation useful in determining V(c), be met. Note that, in the general case of the function f(c, Θ), the differential equation will have the form

$$\frac{d^2V}{dc^2}=\frac{1}{f^2(c,\Theta)}. \tag{16}$$

Upon integrating Eq. (15), we obtain an expression for the separatory potential in the form

$$V(c)=(2c-1)\ln\frac{c}{1-c}+Ac+B+\beta\left[2c\ln\frac{c}{1-c}-\beta\ln(1-c)\right]. \tag{17}$$

The first three terms in this equation coincide with the usual expression for the separatory potential in the case of small enrichments.

A more symmetrical form of the notation is also convenient:

$$V(c)=(1+\beta)\left[\left(2c-\frac{1}{1+\beta}\right)\ln c-\left(2c-(\beta-1)\right)\right]\ln(1-c)+Ac+B. \tag{18}$$

Coefficients A and B have the same value as in the theory of low-enrichment stages. The selection of these variables is usually not a fundamental problem. They can be zero, in particular, or they can be found from the potential inversion conditions and from the derivative of the potential at zero at the feed point, where the concentration c = c_F, i. e., from the condition

$$V(c_F)=\frac{[aV(c)}{dc}=0. \tag{19}$$

In the latter case, the expression for the potential (17) acquires the form

$$V(c)=[2c(1+\beta)-1]\ln\frac{c}{1-c}\Big/\frac{c_F}{1-c_F}+\beta^2\ln\frac{1-c_F}{1-c}-\frac{c-c_F}{c_F(1-c_F)}[c_F(1+\beta)^2-(1-c_F)]. \tag{20}$$

With Eq. (15) taken into account, the expression for the separatory work done by the step (here it is more convenient to refer to the separatory power of the step) is written in the form

$$\delta U=\frac{\gamma^2(\Theta)}{2}\cdot\frac{1-\Theta}{\Theta}L. \tag{21}$$

Formulas for the separatory potential (17) and separatory power (20) can be utilized in order to estimate the total stream in an ideal stage operating at specified external conditions, and in order to shed light on the feasibility of using asymmetrical stages. In an ideal stage, of course, the concentrations of streams being mixed must be identical. If we assume that the value of Θ does not vary very markedly from step to step when the stages are sufficiently long, we can then assume that the separatory potentials of the streams being mixed will be equal for those steps (here we can neglect the difference in the values of $\beta(\Theta)$ in contiguous stages). Upon summing the separatory powers of all the steps under that assumption, and bearing in mind the fact that the potentials of all opposing streams will cancel out in Eq. (12), we find

$$\sum\frac{\gamma^2(\Theta)}{2}\cdot\frac{1-\Theta}{\Theta}L\approx pV(c_p)+WV(c_W)-FV(c_F). \tag{22}$$

This approximate formula is very similar to a similar exact formula used in the theory of low-enrichment stages. The essential difference between the two is that the expression for V(c) contains the coefficient β which is a function of Θ. The quantity Θ remains practically constant along the stage when enrichments are low, and is variable when enrichments are high. The stage-average value of Θ, Θ_{av}, can be introduced for estimates, when dealing with high enrichments. Then, if we neglect the effect of the correction term containing β in the expression for V(c), we can assume that the minimum condition ΣL in Eq. (22) will be the constraint

$$\gamma^2(\Theta_{av})\frac{1-\Theta_{av}}{\Theta_{av}}=\max. \tag{23}$$

Constraint (23) allows us to establish the feasibility of using asymmetrical stages at high enrichments. If the range of concentrations is such that it is safe to assume c(1−c) = const, then Eq. (23) transforms to the constraint

$$\frac{1-\Theta_{av}}{\Theta_{av}}\ln^2\frac{1}{1-\Theta_{ay}}=\max; \tag{24}$$

which is familiar from the theory of low-enrichment stages, and which yields $(\Theta_{av})_{opt}=0.8$, or the value $\Theta=2/3$, which is more interesting from a practical standpoint [8]. Substitution of the appropriate γ values for large and small concentrations in Eq. (23) leads to the formulas

$$(1-\Theta)^{\alpha_0-1}[2(\alpha_0-1)\Theta+1]=1; \tag{25}$$

$$(1-\Theta)^{\frac{\alpha_0-1}{\alpha_0}}\left(2\frac{\alpha_0-1}{\alpha_0}\Theta+1\right)=1. \tag{26}$$

Analysis of these formulas, for the above cases as well, confirms the value $(\Theta_{av})_{opt} = 0.8$ (in practice $\Theta = 2/3$) when α_0 remains within the range from 1.5 to 1.8. At higher values of the separation factor ($\alpha_0 > 2$), we require a more exact analysis (22). Even in those cases, however, the calculations demonstrate the feasibility of employing asymmetrical stages.

Introduction of Θ_{av} also allows us to arrive at the total productivity when the stage is operating under specific external conditions, while at the same time obtaining an a priori estimate of the cost of the facility, and an estimate of the power costs, without having to resort to laborious concrete computations for each variant studied.

Both symmetrical and asymmetrical stages were computed on an electronic computer over a comparatively broad range of parameters: $\alpha_0 = 1.1$; 1.5; 2.0; 2.5; $c_P = 0.1$; 0.9; 0.999; $c_F = 0.001$; 0.1; 0.9; $c_W = 0.01$; 0.001, in order to check the validity of the estimates. The error in the determination of ΣL based on Eq. (23), with Θ_{av} introduced, was within 10-15%.

In summary, we can draw the following conclusions:

1) the relationships for the enrichment function in separation along a channel, while having an implicit form in the general case, turn up approximately in explicit form for three special cases which cover the entire range of concentrations with overlap;

2) a differential equation for the separatory potential for any enrichment function f(c, Θ) was derived, and its solution was found in implicit form for the form of the function adopted;

3) estimating formulas useful for comparing symmetrical and asymmetrical stages and determining the total stream are given;

4) in the case of high-enrichment stages, but of course with certain provisos, the conclusion is retained that an asymmetrical stage such that $\Theta = 0.8$ (in practice $\Theta = 2/3$) is optimal.

LITERATURE CITED

1. N. A. Kolokol'tsov and N. I. Laguntsov, At. Energ., 27, 560 (1969).
2. N. A. Kolokol'tsov and N. I. Laguntsov, ibid., 29, 300 (1970).
3. K. Cohen, The Theory of Isotope Separation, New York (1951).
4. A. M. Rozen, Theory of Isotope Separation in Columns [in Russian], Atomizdat, Moscow (1960).
5. W. Buland et al., Z. Phys. Chem., 214, 249 (1960).
6. A. Boheringer, Arch. Elektrotechnik, 54, 127 (1971).
7. Y. Takashima, Bull. Tokio Inst. Technol., No. 69 (1965).
8. N. A. Kolokol'tsov, At. Energ., 27, 9 (1969).

NEW METHOD FOR DETERMINING HYDROGEN AND HELIUM ISOTOPE CONTENT IN THIN SAMPLES

K. P. Artemov, V. Z. Gol'dberg,
I. P. Petrov, V. P. Rudakov,
I. N. Serikov, and V. A. Timofeev

UDC 543.5

The use of methods developed in nuclear physics for analyzing the element and isotope composition of samples has proven very fruitful. The most widely applied, and apparently the most sensitive, method is activation analysis using beams of neutrons and charged particles. Several other methods have been proposed, based on recording the characteristic emissions, the products of nuclear reactions, elastically scattered particles, etc. It is clear that no method is universal, i.e., there exist, for example, isotopes which either do not activate or give off active products, but whose half-lives or radiation energies are not recordable.

The isotopes of hydrogen and helium (except for radioactive tritium), for example, are isotopes for the analysis of whose content essentially none of the earlier nuclear-physics methods is applicable. These isotopes are not activated upon irradiation by neutrons or by beams of light-charged particles. It is true that analysis of their content is possible using the elastic-scattering method. However, in this case, the group corresponding to scattering by hydrogen will have the smallest energy in the elastic-scattering spectrum (the energy of an elastically-scattered particle at a given angle decreases as the mass of the target nucleus decreases). This means that the given group will lie in the spectral region in which there is a rather large background created by inelastic scattering by other isotopes contained in the analyzed sample, and also caused by scattering of the primary beam at the collimator and various apparatus effects. When the hydrogen content in a sample is less than 10% of the total number of atoms, determining it by the elastic-scattering method becomes difficult.

In the present paper we propose a method for analyzing the hydrogen and helium isotope content in several isotopes of light elements; this method is no less, and is possibly more, sensitive and accurate than other analysis methods. A significant advantage of this method is the fact that it allows one to determine not only the hydrogen and helium isotope content in the sample, but also their depth distribution in the sample. The limitation of the method is the fact that thin ($\leq 100\,\mu$) samples are needed for the analysis, but this limitation is not fundamental and is determined by the energy of the accelerator particle beam.

Analysis Method

The sample in which the hydrogen content is determined is bombarded by a beam of accelerated protons. Two counters working in the coincidence mode record elastically-scattered protons and recoil protons. Inasmuch as there is a strict dependence ($|\theta_{el}| + |\theta_{rec}| = 90°$) between the emission directions of an elastically-scattered proton and a recoil proton in the laboratory coordinate system, the inclusion of the second counter placed at an angle of 90° to the first does not decrease the counting rate of elastically-scattered protons by the first counter. At the same time, all events other than elastic scattering of protons by hydrogen, which cause a proton to enter the first counter, are not recorded, and in the energy spectrum of this counter there remains a single proton group corresponding to scattering by hydrogen. The remaining background in this case is determined by only random coincidences.

Naturally, the better the energy resolution in the measurements, the better the ratio of the effect to the background, and the higher the sensitivity and accuracy of the method. If the protons which are

Translated from Atomnaya Énergiya, Vol. 34, No. 4, pp. 265-270, April, 1973. Original article submitted September 11, 1972.

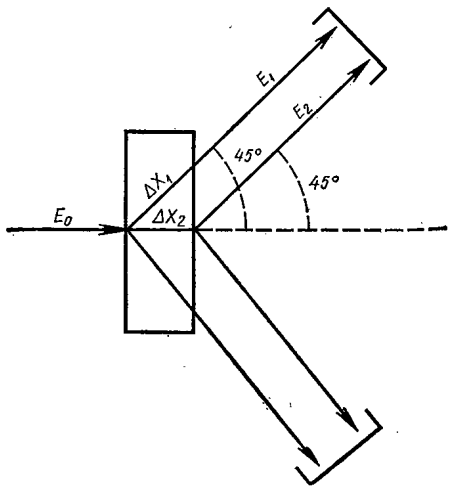

Fig. 1. Scattering of protons by hydrogen contained in various surfaces of the sample. The difference in the combined energy is $\Delta E = 2E_2 - 2E_1 = (dE_0/dx)\Delta x_2 - 2(d(E_0/2)/dx)\Delta x_1$.

elastically scattered by hydrogen are recorded by one counter, then during measurements with a thin target, the fundamental contribution to the width of the peak corresponding to these protons in the energy spectrum will introduce the dependence of the elastic-scattering energy of the proton on the scattering angle ($E = E_0 \cos^2\theta$). Thus, for example, when $E_0 = 16$ MeV and $\theta = 45°$, then we have $\Delta E/\Delta\theta = 270$ keV/deg, which is approximately 4% of the energy of the recorded protons. The contribution from other factors (the energy spread in the proton beam and the target thicknesses, etc.) is usually no more than 1%.

If an elastically-scattered proton and a recoil proton are recorded and their energies added, then in the combined-energy spectrum the kinematic dependence is completely eliminated and does not contribute to the peak width (because of the strict angular correlation of protons $|\theta_{el}| + |\theta_{rec}| = 90°$ the energy change of one proton depending on the angle is compensated by an equal energy change of the second proton, but with the opposite sign).

Good energy resolution in the combined proton-energy spectrum allows us to analyze depth distribution of hydrogen in the sample. If one of the counters is at an angle of +45° to the axis of the proton beam and the second is at −45°, then the energies of an elastically-scattered proton and a recoil proton are equal to half the energy of the incident proton. Since the unit energy losses depend on the total energy of the proton, and since the scattered protons pass through a great sample thickness (see Fig. 1), the depth distribution of hydrogen in the sample will be reflected in the combined-energy spectrum. For instance, when the incident-proton energy is 16 MeV, the difference in the combined energy of protons scattered by hydrogen contained in various aluminum-foil surfaces 5 μ thick is approximately 100 keV. Thus, if the energy resolution is better than 100 keV, then one can analyze the depth distribution of hydrogen in the sample with an accuracy to several microns.

Finally, we should note one more effect which plays a role in these measurements: multiple proton scattering upon passage through the sample. This causes lower efficiency in recording proton-scattering events at hydrogen in proportion to the increase of sample depth at which scattering occurs. This is explained by the fact that some of the protons are outside the boundaries of the solid angle from the sample to the counter. The lowered efficiency can be easily taken into account by calibration or calculation.

The multiple-scattering effect can be used for sequential "scanning" of the hydrogen content over the depth of the sample. Multiple scattering causes smoothing of the rigid angular correlation between the elastically-scattered proton and the recoil proton. Therefore, changing the angle between the two counters allows one to choose a position such that recording of scattering events by hydrogen contained in the surface facing the counter ceases, but where scattering events at hydrogen located in the depth of the sample are recorded. Such measurements can be useful in those cases in which the hydrogen content at the sample surface is considerably greater than its content in the sample depth.

Recording System

In analyzing samples with low hydrogen content, it is obvious that the loading of the counters will be determined by protons which are elastically scattered at nuclei of principal elements of the sample and by nuclear reaction products produced by protons interacting with these nuclei. Such loading, with the purpose of shortening the measurement time, must naturally remain at the maximum allowable level ($\sim 10^4$-10^5 pulses/sec). Then, the counting rate for random coincidences will be rather high. Obviously, most of them will occur in the spectral region in which we have a peak of elastic scattering by the primary material in the sample. Nevertheless, the background may be significant also in the region of the peak for elastic scattering by hydrogen.

There are two possibilities for decreasing the background from random coincidences. First, the particles are recorded using counter telescopes consisting of a narrow ($\sim 30\,\mu$) and a broad (~ 1 mm) semiconductor detector. The first counter measures unit energy losses and the second determines the total particle energy. Analysis of the counter signals using a special identification circuit [1] allows one to

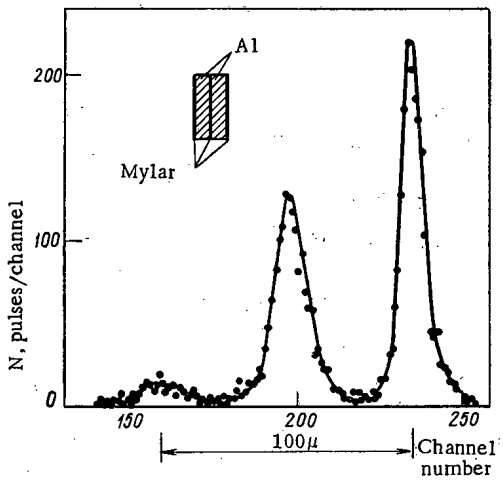

Fig. 2

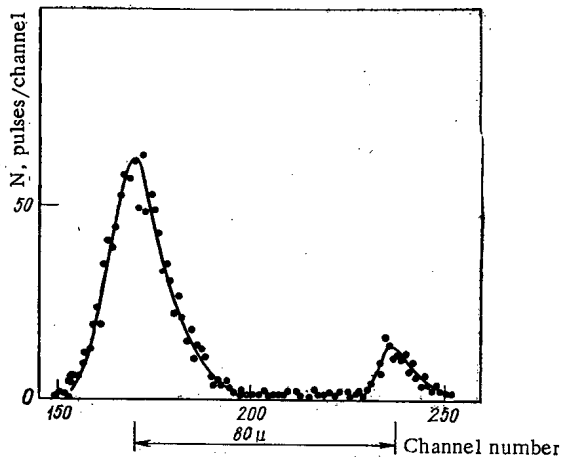

Fig. 3

Fig. 2. Graph of p–p coincidence spectrum in coordinates of the combined energy of coincident protons. A schematic diagram of the sample is shown at the upper left.

Fig. 3. Graph of p–p coincidence spectrum for a Ge sample, in coordinates of the combined energy of coincident protons.

determine uniquely the type of particles recorded by the counter. Thus, by using an identification system, one may separate out from all nuclear reaction products only those particles which are of interest.

The second method for lowering the background level in the spectral region of interest is the presentation of the measurement results as a two-dimensional coincidence spectrum in coordinates of the energy of coincident particles. Under ideal conditions (when there is infinitely good energetic and angular resolution), events corresponding to recording of an elastically-scattered proton and a recoil proton would group themselves in the spectrum at one point with the coordinates $E_1 + E_2 = E_0$, where E_1 and E_2 are the energies of the elastically-scattered proton and the recoil proton, respectively, and E_0 is the energy of the incident proton. Random coincidences, on the other hand, will be more or less evenly distributed over the entire two-dimensional picture, or will group themselves in the energy region corresponding to elastic scattering by the principal sample material.

For the present paper we used just such a recording system, with particle identification and presentation of the results on a two-dimensional coincidence spectrum. This system is described in detail in [2].

Measurement Results

The proposed method for analyzing the hydrogen content was tested experimentally on a proton beam (E_0 = 16 MeV) in the 1.5 m cyclotron at the I. V. Kurchatov Institute of Atomic Energy. The investigated sample was inside a large scattering chamber. Inside were also located two counter telescopes, each of which consisted of a narrow (~32 μ) and a broad (~1.5 mm) semiconductor detector. One telescope was at an angle of +45° relative to the proton-beam axis, while the other was at −45°. The telescope signals entered a recording system as described in [2].

For the test we prepared multilayered samples consisting of a thin (~1 mg/cm^2) hydrogenous Mylar film ($C_{10}H_8O_4$) and aluminum foil (~24 mg/cm^2). We used a sample of Mylar + Al + Mylar + Al + Mylar. The results of the measurements are shown in Fig. 2, where the p–p coincidence spectrum is presented in coordinates of the combined energy of coincident protons. The three spectrum peaks correspond to hydrogen contained in the Mylar films. The Mylar films for the sample contained approximately identical quantities of hydrogen. The difference in intensity among the three proton groups corresponding to scattering from different films is a result of the above-mentioned multiple scattering.

The distribution of the points among the groups reflects mainly not the scattering events at hydrogen contained in the aluminum foil (there is relatively little of it there), but those cases when protons scattered by hydrogen in the Mylar subsequently undergo scattering at the counter apertures or when signal overlap occurs. Such a distribution is the main obstacle to analysis of samples with significantly differing hydrogen content in different layers.

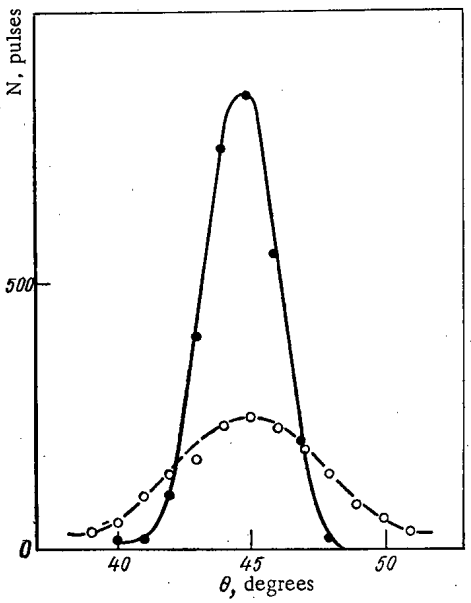

Fig. 4. Dependence of the p–p coincidence counting rate on the angle between the counters.

Figure 2 clearly shows the feasibility of analyzing the hydrogen depth distribution in the sample by the proposed method.

Figure 3 shows a spectrum obtained from a germanium sample. The sample thickness was 80 μ (~40 mg/cm^2). It is clear that practically all the hydrogen is contained in the sample surface; there is much less of it in one surface (that facing the counters) than in the other ($2 \cdot 10^{16}$ atoms/cm^2 and $3 \cdot 10^{18}$ atoms /cm^2, respectively). The hydrogen content within the sample does not exceed $2.4 \cdot 10^{-5}$ atom of H per atom of Ge. Of course, for a more accurate evaluation of the hydrogen content within the sample, one must remove it from the surface. All the quantitative estimates were obtained by simple comparison of the spectra corresponding to a Mylar target with known hydrogen content to the analyzed sample.

It is more accurate to estimate the hydrogen content within the sample when there is a large amount of it on the surface; this can also be done using the multiple-scattering effect. Figure 4 shows the dependence of the coincidence counting rate on the angle between the counters. In these measurements one of the counters remained stationary at an angle of +45° relative to the proton beam. The orientation of the second counter was varied from −39° to −51°. The solid curve is the result of measurements using only a single Mylar film as the target. The angular width of the curve (3.3°) corresponds to the solid angle of the counters and to multiple scattering in the film. The dashed curve was obtained for a target made of the same film and copper foil 13.3 mg/cm^2 thick, where the foil was on the side facing the counters. It is clear that if the counter is at an angle of, for example, −50°, then proton-scattering events at hydrogen located on the side of the foil facing the counters will not be recorded.

Figure 5 shows results for such measurements with a multilayered sample (Mylar + Al + Mylar + Al + Mylar). The upper spectrum reflects the normal counter positions (+45° and −45°), and all three proton groups are visible; the lower spectrum was obtained for angles of +45° and −48°. The proton group corresponding to scattering by hydrogen in the film facing the counters has disappeared, and we may examine in more detail the spectrum region reflecting scattering by hydrogen contained in the aluminum foil.

Thus, the results presented in the figures clearly demonstrate the feasibility of the method. Measurements with Ge, Si, and Cu samples showed that if the sample does not contain a significant quantity of hydrogen at the surface, then it is rather easy to obtain sensitivity of the order of 10^{-4} at.%. We may estimate the maximum sensitivity of the method. We will assume that there are no random coincidences in the spectrum region of interest (in most cases this is actually so). We also assume that the maximum allowable counter loading is 10^4 pulses/sec and the maximum reasonable exposure time is 10^4 sec. If ten pulses corresponding to scattering by hydrogen are recorded in the indicated time, then (if we take into account that the ratio of cross sections for elastic scattering of protons with energy 15-20 MeV through an angle of ~45° by hydrogen and any heavy nucleus is ~10) this will indicate that the hydrogen atoms in the sample comprise 10^{-8} of the total number of atoms in the principal material of the sample.

Using reasonable assumptions, the sensitivity is estimated at 10^{-6} at.%, while the best sensitivity for determining hydrogen content by other methods [3] is 10^{-6} wt.% (which for materials of moderate atomic weight is ~100 times less sensitive).

The way to further increase the sensitivity of the method is also obvious: increasing the counter loading. The actual loading assumed for estimating the sensitivity, which we are using at present, is 10^4 pulses/sec. Increasing it 5-10 times is wholly feasible. This would bring about a similar increase in sensitivity. Of course, we must also take into account the increased number of random coincidences. However, there are at least two methods for lowering this: decreasing the resolution time of the coincidence circuit and using a continuous-beam accelerator instead of a cyclotron.

The accuracy of the method depends on the measuring procedure. It is possible to calculate directly the hydrogen content in the sample based on knowledge of the apparatus parameters and measurement results. Such a method can have an accuracy of the order of 10-20%. One of the main reasons for the limited

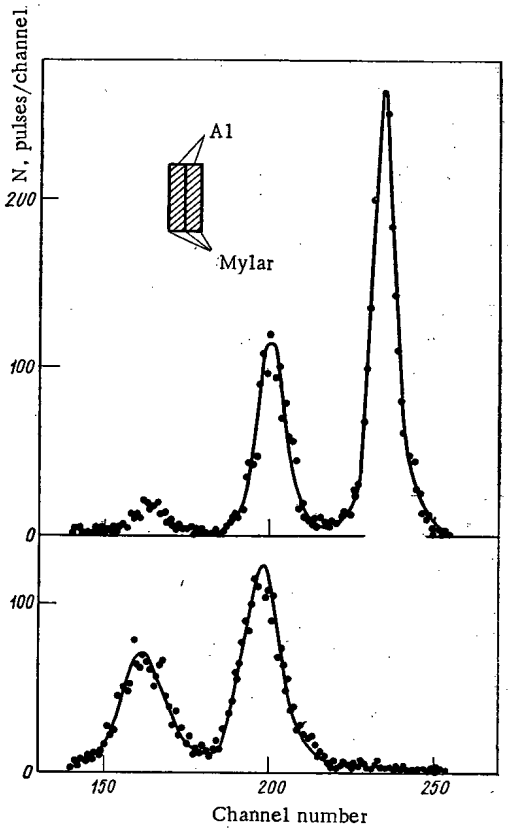

Fig. 5. Graph of p–p coincidence spectrum for a multilayered sample, in coordinates of combined proton energy.

accuracy in this case is the unstable position of the accelerator beam on the target. Another procedure is to use a standard sample. In this case, the accuracy of the method is determined only by one's knowledge of the hydrogen content in the standard sample.

If one must find the hydrogen distribution over the sample thickness, then the sensitivity and accuracy depend on the character of the hydrogen distribution. When there is significant difference in the hydrogen content of neighboring layers, the accuracy of determining it in a depleted layer decreases, as we showed above.

All of our results were obtained using apparatus perfected for a wide range of physical experiments. It was designed for distinct recording of coincidences between particle pairs of different types and for a wide energy range of coincident particles.

It is clear that when one must record coincidences of only protons with practically identical energies, on the one hand, the apparatus may be simplified, and, on the other hand, one may improve some of its parameters (loading and resolution time).

The proposed method may appear rather complex. However, it is no more complex than many widely-used methods. Almost any charged-particle accelerator can be used (and even an accelerator tube if analysis is done on a neutron beam recording, for example, n–p coincidences), and the possibility of linking the counters to a small computer simplifies the solution of the problem.

The method was tested experimentally on only one hydrogen isotope, using protons as bombarding particles. We should note that this method can be used for analyzing the content not only of hydrogen and helium isotopes, but also, in principle, for any element, if one uses an accelerator whose beam is capable of expelling the atoms of such elements from the sample. It is not at all necessary to use a beam with the same nuclei as the atoms whose content is to be determined. The strict correlation between the escape directions of elastically-scattered particles and recoil nuclei is preserved, of course, even for particles which are different. Only the angle between these directions is changed.

Note Added in Proof

After this article was submitted to the editors, B. Skorodumov brought to the authors' attention a paper published in the Journal of Applied Physics [Vol. 43, No. 19 (1972)], in which a similar method is proposed.

LITERATURE CITED

1. A. A. Kurashov and V. V. Paramonov, At. Energ., 19, 400 (1965).
2. K. P. Artemov et al., Yadernaya Fizika, 12, 1108 (1970).
3. Methods for Determining Gases in Metals and Alloys [in Russian], Seminar Papers of the F. E. Dzerzhinskii Moscow House of Scientific and Technical Propaganda, Moscow (1971).

SPACE – AGE DISTRIBUTION OF NEUTRONS ARISING FROM THE SPONTANEOUS FISSION OF URANIUM NUCLEI IN A TWO-LAYER MEDIUM WITH A CYLINDRICAL INTERFACE

Yu. B. Davydov

UDC 550.8:553.495

The recording of neutrons arising from the spontaneous fission of uranium nuclei offers the possibility, in principle, of determining uranium directly in exploratory boreholes; it may be used for studying the geological sections of boreholes in radioactive ore sites. It is therefore particularly interesting to determine the principal laws governing the borehole distribution of spontaneous-fission neutrons.

Uranium nuclei undergoing fission constitute sources of fast neutrons; hence, in order to find the spatial distribution of thermal neutrons, it is first essential to consider the process in which the fast neutrons are slowed down to thermal energy.

The aim of the present investigation is to study the main laws governing the behavior of epithermal neutrons in a borehole/ore seam system. The subject for examination is the slowing down of neutrons arising from the spontaneous fission of uranium nuclei, i.e., a calculation of the space–age distribution of the epithermal neutrons.

Let us consider two media separated by an infinite circular cylinder of radius r_0. The inner medium ($r < r_0$) simulates the borehole and the outer medium ($r > r_0$) the ore seam. The symmetry axis of the inhomogeneous system under consideration coincides with the z axis of the cylindrical coordinate system employed (r, z, φ).

Let the mineralization be one-dimensional, i.e., the number of sources in unit volume of the medium $A(z)$ be a function of one coordinate z. We shall assume that the mineralization does not affect the properties of the ore seam under consideration as regards the transport of neutrons; the slowing-down properties of the ore and surrounding rocks will then be identical. We require to find the slowing-down density of the spontaneous-fission neutrons in the two media.

We shall use the age approximation of transport theory, representing the retardation as a process of three-dimensional neutron diffusion, accompanied by a continuous loss of energy.

Analysis of theoretical and experimental data indicates that the age approximation defines the behavior of the neutrons at short distances from the source fairly accurately in media of arbitrary isotopic composition. Even in describing the spatial distribution of neutrons retarded in water, the age approximation is accurate up to a distance of the order of 10 cm from the source [1]. The geometrical conditions normally employed in measuring the density of neutrons arising from the spontaneous fission of uranium nuclei in ore borings (the mean radius of the boreholes usually lies between 5 and 6 cm) indicate that the age approximation may validly be used for solving this problem, since the average distances traveled by the neutrons in the borehole lie within the range of practical applicability of the age approximation.

Mathematically, the problem of the slowing down of spontaneous-fission neutrons may be solved by using the system of age equations

$$L^k q_k(r,\ z,\ \tau_k) = 0 \qquad (k = 1,\ 2) \tag{1}$$

Translated from Atomnaya Énergiya, Vol. 34, No. 4, pp. 271-275, April, 1973. Original article submitted April 3, 1972.

with the following boundary conditions

$$q_1(r,\ z,\ \tau_1)|_{r=0} < \infty; \tag{2}$$

$$q_2(r,\ z,\ \tau_2)|_{r\to\infty} < \infty; \tag{3}$$

the following matching conditions at the interface between the media

$$\left.\frac{q_1(r,\ z,\ \tau_1)}{\xi_1\Sigma_{sk}}\right|_{r=r_0} = \left.\frac{q_2(r,\ z,\ \tau_2)}{\xi_2\Sigma_{sk}}\right|_{r=r_0}; \tag{4}$$

$$\left.\frac{D_1}{\xi_1\Sigma_{sk}}\cdot\frac{\partial q_1(r,\ z,\ \tau_1)}{\partial r}\right|_{r=r_0} = \left.\frac{D_2}{\xi_2\Sigma_{sk}}\cdot\frac{\partial q_2(r,\ z,\ \tau_2)}{\partial r}\right|_{r=r_0}; \tag{5}$$

and the initial conditions

$$q_k(r,\ z,\ 0) = S_k(z) \qquad (k=1,\ 2), \tag{6}$$

where k = 1, 2 is the index of the medium (borehole and ore seam, respectively); $q_k(r, z, \tau_k)$ is the neutron slowing-down density; L^k is a differential operator defined by the relation

$$L^k = \frac{\partial^2}{\partial r^2} + \frac{1}{r}\cdot\frac{\partial}{\partial r} + \frac{\partial^2}{\partial z^2} - \frac{\partial}{\partial\tau_k} \quad (k=1,\ 2);$$

$S_k(z)$ is the density of the sources; ξ_k is the logarithmic mean of the energy loss in collision; $\Sigma_{\rho k}(u)$ is the macroscopic scattering cross section; $D_k(u)$ is the diffusion coefficient defined by the equation

$$D_k(u) = \frac{1}{3\Sigma_{sk}(u)[1-\overline{\cos\alpha(u)}]};$$

$\overline{\cos\alpha(u)}$ is the mean cosine of the scattering angle; $\tau_k(u)$ is the age of the neutrons; u is the lethargy.

The initial conditions (6) are a consequence of the physically obvious assertion to the effect that the slowing-down density of neutrons of zero age equals the density of the sources.

The solution of the age equation within each homogeneous component of the heterogeneous medium is perfectly easy; however, at the interface between the media the solutions for each medium have to be appropriately matched by the use of physically obvious boundary conditions.

When using the age approximation to solve problems regarding the slowing down of neutrons in heterogeneous media, additional difficulties associated with the presence of the age coordinate arise. Each homogeneous part of the heterogeneous medium is characterized by its own particular age, this being a complicated function of the lethargy. However, the system of age equations can only be solved if the age is an independent variable of the system as a whole.

Hence, in solving problems relating to the slowing down of neutrons in heterogeneous media, simplifying restrictions are necessarily imposed on the age of the neutrons. Usually it is assumed that there is a linear relationship between the ages of the neutrons in the individual homogeneous parts of the medium for all lethargy values [2].

According to the definition of age

$$\tau_i(u) = \frac{1}{3\xi}\int_0^u \frac{du}{\Sigma_{si}(u)\Sigma_{ti}(u)}, \tag{7}$$

where i is the index of the homogeneous part of the heterogeneous medium, $\Sigma_{si}(u)$, $\Sigma_{ti}(u)$ are macroscopic scattering and transport cross sections.

Equation (7) may be integrated if we introduce the values of $\overline{\Sigma}_{si}$ and $\overline{\Sigma}_{ti}$ averaged over the spectrum. Then

$$\tau_i(u) = \frac{u}{3\xi\overline{\Sigma}_{si}\overline{\Sigma}_{ti}}, \tag{8}$$

from which it follows that

$$\tau_i(u) = \frac{\overline{\Sigma}_{sj}\overline{\Sigma}_{tj}}{\overline{\Sigma}_{si}\overline{\Sigma}_{ti}}\tau_j(u) = a_{ij}\tau_i(u), \tag{9}$$

where a_{ij} is a constant.

Equation (9) indicates that, to a first approximation, the relationship between the age in the i-th and j-th media may be regarded as linear.

Remembering the foregoing remarks as to the age of neutrons, we shall accept as valid the assertion that there is a direct proportionality between the neutron ages in the borehole and the seam, i.e., for all lethargy values

$$\tau_k(u) = a_k \tau(u) \qquad (a_k \geqslant 1), \tag{10}$$

where $\tau(u)$ is the age used subsequently as an independent variable for the whole system (1).

From the conditions of the problem, sources of neutrons only exist in the external active medium; hence

$$S_k(z) = A_k(z)\,\delta_{mk}, \tag{11}$$

where $A_k(z)$ is the density of the sources; δ_{mk} is the Kronecker–Weierstrass symbol, equal to unity for $m = k$ and zero for $m \neq k$.

The problem is solved by the successive application of direct Laplace and Fourier transformations with respect to τ and z, and the subsequent application of the inverse transformations.

In order to solve the problem for an arbitrary unidimensional distribution of sources $A_2(z') = A(z')$, we used a method based on Green's functions [3] with respect to the variable z, i.e., we find the influence function of the plane source $z = z'$ and integrate the result over the whole interval of source distribution. Then the density of the sources may be expressed in the form

$$A(z') = \delta(z - z'), \tag{12}$$

where $\delta(z - z')$ is the Dirac delta function.

We introduce the Laplace–Fourier transform $Q_k(r, k^2, p)$ of the neutron slowing-down density $q_k(r, z, \tau)$. The Green's function $G_k(r, z - z', \tau)$ by definition constitutes the solution of the problem (1-6) for the plane source (12) and takes the form

$$G_k(r,\ z - z'\ \tau) = \frac{1}{\pi} \cdot \frac{1}{2\pi i} \int_{\sigma - i\infty}^{\sigma + i\infty} e^{p\tau}\, dp \int_0^{\infty} Q_k(r,\ k^2,\ p)\, \cos k(z - z')\, dk, \tag{13}$$

where

$$Q_1(r,\ k^2,\ p) = \beta_1(k^2,\ p)\, I_0(\nu_1 r); \tag{14}$$

$$Q_2(r,\ k^2,\ p) = \beta_2(k^2,\ p)\, K_0(\nu_2 r) + \frac{1}{a_2 \nu_2^2}; \tag{15}$$

$$\beta_1(k^2,\ p) = \frac{\xi_1 \Sigma_{s1}}{\xi_2 \Sigma_{s2}} \cdot \frac{K_1(\nu_2 r_0)\, \nu_2 D_2}{\Delta a_2 \nu_2^2}; \tag{16}$$

$$\beta_2(k^2,\ p) = -\frac{I_1(\nu_1 r_0)\, \nu_1 D_1}{\Delta a_2 \nu_2^2}; \tag{17}$$

$$\Delta = D_2 \nu_2 I_0(\nu_1 r_0)\, K_1(\nu_1 r_0) + D_1 \nu_1 K_0(\nu_2 r_0)\, I_1(\nu_1 r_0);$$

$$\nu_k^2 = k^2 + \frac{p}{a_k};$$

$I_\nu(x)$, $K_\nu(x)$ are modified Bessel functions of the first and second kind of order ν.

Integrating the Green's function (13) over the whole range of distribution of the sources, we obtain a solution to the problem (1-6) for an arbitrary law of source distribution $A_2(z') = A(z')$ in integral form:

$$q_k(r,\ z,\ \tau) = \frac{1}{\pi} \cdot \frac{1}{2\pi i} \int_{-\infty}^{+\infty} A(z')\, dz' \int_{\sigma - i\infty}^{\sigma + i\infty} e^{p\tau}\, dp \int_0^{\infty} Q_k(r, k^2, p) \cos k(z - z')\, dk. \tag{18}$$

In the particular case of a seam of finite width with homogeneous mineralization $A(z') = A$, $|z'| \leq h$, the solution to the problem takes the form

$$q_k(r,\ z,\ \tau) = \frac{2}{\pi} \cdot \frac{A}{2\pi i} \int_{\sigma - i\infty}^{\sigma + i\infty} e^{p\tau}\, dp \int_0^{\infty} Q_k(r,\ k^2,\ p)\, \frac{\cos kz \sin kh}{k}\, dk. \tag{19}$$

Equation (19) may be used for calculating the slowing-down density in certain particular cases of practical interest. For example, practical cases are often encountered in which we may neglect either the influence of the borehole or the influence of the surrounding rocks.

In the case in which the perturbing effect of the borehole may be neglected, the neutron slowing-down density distribution may be found by making the limiting transition $r_0 \to 0$ in Eq. (19). Then we have

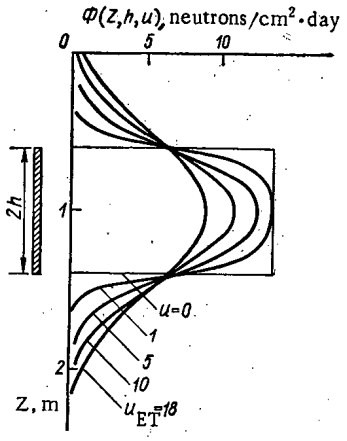

Fig. 1

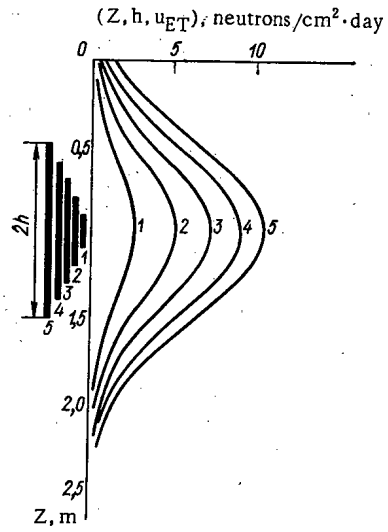

Fig. 2

Fig. 1. Neutron flux distribution along the axis of a borehole for a seam of width 2h = 1 m. The figures on the curves indicate the lethargy of the neutrons.

Fig. 2. Flux distribution of epithermal neutrons for seams of various widths: 1) 2h = 20 cm; 2) 2h = 40 cm; 3) 2h = 60 cm; 4) 2h = 80 cm; 5) 2h = 100 cm.

$$q_1(z, h, \tau) = \frac{\xi_1 \Sigma_{s1}}{\xi_2 \Sigma_{s2}} \cdot \frac{A}{2} \left(\operatorname{erf} \frac{z+h}{2\sqrt{\tau_2}} - \operatorname{erf} \frac{z-h}{2\sqrt{\tau_2}} \right), \tag{20}$$

where

$$\operatorname{erf} x = \frac{2}{\sqrt{\pi}} \int_0^x e^{-t^2} dt.$$

In the second case, in which the effect of the surrounding rocks may be neglected, we make the limiting transition $h \to \infty$. After carrying out this limiting transition, we find the neutron slowing-down density distribution for an active seam of infinitely great width with uniform mineralization:

$$q_h(r, \tau) = \frac{A}{2\pi i} \int_{\sigma - i\infty}^{\sigma + i\infty} Q_h(r, 0, p)\, e^{p\tau} dp. \tag{21}$$

It is impossible to obtain an exact solution of the problem in finite form except for the case in which the influence of the borehole may be neglected. Subsequent analysis of the results will therefore be carried out numerically.

Figures 1-4 show some results of the numerical calculation of the neutron flux arising from the spontaneous fission of uranium nuclei $\Phi(\mathbf{r}, u)$, which is related to the slowing-down density $q(\mathbf{r}, u)$ [4] by the equation

$$\Phi(\mathbf{r}, u) = \Phi[\mathbf{r}, \tau(u)] = \frac{q[\mathbf{r}, \tau(u)]}{\xi \Sigma_s}.$$

The distribution of the retarded neutrons is calculated for the case in which the borehole, filled with fresh water, intersects an active seam folded with dense quartz sandstone of density $\rho = 2.65$ g/cm^3. The initial energy of the fission neutrons equals 2 MeV.

In the calculation we assumed a direct proportionality between the ages of the neutrons in the borehole and in the seam. The total age of the neutrons was calculated approximately from the known lethargy by using the scattering and transport cross sections, averaged over the spectrum. In order to calculate the averaged cross sections, we used exact calculations of total age for epithermal neutrons in water and sand, as given in [5-7]. The averaged cross sections so calculated were subsequently used in calculating the total age for all lethargy values.

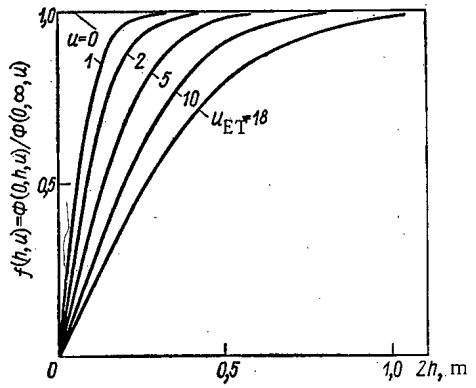

Fig. 3

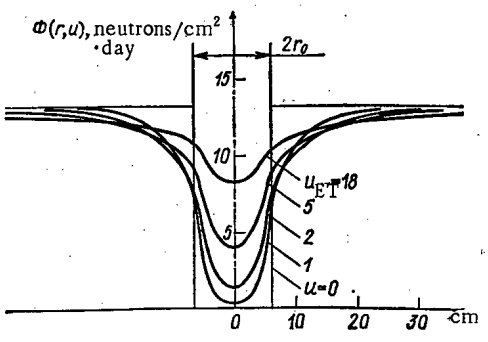

Fig. 4

Fig. 3. Normalized saturation functions for neutrons of various energies. The numbers on the curves give the lethargies of the neutrons.

Fig. 4. Radial neutron flux distribution for a borehole of radius r_0 = 6 cm. The numbers on the curves give the lethargies of the neutrons.

Figure 1 shows the flux distribution of spontaneous-fission neutrons along the axis of the borehole for the case in which the influence of the latter may be neglected. On reducing the energy of the retarded neutrons, i.e., on increasing their lethargy, the flux distribution becomes more slanting.

The flux distribution of the epithermal neutrons is shown in Fig. 2 as a function of the width of the active seam. With increasing width of the ore vein, the absolute value of the flux increases, asymptotically approaching the value corresponding to a seam of infinite width. The maximum flux Φ_{max} is reached in the center of the seam at the point z = 0, $\Phi_{max} = \Phi(0, h, u)$. The value of the flux for a seam of infinite width Φ_∞ may be found by making the limiting transition $h \to \infty$, i.e., $\Phi_\infty = \Phi(0, \infty, u)$. The relationship between the flux in the center of the seam and the width of the latter expressed in units of Φ_∞ is called the normalized saturation function. The saturation functions for neutrons of various energies are presented in Fig. 3.

Analysis of the saturation curves indicates that, for small lethargies (high-energy neutrons), saturation sets in earlier. For example, in the case of epithermal neutrons, u_{ET} = 18, to within an error of 5%, saturation sets in for a seam width of 80 cm, while in the case of fast neutrons, u = 1, it sets in for a width of under 20 cm.

A calculation of the radial neutron flux distribution for a borehole of radius r_0 = 6 cm is presented in Fig. 4. In the active seam at a fair distance from the borehole, the flux is independent of the lethargy and remains constant, i.e., neutrons of all energies are present in the seam. In the borehole there are more low-energy than fast neutrons. With diminishing energy of the neutrons the number of these in the borehole increases.

Allowing for the comparatively low initial energy of the fission neutrons and the comparatively small diameters of the ore boreholes, the age approximation should yield excellent agreement with the true picture of the low-energy neutron distribution.

For neutrons with energies close or equal to the initial energy, the accuracy of the calculation is poor, especially for hydrogen-containing media. More precise results may be obtained by using first collision sources [8].

The simplifying assumptions imposed upon the sources and the age of the neutrons, and also the general limitations of diffusion theory in relation to heterogeneous media, have the effect that the results of the calculations may only be used for establishing very general relationships for the distribution of retarded neutrons in a borehole.

The author is grateful to S. A. Kantor for consultations and help in the numerical realization of the calculations.

LITERATURE CITED

1. D. A. Kozhevnikov, in: Problems of Nuclear Geophysics [in Russian], Nedra, Moscow (1964), p. 40.
2. O. Czubek, Nucleonika, 7, No. 12 (1962).
3. D. Ivanenko and A. Sokolov, Classical Field Theory [in Russian], Gostekhizdat, Moscow (1951).
4. K. Berkurtz and K. Wirtz, Neutron Physics [Russian translation], Atomizdat, Moscow (1968).
5. D. A. Kozhevnikov, in: Industrial Geophysics, No. 41 [in Russian], GTTI, Moscow (1963), p. 54.
6. R. A. Rezvanov, in: Applied Geophysics, No. 39 [in Russian], Nedra, Moscow (1964), p. 136.
7. S. A. Denisik, R. A. Rezvanov, and B. E. Lukhminskii, in: Nuclear Geophysics, No. 3 [in Russian], Nedra, Moscow (1968), p. 106.
8. S. A. Kantor, ibid., p. 3.

THE METROLOGY OF NEUTRON MEASUREMENT IN NUCLEAR REACTORS

R. D. Vasil'ev

UDC 621.039.512.45

One of the most important problems in applied nuclear physics is the design of economical, safe, and easily controlled reactors. This requires the availability of accurate information about such topics as the degree and uniformity of fuel burnout, the radiation resistance of materials employed in the reactor, the efficiency of biological protection systems, etc. To obtain such information one has to find the characteristics of neutron fields in operating reactors and critical installations. The results obtained in different reactors using identical or different measuring techniques and devices should agree to within the required degree of reliability. A comprehensive solution of this problem encompasses questions of both scientific and administrative nature and forms the main subjects of applied metrological research.

In the present article we consider the experimental and theoretical aspects of metrological aids to neutron field measurements in reactors and primarily to in-reactor measurements which are the most important and difficult from an experimental point of view.

Metrological Classification of Neutron Measurement Techniques

Neutron fields are described by derivative radiometric quantities characteristic for neutron radiation and by their dependences on other quantities (spectra). The most frequently measured radiometric quantities are neutron density (neutron/cm^3), neutron flux density (neutron/$cm^2 \cdot sec$), and neutron fluence (neutron/cm^2). Most frequently measured radiometric relations include differential and integral functions that describe energy, angular, spatial, and time distributions of these quantities. In some cases it is necessary to know more involved functions such as, for example, the energy and angle dependence of neutron flux density (neutron/$cm^2 \cdot sec \cdot eV \cdot sr$). Other commonly-used quantities include effective neutron temperature, spectral index, etc., which can be either measured directly or calculated from appropriate relations.

The techniques used to measure the above quantities and to find the respective relations are usually classified on the basis of the neutron detection methods, readout instruments, etc. We shall use a classification of a metrological nature based on the method by which the results are obtained. In such a classification the measurements are subdivided into three types: direct measurements, indirect measurements, and joint measurements [1]. Direct and indirect measurements are used to find the magnitudes of separate quantities, whereas joint measurements provide quantitative relationships between different quantities. This approach stems from the fact that the main subjects of investigation in metrology are quantities and relationships, units of their measurement, measuring techniques, and the reliability of the obtained results. The reliability of results is commonly described by random and systematic errors. Random errors characterize the precision of a result and systematic errors its accuracy (the result is the more precise the lower the random error, and the closer to the true value of a quantity the lower the systematic error [2]). Obviously, reduction of random errors does not automatically ensure that the obtained results are more reliable. Of much greater importance is to find, account for, and eliminate sources of systematic errors since the deviations from true value caused by these errors are frequently much greater than random errors. Thus, provision of conditions that ensure the least systematic errors is the most important task of the metrology of direct measurements.

Translated from Atomnaya Énergiya, Vol. 34, No. 4, pp. 277-282, April, 1973. Original article submitted May 18, 1972; revision submitted October 16, 1972.

Metrology of Direct Measurements

Direct measurements can be used to find the values of a restricted group of radiometric quantities that describe neutron fields (e.g., flux density, and occasionally neutron density). In direct measurements the value of a desired quantity is determined by one of the two following methods: 1) by comparing it with a standard measure directly or by means of a comparison device; 2) from the readings of an instrument calibrated in advance with the aid of standards. Only the second method is used in reactor measurements. The instruments are calibrated in units of the desired quantity thus establishing a definite relationship between the instrument reading and the value of the measured quantity. Calibration is performed either with the aid of neutron fields having variable characteristics or with a set of fixed neutron fields with different magnitudes of these characteristics. From a metrological point of view such calibration fields are measures of physical entities, i.e., materialized (substantiated, reproduced) units of measurement. Instrument calibration is preceded by measurements of the quantity that characterizes the calibration field. Various indirect methods are employed to obtain the most reliable values of the given quantity.

When using precalibrated measuring instruments their readings must be multiplied by so-called influencing factors. These factors take into account the differences in the characteristics of the calibration and measured fields represented by the respective relations (energy, angular, or other distributions of the calibrated quantity), as well as the different conditions of measurement and calibration (ambient temperature, background, etc.). In direct measurements, the influencing factors, together with the calibration functions, are the sole source of systematic errors. These factors must be allowed for as otherwise the obtained results are liable to deviate from true values by tens and hundreds percent.

From the above follows that a metrologically valid approach to direct measurements requires: 1) appropriate standard measure in the form of calibration neutron fields and instruments for measuring the quantities that describe these fields; 2) techniques for calibrating the instruments; and 3) methods of detecting and measuring influencing factors.

This approach is implemented in many national metrological laboratories in concrete applications. Now under development are standards of only one of the quantities that describe a neutron field: standards of neutron flux density. However, the properties of these standards are such that their usefulness is limited to a narrow group of problems. Neutron fields of isotopic sources are frequently used as flux density standards. Accelerators and reactors, by means of which it is possible to obtain neutron fields of highest intensities, are currently used in the development of standard measures [3, 4]. Neutron flux densities are determined by indirect measuring methods having a minimum error approaching 1-5%. Thus obtained neutron fields can be used to calibrate direct-measuring instruments and their detectors (counters, ionization chambers, etc.). To ensure that the calibrated instruments provide the desired reliability, recommendations are given on how to estimate the influencing factors applying to conditions that are of interest to the widest possible group of users.

The results of direct measurements are most reliable when the influencing factors are either negligible or their effect can be reduced to a minimum. This can be achieved with instruments that are little sensitive to influencing factors. However, since no such instruments suitable for in-reactor operation are now available, many experimenters are compelled to abandon the above traditional metrological approach. They rather use a different way which makes it possible to neglect the majority of influencing factors. In this approach, the investigated reactor neutron fields serve at the same time as the calibration fields. Their characteristics are determined by various means and techniques of indirect and joint measurements. Each group of experimenters develops its own technique for calibrating instruments for direct measurements. Such a situation demands a fundamentally different metrological approach to direct measurements in reactors [5]. This requires the development of standard devices and methods of indirect and joint measurements and of appropriate methods of their certification, and the creation of standard instrument calibration techniques.

Naturally, since no standard technique can encompass the various possible measurement and calibration conditions, the methods should provide recommendations of a fundamental nature.

This second approach to the metrology of direct measurements in reactors is also implemented in practice. An example of such implementation are standardization studies involving calibration of direct-charge detectors and fission chambers in reactor neutron fields [3].

Metrology of Indirect and Joint Measurements

Unlike direct measurements, indirect measurements make it possible to determine practically any derivative quantity with a high degree of reliability. The results of indirect measurements of a given quantity are found by calculations based on direct measurements of fundamental and other derivative quantities related to the desired quantity in a known way. It should be noted that indirect measurements of neutron field characteristics (or any other derivative quantities) in a given sense precede direct measurements as the characteristics of standards used in direct measurements are determined on the basis of results found in indirect measurements.

Experimental relations are found from results of joint measurements of two or more quantities involved in these relations. For example, the differential neutron energy flux density is determined from a set of interrelated values of flux density and neutron energy, the former being obtained by either direct or indirect measurements and the latter by indirect measurements only.

The metrological approach to indirect and joint measurements becomes more and more important because of the increasing demands imposed on the reliability of obtained results. This explains the great interest shown by most national metrological laboratories. A metrological analysis of indirect and joint measuring techniques has been undertaken in [5]. The results proved that at the basis of these techniques lie on the one hand so-called basic quantities and relations, and on the other hand, the influencing factors. To basic quantities and relations belong: 1) the cross section or its energy dependence of a reaction; 2) the number of nuclei of a given isotope in a sample of material intended for neutron counting; 3) the rate of interaction of neutrons with the sample nuclei or the energy dependence of this interaction rate. The reaction cross section is a constant of nuclear physics which most frequently limits the reliability of measuring results in the absence of influencing factors. The number of nuclei in a sample characterizes the material composition. The interaction rate gives the number of interaction events between neutrons and the sample nuclei which is converted into an instrument reading as a result of various effects accounted for by correction factors; some of these factors can depend on constants, e.g., on the half-life of activated nuclei. It is frequently these constants and not the cross sections that limit the reliability of the measured results. In indirect and joint measurements the influencing factors allow for the effect of assumptions used in the derivation of the standard working equations for the given measuring method, approximation technique, or environmental measuring conditions.

The basic quantities and relations, together with the influencing factors, are the sole cause of neglected systematic errors and thus also the only reason for the inconsistency of measured results. From this follows that to ensure reliable indirect and joint measurements metrology must provide conditions for correct determination of the given quantities and relationships. On this basis detailed programs have been formulated for the development of metrological aids for indirect and joint measurements of neutron field characteristics; the main points of this program are:

1) analysis and establishment of most reliable standard (preferred) values of nuclear-physics constants that describe standard samples; experimental determination of new constants and of more accurate values of old ones;

2) development of standard samples of materials and methods of their metrological certification concerning the number of nuclei, isotopic composition, etc.; in neutron measurements such standards can be either isolated from the counting equipment (activation materials), or in touch with the counter (gaseous or solid materials), or placed near the counter (emitters);

3) development of standard techniques for the determination of reaction rates in a sample from instrument readings; methods of detection, allowing for, and elimination of influencing factors; techniques for indirect and joint measurements, and also methods for evaluating the reliability of measured results.

Until quite recently the program was carried out mainly by organizations of a nonmetrological character. Work in this direction proceeds in four international nuclear centers (Obninsk, Brookhaven, Saclay, and Vienna), at various international and national laboratories engaged in the production and analysis of pure materials on the basis of stable and fissionable isotopes used in nuclear measurements in reactors. Metrological laboratories are becoming more and more active in these works. These laboratories put most emphasis on the development and certification of standard samples of materials and of standard measuring techniques.

Of special importance in the problem of metrological aids to indirect and joint measurements is the comparison of measuring techniques and instruments used in experimental practice. In 1970 and 1971 the International Atomic Energy Agency carried out an international comparison of the results of indirect and joint measurements in pulse reactors. An extensive program of comparison of neutron activation means and methods is now being carried out in the USSR [3]. Actually, such comparisons allow not only the evaluation of the true state of the given field of measurement but also reveal the most urgent requirements of metrology.

Measuring Errors

At the present time the allowed error in the measurement of radiometric quantities of neutron fields in reactors does not exceed 1% [6, 7]. The permissible error of radiometric relationships approaches several percent.

In principle, an error of nearly 1% can be obtained only in the determination of thermal neutron densities by indirect measuring techniques. Similar measurements of other quantities in reactor fields of thermal and epithermal neutrons give as a rule errors of at least 5-10%. This error is even higher because of the difficulties associated with the determination of individual influencing factors and the corresponding systematic errors. Direct measurements give a similar error only if the instrument has been calibrated in the investigated field whose characteristics have been determined in advance by means of indirect or joint measurements. It must be noted that no standard methods are available at present for the estimation of errors in relationships determined on the basis of joint measurements (e.g., from neutron energy spectra). The actual error in the determination of relationships can be only approximately estimated. This error probably exceeds 10-20% even in the most favorable circumstances.

A comparison of the results of precision indirect and joint measurements carried out at different laboratories indicates that the authors often cite errors approaching the minimum theoretically attainable. At the same time, however, one frequently observes a discrepancy of results which greatly exceeds the indicated error limits. In direct measurements the discrepancies are even greater.

Developments of Metrological Laboratories

A suitable metrological approach can ensure consistent results of various reactor measurements at a level satisfying the ever-increasing practical needs. The basic aspects of this problem as applied to neutron measurements in reactors have been discussed at the First All-Union Conference on the Metrology of Nuclear Radiation [3]. The various specific developments of local metrological laboratories have been reported at this Conference.

As can be learned from the published papers [3], standard measures of thermal neutron flux density based on the NG-160 low-voltage accelerator and the F-1 graphite reactor have been developed for use in direct measurements. These measures consist of stable neutron fields with a variable flux density of 10^3 to 10^7 neutron/cm^2 · sec ± 1-2% in the accelerator and 10^5 to 10^{10} neutron/cm^2 · sec ± 2.5-7% in the reactor. Under development are standards of flux density of monoenergetic neutrons with energies ranging between 0.01 to 3 MeV and 12 to 17 MeV. Electrostatic accelerators EG-2.5 and EG-2M and type NG accelerators are used for this purpose; appropriate conditions and devices have been developed for neutron field stabilization (the neutron flux density is maintained constant to within ±0.5% for a whole day). Precision equipment has been designed for measuring the yield and flux density of neutrons by the manganese bath method, by accelerator target activation, associated-particle counting, etc. The industry manufactures instruments with counters based on hydrogen, He^4 (recoil nuclei counters), and He^3 for measuring the spectrum of neutrons with energies up to 1 MeV.

Neutron flux density standards and instruments for its measurement were designed for the calibration of radiometric, dosimetric, and spectrometric devices, for certification of neutron counters and chambers, for certification of standard samples of materials in accordance with the number of neutrons by the neutron activation method, and for precision measurement of cross sections (primarily of reference cross sections). Obviously, these problems require the application of metrological aids for direct as well as indirect and joint measurements.

To solve problems associated with indirect and joint measurements, instruments and methods are being developed for neutron activation measurements of neutron fields with energies from thermal to 20 MeV. To these devices belong sets of standard neutron-activation detectors and detectors with a fissionable

layer; radioactive γ-, β-, and α-calibration sources, neutron tracking detectors, neutron activation assemblies, activation neutron detectors, standard spectrometric γ-sources, etc. The devices included in such sets are certified by means of standard and reference setups consisting of precision equipment for measuring the activity and spectra of different kinds of radiation, standard neutron fields, etc. The list of standard detectors and sources increases continuously. Considerable attention is devoted to their metrological certification with reference to the respective quantities (number of nuclei, isotopic composition, activity, uniform distribution of nuclei, etc.). In addition to standard detectors and sources, standard methods are being developed for indirect and joint measurements of effective temperature, spectral index, flux density and density of thermal neutrons, and measurements of transport, flux density, spectral index, and energy spectra of intermediate and fast neutrons. Standard techniques are devised for calibrating instruments in reactor neutron fields with the aid of indirect and joint measurements, for evaluating the reliability of results, etc., experimental and theoretical methods are analyzed for estimating the effects of influencing factors, and much attention is devoted to ensure a unified terminology.

Modern requirements of accuracy and consistency of the results of in-reactor measurements are not always satisfied by the properties of commercially produced devices. Further metrological research can help to solve this problem. It can be expected that future developments in metrology will continue the present trends. Much attention will be probably devoted to the development of metrological aids to indirect measurements as the most accurate and to joint measurements as least studied from a metrological point of view.

LITERATURE CITED

1. Metrology. Terminology and Definitions, GOST 16263-70 [in Russian], Standarty, Moscow (1970).
2. M. F. Malikov, Principles of Metrology [in Russian], Standartov, Moscow (1949).
3. Metrology of Neutron Radiation in Reactors and Accelerators, Proceedings of the First All-Union Conference on the Metrology of Neutron Radiation (Moscow, 1971) [in Russian], Vols. 1, 2, Standarty, Moscow (1972).
4. E. Axton, Neutron Monitoring, Vienna, IAEA (1967), p. 669.
5. R. D. Vasil'ev, Principles of the Metrology of Neutron Radiation [in Russian], Atomizdat, Moscow (1972).
6. Proceedings of the First International Conference on Nuclear Data for Reactors (Paris, 1966), IAEA, Vienna (1967).
7. Proceedings of the Second International Conference on Nuclear Data for Reactors (Helsinki), IAEA, Vienna (1970).

MODERATION OF RESONANCE NEUTRONS IN MATTER

COMMUNICATION 5

D. A. Kozhevnikov, V. S. Khavkin, and V. A. Belizhanin

UDC 621.039.512.4

The spatial dependence of the neutron moderation time and the three-dimensional distribution of moderated neutrons at large distances from the source in anisotropic scattering are considered.

Analysis of the spatial dependence of the total neutron moderation time, even for simple models, makes it possible to determine the effect of the energy dependence of interaction cross sections on the neutron moderation kinetics. The following result is obtained for an arbitrary energy dependence of interaction cross sections and an arbitrary angular scattering anisotropy (the source is assumed to be isotropic):

$$\langle t(r, u)\rangle = t_s(u) + \frac{r^2}{4\tau_0(u)}\left[\frac{\tau(u)\lambda^2(u)}{1-h(u)\overline{\mu_0(u)}} + \int_0^u h(u')\tau(u')\lambda(u')\lambda_{tr}(u')\frac{du'}{\xi(u')}\right]. \quad (1)$$

This expression* has been obtained in Wigner's spectral approximation [1-4]; its scope of application is determined by the inequality $r \ll 2\tau_0(u)/\lambda_{max}$. At very large distances from the source, in the case of a narrow and deep interference minimum of the cross section, we have

$$\langle t(r, u)\rangle = t_s(u) + \frac{r}{v_{res}}, \quad (2)$$

where v_{res} is the neutron velocity at the "negative" resonance energy. If the mean free path of neutrons is constant, then

$$\langle t(r, u)\rangle = \tau(u) + \frac{2r}{u}\left(\frac{1}{v} - \frac{1}{v_0}\right). \quad (3)$$

The present article explains the contradictions between the available experimental data [5] and the calculation data obtained by means of the Monte Carlo method [6] on the basis of the obtained results and provides a theoretical interpretation of these contradictions.

Recurrent calculation of the transform of the distribution function $\psi_0^{(N)}(\zeta, u)$ for any assigned order of the angular anisotropy N is proposed for the general case of anisotropic scattering. For constant cross sections, Wigner's spectral B_1-approximation leads to the following asymptotic result:

$$\psi_0(z, u) \approx \frac{\psi_0(u)C_{-1}}{\lambda\sqrt{2\pi}}\left[4a_{-1}(u)\frac{z}{\lambda}\right]^{-1/4}\exp\left[-x_0\frac{z}{\lambda} + \sqrt{\frac{a_{-1}(u)z}{\lambda}} + a^0(u)\right] \quad (4)$$

(explicit expressions are given for the coefficients).

In the transport approximation, the canonic transport equation corresponds to the generalized Weinberg–Wigner–Korngold–Orlov equation, where the generalized Placzek function is determined by the expression

$$R\begin{pmatrix} u' \to u \\ \omega' \to \omega \end{pmatrix} = \frac{1}{4\pi}R_0(u' \to u) + \frac{1}{4\pi}R_1(u' \to u)\{\delta[(\omega'\omega) - 1] - 1\}, \quad (5)$$

* The notation used is defined in the article.

Translated from Atomnaya Énergiya, Vol. 34, No. 4, pp. 283-284, April, 1973. Original article submitted December 16, 1971.

where

$$R_1(u' \to u) = \frac{\overline{\mu_0(u)}}{1-\overline{\mu_0(u)}}\,\delta(u-u').$$

For the single negative resonance model, using Wigner's transport approximation for large distances from the source, we write the following:

$$\psi_0(z, u) = B(u)\,F(z)\,[1+0(e^{-z/\lambda^*})],$$

$$F(z) \approx \frac{b\sqrt{\pi K(z)}}{a^2 z}\ln^{-2}\left(\frac{z}{a\Lambda_{tr}}\right)\exp\left(-\frac{z}{\Lambda_{tr}}+\frac{b}{a}\right),$$

where K(z) is a slowly varying function of z; the coefficients a and b are determined. The asymptotic result corresponding to the constant cross section model is given in the article.

LITERATURE CITED

1. D. A. Kozhevnikov and V. S. Khavkin, At. Energ., 27, 142 (1969).
2. D. A. Kozhevnikov and V. S. Khavkin, ibid., 27, 143 (1969).
3. D. A. Kozhevnikov and V. S. Khavkin, ibid., 29, 365 (1970).
4. D. A. Kozhevnikov and V. S. Khavkin, ibid., 29, 448 (1970).
5. A. Takahaschi and K. Sumita, J. Nucl. Sci. Technol., 4, 503 (1967).
6. S. Chen and I. Lidofsky, Nucl. Sci. and Engng., 29, 198 (1967).

CALCULATION OF THE EFFECTIVE ATTENUATION FACTOR OF γ-RADIATION IN A MICROSCOPICALLY INHOMOGENEOUS MEDIUM

L. I. Shmonin and G. K. Potrebenikov

UDC 539.173

A method is shown for calculating the effective attenuation factor for γ-radiation in a homogeneous continuous medium H in the form of a barrier with plane boundaries which contains occlusions (granules) of another material A randomly distributed throughout its volume. The fraction of the volume occupied by the occluded material A is small ($v \ll 1$). A plane unidirectional source of radiation of energy E was chosen.

The behavior of the effective attenuation factor of γ-rays with energy E was studied as a function of the size of the occlusions, their shape, and orientation relative to the direction of propagation of the γ-rays. In this study occlusions were of the same size distributed randomly with a Poisson distribution. Their shape was either spherical or one of several convex figures (e.g., cube, tetrahedron, octahedron, ellipsoid of rotation) oriented in a certain way relative to the direction of propagation of the γ-radiation. A formula for the effective linear attenuation factor μ' was obtained:

$$\mu' = \mu - Bv\Delta\mu\sum_{n=1}^{\infty}\frac{(-1)^{n-1}(n+k)C^n[v_1^{1/3}\Delta\mu]^n}{(n+i)!},$$

where $\mu = \mu^A v + (1-v)\mu^H$ is the average linear attenuation factor of a homogeneous mixture of components A and H, $\Delta\mu = \mu^A - \mu^H$; v_1 is the volume of one granule; B, C, k, and i are parameters whose values are determined by the form and orientation of the occlusions. The article gives values of B, C, k, and i which were calculated for various special cases.

The effective attenuation factor μ' is less than the average linear attenuation factor μ by an amount which increases with the size of the occlusions. This result agrees with calculations which have been made

Translated from Atomnaya Énergiya, Vol. 34, No. 4, p. 284, April, 1973. Original article submitted January 31, 1972.

by other workers. In the present article it is shown that for a medium containing occlusions of compact shape (spherical or regular polyhedra), variations in the shape or orientation of the occlusions can cause the effective and average attenuation factors to differ by at most 10%, provided that $v_i^{1/3}\Delta\mu > 0.5$. For highly deformed occlusions (prolate or oblate ellipsoids), the attenuation properties of the medium may depend critically on their form, especially if the orientation of these occlusions relative to the direction of propagation of the γ-rays is clearly defined.

It was proven that measurements of the effective attenuation factor of an absorber can be used to determine the size of foreign occlusions distributed throughout the volume of the absorber.

γ-SCANNING DISTRIBUTION OF HEAVY ELEMENTS OVER POLISHED SECTIONS OF SPENT FUEL ELEMENTS

V. K. Shashurin, E. F. Davydov,
A. V. Sukhikh, and M. I. Krapivin

UDC 621.039.548:621.039.84

The relative distribution of heavy elements over the area of polished sections cut from spent fuel elements may be useful in studies of the intensity of characteristic x-radiation induced by γ-emission on the part of fission products. Because of the high average energy, and the concomitant adequate penetrability of the exciting radiation in studies of fuel elements where cooldown times stretch beyond three months in some instances, the distribution of fission-product activity over the area of the polished section need not be taken into account, and that simplifies the interpretation of results of measurements of the intensity of x-radiation. The β-emission from the fission products does not produce any substantial x-radiation from the heavy elements because the interaction cross section is so small compared to that for γ-emission.

An experimental verification was carried out on a facility designed for studying the distribution of radioactive isotopes by the γ-scanning method [1]. A standard Ge(Li)-detector was employed to identify peaks due to recording x-radiation on spectra obtained in the investigation of the polished sections.

The article cites results of measurements of the distribution of some fission products and the distribution of heavy elements, obtained by the proposed method, over the diameter of a polished section of the fuel element, which contained pellets of uranium monocarbide enriched to 6% burnup, and where cooldown times were of the order of one year.

LITERATURE CITED

1. A. V. Sukhikh et al., At. Energ., 32, No. 4, 318 (1972).

Translated from Atomnaya Énergiya, Vol. 34, No. 4, pp. 284-285, April, 1973. Original article submitted February 10, 1972.

DISTRIBUTION OF NEUTRONS IN WORKROOMS AT NUCLEAR INSTALLATIONS

L. S. Andreeva, A. A. Savinskii, and I. V. Filyushkin

UDC 539.12.08

The paper describes rather simple relationships from which one can obtain the characteristics of a field of neutrons scattered by the floor, walls, and ceiling of a one-room experimental hall. The given relationships were obtained as a result of measurements of the scattered-neutron field using the many-sphere spectrometry method in three experimental halls of different sizes, and also based on published data on the neutron albedo.

The following general laws were established for the formation of a scattered-neutron field in an experimental hall: 1) if the point neutron source is near the geometrical center of the hall the scattered-neutron flux is constant over the hall volume; this holds also for the case in which the neutron source is part of the floor or wall; 2) the angular distribution of the scattered-neutron flux is isotropic; 3) the scattered-neutron spectrum for a monochromatic source is Fermian.

The flux of fast and intermediate scattered neutrons in a one-room hall shaped like a parallelepiped with concrete walls, floor, and ceiling can be determined from the relationship

$$\Phi_{scat}=\frac{0{,}4A}{4\pi R^2_{eff}}.$$

Here, A is the source output into 4π (or into 2π if only part of the floor, wall, or ceiling is studied), and

$$R^2_{eff}=\frac{1}{3}\sum_{i=1}^{3}\frac{1}{R_i^2}(1-\cos^3\alpha_i),$$

where R_1, R_2, and R_3 are the half-length, half-width, and half-height of the hall, respectively:

$$\alpha_i=\operatorname{arctg}\left(\frac{4R_jR_k}{\pi R_i}\right)^{1/2}.$$

It is established that the unit dose equivalent (kerma) of scattered neutrons is a factor of 5.4 smaller than the analogous values for the source neutron spectrum.

The relationships given hold at least for experimental halls whose length-to-width ratio does not exceed 3 : 1. The article compares calculated scattered-neutron field characteristics with the measured characteristics; practical applications of the given relationships are also examined.

The relationships found between a flux of neutrons "injected" into a one-room experimental hall and the space–energy distribution of the fluxes of neutrons scattered in it can be used for determining the equivalent dose power behind a biological shield, for determining the background of neutrons ejected through experimental channels, for choosing the experimental-hall dimensions from the allowable size of the scattered-neutron background, for determining hardness dependence of individual neutron dosimeters, etc.

Translated from Atomnaya Énergiya, Vol. 34, No. 4, p. 285, April, 1973. Original article submitted April 17, 1972.

EFFICIENCY OF THE DECONTAMINATION SYSTEM FOR RADIOACTIVE-GAS WASTE AT THE VK-50 ATOMIC POWER STATION

E. K. Yakshin, A. G. Cherepov,
Yu. V. Chechetkin, B. R. Keier,
and G. Z. Chukhlov

UDC 621.039.524.4-97.621.039.72

Dynamic adsorption of krypton and xenon from the gas flow by activated carbon is now widely used for lowering the radioactivity of gaseous wastes at single-circuit atomic power stations having boiling-water reactors. This principle is the basis of the decontamination system at the VK-50 atomic power station.

The system efficiency (decontamination factor K) depends on the gas-adsorption coefficients of the carbon (see Table 2), the carbon volume V, the gas flow rate G, and the composition of radioactive gaseous isotopes entering. Table 1 shows the relative composition and activity of the radioisotopes in gaseous wastes (the radioactivity of Kr^{87} is taken as unity).

Using the adsorption coefficient and composition of the isotopes, we find K (see Table 3) for the given carbon temperature T and ratio V/G. Table 3 can be used to determine the size of the adsorption site.

We expect that the flow rate of ejector gases (mainly air) of 1000-1500 MW industrial atomic power stations reaches 100-200 m^3/h, while the radioactivity is several hundred thousand curies per day. Decontamination by a factor of 200-300 will lower the radioactivity to allowable safety norms; the carbon volume at 25°C will be about 200 m^3. This is a huge installation. Decreasing the volume of gaseous wastes to 0.03 $m^3/h \cdot MW$ (elec.) and cooling the carbon to −25°C presents no technical problems. With such parameters, the given decontamination factor can be achieved by using 10-15 m^3 of carbon.

TABLE 1

Kr^{85}	Kr^{83m}	Kr^{85m}	Kr^{87}	Kr^{88}	Kr^{89}	Kr^{90}	Xe^{131m}	Xe^{133}	Xe^{135}	Xe^{135m}	Xe^{137}	Xe^{138}	Xe^{139}
$4{,}5 \cdot 10^{-4}$	0,1	0,55	1,0	0,8	6	1	$1{,}5 \cdot 10^{-3}$	0,8	2	3	9	9	2

TABLE 2. Dependence of the Krypton and Xenon Adsorption Coefficients on Temperature, cm^3/g

Temperature, °C	Kr	Xe
40	40	530
20	57	1 000
0	84	1 820
−20	130	3 600
−40	230	8 400
−60	420	24 400

TABLE 3. Decontamination Factor for Radioactive Gaseous Wastes

V/G, h	T, °C				
	25	0	−10	−20	−40
0,05	13	16	20	28	50
0,1	20	27	35	50	160
0,2	35	60	90	160	1 300
0,5	90	320	850	2 900	62 000
1,0	300	3 500	18 400	58 000	76 000
1,5	1000	24 000	66 000	75 000	76 000
2,0	3000	60 000	75 000	76 000	76 000

Translated from Atomnaya Énergiya, Vol. 34, No. 4, pp. 285-286, April, 1973. Original article submitted June 12, 1972.

HIGH BURNUP IN URANIUM CERMET ALLOYS*

A. I. Voloshchuk, V. V. Votinova,
Yu. M. Golovchenko, A. Ya. Zavgorodnii,
V. F. Zelenskii, Yu. F. Konotop,
and R. A. Timchenko

UDC 621.039.543.45:669.822.5

Results of irradiation of uranium hardened by disperse particles of beryllium oxide [1, 2] and of alloys containing molybdenum, aluminum, and some additions of iron and silicon, in the SM-2 reactor in capsules, and under conditions of free swelling at temperatures in the 250-600°C range and at maximum thermal loads from 30 to 250 W/g are reported. Different burnup levels from 0.4% to 3% were attained in one experiment through the use of differentially enriched uranium.

The following basic findings were obtained.

1. In the case where high burnup is attained through intensifying the fission rate, the burnup level exerts no decisive influence on swelling of the alloys (within the range of burnup level investigated). At low irradiation temperatures (250-350°C), swelling of alloys with 0.4% and 3% burnup is practically the same. At temperatures 450-600°C, swelling of some alloys with 0.4% burnup is found to be greater than in the case of alloys with 3% burnup.

2. Irradiation at low temperatures and high fission rates is accompanied by the formation of porosity predominantly of vacancy derivation, in contrast to high-temperature irradiation, when pore growth is brought about by excess pressure exerted by gaseous fission fragments. Intensive swelling is observed in the case of heterogeneous alloys containing molybdenum and aluminum.

3. A tendency toward the formation of a honeycomb or block-mosaic structure is observed in the structure of the irradiated specimens. Cracks or voids show up preponderantly on the boundaries of the mosaic blocks. Disperse beryllia particles contribute to the formation of a fine mosaic structure, which is viewed as one of the reasons for the high radiation stability of dispersion-hardened uranium.

LITERATURE CITED

1. V. E. Ivanov, At. Energ., 29, 178 (1970).
2. A. I. Voloshchuk, ibid., 29, 416 (1970).

AUTORADIOGRAPHY OF MICROSEGREGATIONS IN A RADIOACTIVE MATRIX†

V. N. Chernikov and A. P. Zakharov

UDC 620.18+620.183.6

The radiation signal/background ratio in the plane of the surface of a test object above a source of radiation acting in the specimen is calculated as a function of the ratio of the concentration of radioactive isotope in the specimen to the isotope concentration in the surrounding matrix, and also as a function of other parameters determined by the mode of radiation, by the material comprising the test object, and by

* Translated from Atomnaya Énergiya, Vol. 34, No. 4, pp. 286-287, April, 1973. Original article submitted July 24, 1972.
† Translated from Atomnaya Énergiya, Vol. 34, No. 4, pp. 287, April, 1973. Original article submitted August 28, 1972.

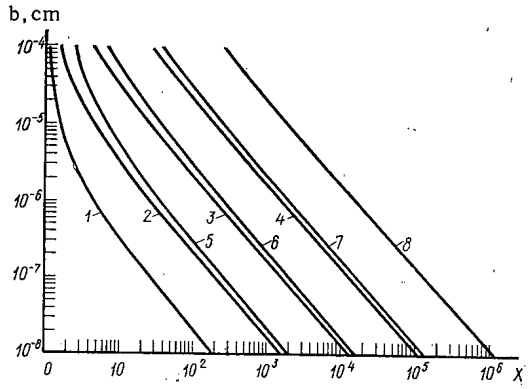

Fig. 1. Two series of curves plotted on the basis of Eq. (1).

the geometry of the source to begin with. Sources considered are uniformly activated semiinfinite boundaries (of width b) and cylinders (of radius r_0) oriented perpendicular to the surface of the specimen as well as a sphere (radius r_{sph}) situated at a distance h from the surface of the object. The radiation signal/background ratio resulting in the case of a specific source of radiation uniquely and completely specifies the signal/background ratio in its autoradiographic image if the experiment is conducted within the region of normal exposures on the characteristic curve of the photodetector employed. That applies to conventional autoradiographic procedures in which comparatively thick emulsion layers [1] are used, and equally well to the method of electron-microscopic autoradiography [2, 3].

In all cases, the same law for the dependence of the radiation signal/background ratio (Y) on the ratio of the isotope concentrations in the source and in the matrix (X) holds:

$$Y = (1 - \eta) X + \eta, \quad (1)$$

where η is a variable determined by the mode of radiation, by the stopping power of the material and by the geometry of the system. Analytical expressions for the coefficients η were derived in general form. An electronic computer was employed to calculate the relationships for several concrete cases, on the basis of Eq. (1), and the results were displayed in graphical form.

As an example, Fig. 1 here shows two series of curves (1-4 and 5-8) constituting the relationships between the width of the semiinfinite boundary b and the minimum ratio of concentrations of β-emitter in the boundary and in the matrix X needed in order for the quantity Y–1 to be 0.1 in the plane of the object above the source, for the first series of curves, and correspondingly 1.0 for the second series of curves. Within each distinct series of curves, the values of linear absorption coefficients of the matrix are distinguished, and found to be 10^4, 10^3, 10^2, and 10 cm^{-1}, respectively.

The results we arrived at enable us, on the basis of autoradiographic data, to obtain quantitative information on fine details of the inner structure of the test object, and also provide information on certain limitations of the autoradiographic method.

LITERATURE CITED

1. B. I. Bruk, Autoradiographic Investigation of Metals [in Russian], Sudostroenie, Leningrad (1966).
2. S. Z. Bokshtein, Structure and Properties of Metal Alloys [in Russian], Metallurgiya, Moscow (1971).
3. V. N. Chernikov et al., At. Energ., 31, 509 (1971).

CALCULATION OF INNER-GROUP FAST NEUTRON SPECTRA

V. N. Gurin, V. S. Dmitrieva, and G. Ya. Rumyantsev

UDC 621.039.51

A detailed knowledge of the spectra of neutrons in energy groups is needed to solve a number of the problems arising in fast reactor physics. To solve such problems, one needs to analyze the experimental results obtained in measuring spectra in various sections of a fast reactor, and also to obtain more accurate

Translated from Atomnaya Énergiya, Vol. 34, No. 4, p. 288, April, 1973. Original article submitted October 2, 1972.

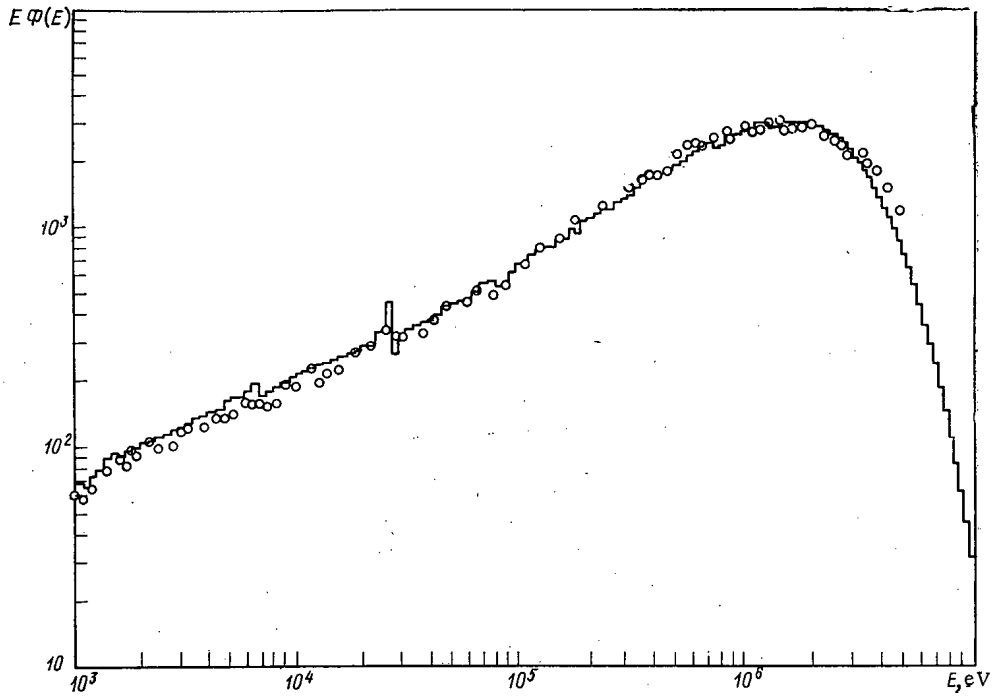

Fig. 1. Neutron spectrum in a fast hydrogen assembly [1]. The histogram was calculated by means of a computer; the points represent experimental results.

constants pertaining to the physics of grouped neutrons (mainly their elastic moderation cross sections). A special "spectral" program, employing a large number of groups, is used to compute the spectra.

The algorithms of such programs are usually based on the solution of Fourier-transformed neutron moderation equations in the P_1 approximation, which is equivalent to the solution of a problem involving energy alone. Elastic moderation is taken into account either in matrix form, or within the framework of a continuous moderation model.

An effective algorithm based on the Gruling–Herzl continuous moderation model is proposed for the detailed calculation of neutron spectra. The amount of input information needed to calculate elastic moderation is much less when this algorithm is used than when the calculation is done by a matrix method. An essential feature of this algorithm, which distinguishes it from those described in the literature, is that it may be used for zones whose neutron spectra have considerable space dependence. The appropriate computer program was written (with the code name ChGG), and a library of microcross sections and elastic scattering anisotropy parameters was assembled.

The calculated spectra are compared with experiments at two fast assemblies [1, 2]. The calculated results for one assembly [1] are shown in Fig. 1.

LITERATURE CITED

1. S. Cohen et al., Nucl. Sci. Eng., 37, 111 (1969).
2. C. Preskitt, J. Neill, and C. Stevens, Trans. Am. Nucl. Soc., 11, 1 (1969).

EFFECT OF BURNUP OF INDIUM ON THE MELTING POINTS OF γ-CARRIERS OF HOT LOOPS

D. M. Zakharov, G. I. Kiknadze, and R. B. Lyudigov

UDC 621.039.553:669.872

In In–Ga and In–Ga–Sn γ-carriers radiative capture by In^{115} nuclei takes place by the following reaction: $_{49}In^{115} + n \rightarrow {}_{49}In^{116m} + \gamma$. As it decomposes, the radiative isotope $_{49}In^{116m}$ ($T_{1/2} \approx 54$ min) is converted to the stable isotope $_{50}Sn^{116}$. This burnup of indium increases the tin content by replacement of the indium; the binary indium–gallium γ-carrier is converted to a ternary indium–gallium–tin alloy, and in the ternary alloy the tin content is higher than that of the eutectic alloy. It is therefore important to assess the effect of accumulation of tin on the liquidus temperature of the alloys formed. A qualitative solution of this problem may be obtained on the basis of the concentration triangle of the system gallium–indium–tin [1]. Prokhorenko et al. [2] have established that the eutectic alloy contains 67 wt.% gallium, 20.5 wt.% indium, 12.5 wt.% tin, and that the melting point of the eutectic is 10.6°C.

Figure 1 shows the concentration triangle of the system gallium–indium–tin; owing to the absence of reliable data, the binary eutectic curves are represented by straight lines, but this has no effect on our argument.

During burnup of indium from the binary indium–gallium alloy of eutectic concentration (the alloy has 20.5 wt.% indium and the melting point is 15.8°C [3]) the composition of the γ-carrier changes in the direction shown by the arrow dk. The liquidus temperatures of the ternary alloys formed within the limits of the sector *abed* will not differ appreciably from the eutectic temperature. This follows from the fact that the liquidus surface *abed* is bounded by low temperatures: the melting point of gallium (29.8°C) and the melting points of gallium–tin (20°C), indium–gallium (15.8°C), and gallium–indium–tin (10.6°C) eutectics.

During burnup of indium from the ternary alloy indium–gallium–tin of eutectic concentration, an increase in the tin content will displace the composition of the ternary alloy from the lowest (temperature-wise) point e onto the liquidus surface benm in the direction shown by the arrow ef. Owing to such displacement the liquidus temperatures of the alloys increase; this is attributable to the fact that the surface benm is bounded by the fairly high melting points of tin (232°C) and the indium–tin eutectic (171°C).

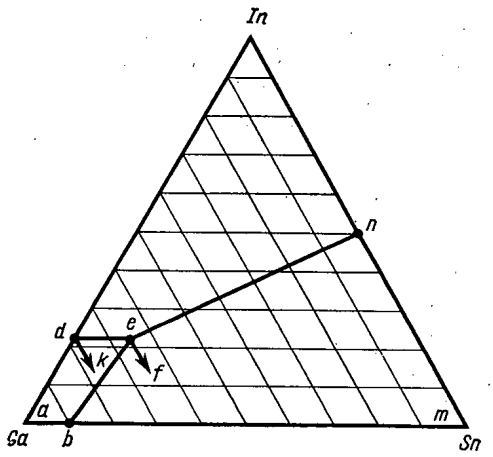

Fig. 1. Concentration triangle of the system gallium–indium–tin.

These conclusions were experimentally confirmed. Burnup of indium in these liquid metal systems may be modeled by replacing indium by a corresponding amount of tin (the gallium content is constant in all cases and remains equal to the eutectic concentration). The problem reduces to determination of the temperature of the end (or beginning) of phase transition due to fusion (or crystallization) of the tin phase (we have in mind burnup of indium from the ternary alloy indium–gallium–tin) or of the gallium phase (during burnup of indium from the binary indium–gallium alloy).

In this experimental work the liquidus temperatures of these alloys were determined from the curves obtained by

Translated from Atomnaya Énergiya, Vol. 34, No. 4, pp. 289-290, April, 1973. Original article submitted May 18, 1972.

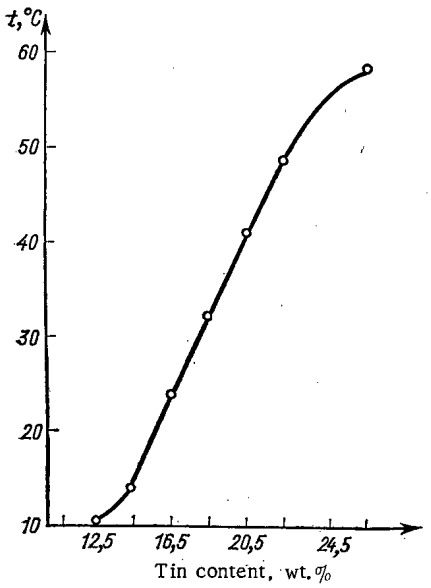

Fig. 2. Melting point of γ-carrier, plotted vs burnup of indium from the ternary alloy indium–gallium–tin of eutectic concentration.

plotting the electrical conductivity vs temperature. For these measurements we used the contact method; they were performed in a specially-designed conductometric apparatus developed in the Institute of Physics of the Georgian Academy of Sciences.

Figure 2 shows the increase in the liquidus temperature during burnup of indium from the ternary alloy indium–gallium–tin of eutectic concentration. The temperature was determined to within ±0.1°C.

All the measurements were performed as the alloys were heated, so that the liquidus temperatures correspond to transition of the two-phase state of the system to the one-phase state, corresponding to the completion of fusion of the tin phase. Such a transition cannot always be determined on the basis of thermal curves obtained in an apparatus of the Kurnakov pyrometer type; however, it can be recorded exactly by measuring the electrical conductivity (a structure-sensitive property).

Note that burnup of indium from a binary indium–gallium alloy of eutectic concentration somewhat reduces the melting point of the γ-carrier. The experimental data show in particular that when indium burnup is 50% the liquidus temperature of the ternary alloy indium–gallium–tin formed is 14.9°C (the initial melting point of the binary γ-carrier is 15.8°C).

We also investigated the dynamics of indium burnup. We determined the reduction in the indium concentration after operation of a hot loop for one year.

Indium burnup in 1 cm^3 of γ-carrier in 1 sec may be calculated from the equation:

$$P = \frac{A}{N} \cdot \frac{\sigma_{act}}{\sigma_{abso}} \bar{\varphi} \Sigma_{act},$$

where A is the atomic weight of the isotope $_{49}In^{115}$; N is the Avogadro number; σ_{act} and σ_{abso} are, respectively, the microscopic cross sections of activation and absorption of neutrons by $_{49}In^{115}$; $\bar{\varphi}$ is the mean neutron flux in the activation zone; and Σ_{act} is the macroscopic activation cross section of this isotope.

If one assumes that $\bar{\varphi} = 10^{13}$ neutrons/$cm^2 \cdot$ sec, the value of P will be $16.7 \cdot 10^{-10}$ g/($cm^3 \cdot$ sec). It can now be readily seen that the loss of indium in the γ-carrier after operation of the hot loop for one year is 0.82 wt.%, and after five years 4.1 wt.%. Thus burnup of indium in liquid metal γ-carriers does not lead to insuperable difficulties. Losses of indium due to burnup can be made good by topping up the γ-carrier with indium from time to time, or simultaneously with indium and gallium. This enables one to control the melting point of the γ-carrier, i.e., to reduce it where necessary, and to restore the radiation power of the loop.

We thank Z. P. Danelyan and Yu. B. Klyuzner for their help with the experiment.

LITERATURE CITED

1. H. Spengler, Z. Metallkunde, 46, 464 (1955).
2. B. Ya. Prokhorenko et al., Teplofiz. Vys. Temp., 2, 374 (1970).
3. G. I. Kiknadze et al., At. Energy., 19, 178 (1965).

DIFFUSION OF CARBON IN BERYLLIUM OXIDE

V. P. Gladkov, V. S. Zotov, and D. M. Skorov

UDC 539.125.525

Self-diffusion of beryllium and oxygen in beryllium oxide is dealt with in a number of communications (for example [1]), but the literature gives very little information on diffusion of impurities.

We have studied diffusion of C^{14} in sintered beryllium oxide. The diffusion source was a layer of elementary carbon deposited in the form of a suspension in cellulose nitrate varnish on the surfaces of plane-parallel specimens.

Diffusion annealing was performed in a TVV-4 furnace with a tungsten heater in a vacuum of not less than 10^{-4} torr. After annealing the integral radioactivity of the residue of the specimen was determined by layerwise measurement (G. L. Gruzin's method). From the data thus obtained we calculated the coefficient of diffusion of carbon in beryllium oxide at five different temperatures:

T, °C	D, cm^2/sec
1250 ± 20	$(6.0 \pm 2.0) \cdot 10^{-12}$
1427 ± 10	$(7.5 \pm 0.5) \cdot 10^{-11}$
1540 ± 15	$(2.3 \pm 0.4) \cdot 10^{-10}$
1670 ± 40	$(5.1 \pm 0.6) \cdot 10^{-10}$
1800 ± 30	$(1.6 \pm 0.3) \cdot 10^{-9}$

The temperature dependence of the coefficient of diffusion of carbon in beryllium oxides may be represented as follows:

$$D_{C \to BeO} = (4 \pm 1) \cdot 10^{-3} \exp\left[-(60.4 \pm 0.9)/RT\right] \text{ cm}^2/\text{sec}.$$

The diffusion parameters of C^{14} thus obtained coincide with the analogous values of diffusion of Be^7 in unirradiated beryllium oxide [1].

In the range 1150-1180°C the temperature dependence of diffusion of Be^7 is as follows [1]:

$$D_{Be \to BeO} = 2.49 \cdot 10^{-3} \exp\left(-62.5/RT\right) \text{ cm}^2/\text{sec}.$$

The similarity of the activation energies and preexponential factors indicate that the diffusion mechanism of beryllium and carbon in beryllium oxide is apparently the same. Calculations show [2] that the energy of formation of a vacancy in beryllium oxide is very high (45.4 eV), so that vacancies could hardly be involved in transfer of the substance. However, the energy of formation of interstitial defects is much lower (by nearly one order of magnitude [2]). It may be assumed that, like self-diffusion of beryllium in beryllium oxide, diffusion of carbon in the latter is effected by an interstitial mechanism.

LITERATURE CITED

1. H. Bruin and G. Watson, J. Nucl. Mater., 14, 239 (1964).
2. A. Pryor, ibid., 14, 258 (1964).

Translated from Atomnaya Energiya, Vol. 34, No. 4, pp. 290-291, April, 1973. Original article submitted April 6, 1972; revision submitted December 13, 1972.

DETERMINATION OF THE INTEGRAL PARAMETERS OF THE INTERACTION OF NEUTRONS WITH CARBON

V. T. Shchebolev

UDC 539.125.5.17

Our experimental arrangement was part of a standard neutron flux apparatus. As shown in Fig. 1, it consists of a graphite sphere of diameter a = 4 m with a central cavity of diameter a' = 0.04 m.

Wallace [2] found the thermal neutron distribution function in a moderator of this form for fast neutrons from a point or distributed source giving a flux Q. The thermal neutron density $\rho(r)$ at a distance r from the center of the source has the form

$$\rho(r)=\frac{QT}{2\pi}\sum_{m=1}^{\infty}\frac{(-1)^{m+1}\alpha_m\sqrt{1+(a_1\alpha_m)^2}}{a+(a-a_1)(a\alpha_m)^2}\times\frac{\sin\alpha_m(a-r)}{r}\cdot\frac{e^{-\alpha_m^2\tau_0}}{1+\alpha_m^2L^2}, \quad (1)$$

where α_m is a root of the transcendental equation $\tan\alpha(a-a_1) = -a_1\alpha$; $\sqrt{\tau_0} = L_S$ is the slowing down length of thermal neutrons; L is the diffusion length; and T is the lifetime of thermal neutrons. Analysis of Eq. (1) shows that in media with $L > L_S$ there is a spherical layer of average radius r_0 at each point of which the thermal neutron density is independent of the source spectrum in the range ~0.5-15 MeV.

We consider the quantity

$$b(r)=\frac{N(r)}{\int N(r)\,r^2\,dr}, \quad (2)$$

where $N(r) = N'(r) - N_{Cd}(r)$; $N'(r)$ is the thermal neutron detector counting rate at point r in the moderator; and $N_{Cd}(r)$ is the counting rate due to epicadmium neutrons and the background of accompanying radiation.

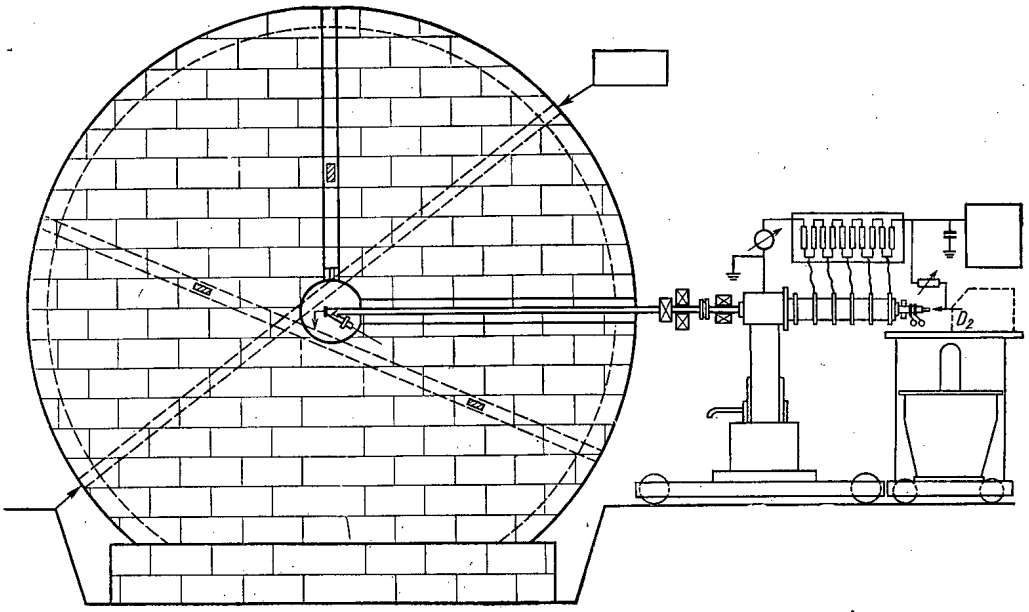

Fig. 1. Schematic diagram of experimental arrangement.

Translated from Atomnaya Énergiya, Vol. 34, No. 4, pp. 291-293, April, 1973. Original article submitted November 10, 1971; revision submitted January 19, 1973.

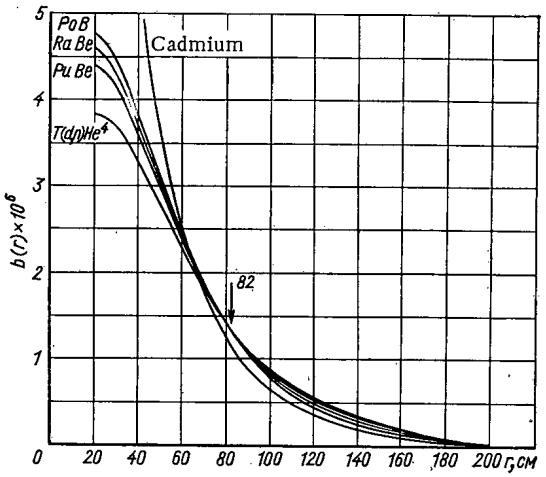

Fig. 2. Normalized thermal neutron distribution curves in graphite.

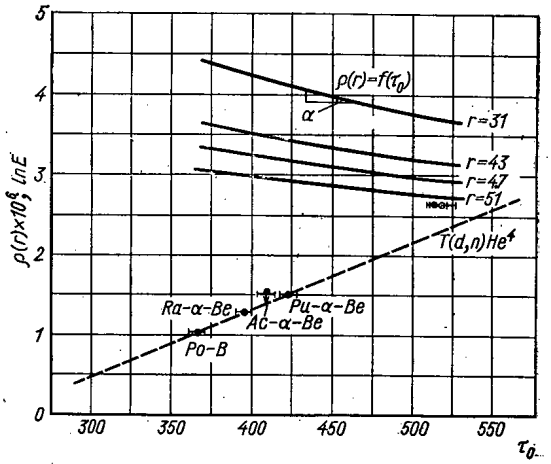

Fig. 3. Determination of the age and mean energy of neutrons from various sources: ○, ●) data obtained at FIAN and VNIIM respectively.

TABLE 1. Measured Values of Slowing Down Length

Neutron source	L_s, cm	E_i, MeV
T (d, n) He^4	22,70	14,1
Pu—Be (α, n)	20,54	4,5
Ac—Be (α, n)	20,22	4,6
Pa—Be (α, n)	19,91	3,6
Po—B (α, n)	19,11	2,8
T (d, n) He^4 [6]	22,78	14,1

Assuming that the thermal neutron counting efficiency is independent of r we find $b(r) = k\rho(r)$, where k = const. It follows from (2) that $\int b_i(r)r^2dr = 1$, where the subscript i indicates that the curve $b_i(r)$ is obtained for a source which yields a flux Q_i of neutrons of energy E_i.

It should be noted that b(r) is independent of the properties of the detector and the counting equipment. Figure 2 shows the experimental results for the sources T(d, n) He^4, Pu—Be(α, n), Ra—Be(α, n), Po—B(α, n), and a thermal source (Cd). They show that in graphite the region of constant sensitivity is at a distance of 0.82 m; i.e., the results agree with the theory. The same result was obtained with Po—Be(α, n), Ac—Be(α, n) sources and with a spontaneous Pu^{240} source. However, the sensitivity for a Ra—Be(γ, n) source was approximately 4.8% lower, and that for the thermal (Cd) source about 13% lower.

If a spherically symmetric source of thermal neutrons is placed in a cavity in a moderator the density distribution is given by

$$\rho(r) = \frac{QT}{4\pi L^2\left(1+\frac{a_1}{L}\right)} \cdot \frac{e^{-\frac{r-a_1}{L}}}{r}. \qquad (3)$$

A thermal neutron source was obtained by placing a cadmium sphere in a cavity in the graphite sphere and a fast neutron source at its center. A series of accurate measurements showed that the diffusion length L = 0.520 ± 0.002 m.

The fact that the functions $\rho_i(r)$ and $b_i(r)$ can differ only by a multiplicative constant permits the determination of the neutron age τ_{0i} by a comparison of these curves provided that at the point r_0 where the spectral sensitivity is constant $\rho_i(r_0) \equiv b_i(r_0)$. They must agree at all values of r if the correct values of τ_{0i} and L are used in the calculation.

Since the relation $\rho = \rho(r, \tau_0, L)$ cannot be expressed in terms of elementary functions with a factor τ_0, the age was determined by a trial and error minimizing of the dispersion of the equation obtained.

In the 0.3-0.6 m region where the function $\rho(r, \tau_0, L)$ is most sensitive to a change in τ_0 the experimental and calculated values of the density of thermal neutrons from the T(d, n)He^4 reaction agree within 0.2-0.4%.

In determining the age by the method proposed the error $\delta\tau_0$ depends on the errors of the experimentally determined quantities $N(r) \approx \rho(r)$ and L.

If it is assumed that the dispersion $D(L) = 0$ the dispersion $D(\tau_0)$ is found from the relation $\rho(r) = f(\tau_0)|_{L=\text{const}}$. Then we obtain $D(\rho) = \tan^2\alpha D(\tau_0)$ (Fig. 3). The average value of $1/\tan\alpha \approx 2 \cdot 10^8$, and the mean square error $S(\rho) \leq 10^{-8}$. In addition it can be assumed that $\delta\rho = k\delta\tau_0|_{L=\text{const}} = k\delta L|_{\tau_0=\text{const}}$, i.e., $\delta\tau_0 = \delta L$ for $D(\rho) = 0$. Thus the maximum error in determining the age is $\delta\tau_0 = \delta\rho + \delta L = 0.8\%$.

Table 1 lists the measured values of $L = \sqrt{\tau_0}$ in graphite with a diffusion length of 0.520 m for neutrons emitted by various sources; the average energies are taken from [3-5].

It is easy to see that the ages of neutrons from the reaction $T(d, n)He^4$ determined by a pulsed method [6] (error ~2%) and by our method (error 0.8%) agree. This indicates that there are no significant systematic errors in these measurements.

Figure 3 shows the relation $\ln E_i = f(\tau_{0i})$ which should be a straight line according to Marshak's theory for 2 MeV < E_i < 5 MeV. If it is assumed that the mean energies of the neutrons from Po–B, Ra–Be, and Pu–Be sources have been determined correctly, the mean energy of neutrons from an Ac–Be source, measured by the method of nuclear recoil, is an overestimate; it should be taken as 4.1 MeV. A similar conclusion was drawn in [7] where the fraction of neutrons with energies below 1 MeV in the spectrum of an Ac–Be source was determined.

LITERATURE CITED

1. V. T. Shchebolev, Trudy Metrologicheskikh Institutov SSSR, 89 (149), 133 (1967).
2. P. Wallace, Nucleonics, 4, No. 2 (1949).
3. J. De Pangher, J. Nucl. Instrum. and Methods, 5, 61 (1959).
4. K. Yeiger and J. Jarvis, Canad. J. Phys., 40, 33 (1962).
5. O. Runnals and R. Boucher, ibid., 34, 949 (1956).
6. Z. Dlougly, Atomnaya Energiya, 9, 182 (1960).
7. B. N. Krylov and V. I. Fominykh, Trudy Metrologicheskikh Institutov SSSR, 124 (184), 198 (1970).

A PROCEDURE FOR COMPARING VARIOUS ATOMIC ELECTRIC POWER PLANT SYSTEMS

G. P. Verkhivker

UDC 621.039.553.34

Comparing various thermal systems of atomic electric power plants (AEP) is much more complicated than comparing systems of thermal electric power plants (TEP) operating on fossil fuels. A change in efficiency at constant electric power leads to a change in thermal power, and consequently to changes in the capital investments in the reactor and the fuel component, determined not only by the thermal but also by the neutron-physical design. The comparison of different versions is simplified by assuming that the thermal power of the reactor is constant. Then the cost of the reactor and the fuel component remains unchanged for all versions of one kind of reactor; the change in electric power is compensated by the electric power output of a replacement plant which operates on fuel, closing the power balance in the economic region under consideration.

This is particularly true of reactor-multipliers which combine the generation of electric power with the production of secondary fuel, proportional to the neutron flux and consequently also to the thermal power. Since making secondary fuel is very important for the development of nuclear power, it seems that the thermal power of reactor-multipliers of a given type should be chosen as large as possible, and an AEP should operate in the base load band of the load curve [1]. With such an arrangement the popular notion that fast reactor power plants have a low efficiency when the fuel component is small turns out to be wrong. A change in efficiency will not lead to a decrease in the amount of nuclear fuel consumed by a particular atomic power plant, but to a saving in the fuel inventory, which is known to be the most expensive for a given economic region.

To derive analytic relations determining the effectiveness of various changes in an AEP we use the idea of a "basic version" proposed by Yu. D. Arsen'ev [2]. We denote the efficiency of the basic version by η^* and the capital investment by K^*; the efficiency and cost of any other comparable AEP are η_i and

$$K_i = K^* + \Delta, \tag{1}$$

where Δ is the difference between the investment in the installation and that in the basic version; Δ can be positive or negative.

The total investment in the power system (p.s.) for the variant as compared with the basic version is found from the expression

$$K_{\text{p. s.}} = K_i + Q_T(\eta^* - \eta_i) K_{\text{rep}}. \tag{2}$$

The cost of the fuel consumed per year at the replacement plant is given by

$$C_T = \frac{Q_T(\eta^* - \eta_i)\tau}{\eta_{\text{rep}} Q_p^H} c_T; \tag{3}$$

K_{rep} is the specific capital investment in replacement power; Q_T is the thermal power of the AEP, η_{rep} is the efficiency of the replacement plant; C_T is the cost per ton of the fuel inventory; Q_p^H is the heating power of this fuel; and τ is the number of hours of use of the installed power per year. Knowing the investment in the versions being compared and the cost of the fuel consumed, it is easy to determine the estimated cost of each version.

To determine the economic efficiency of a change in the installation in comparison with the basic version we use the concept of fixed charges for electric power. Then the variable part of the estimated cost of a given variant is

Translated from Atomnaya Énergiya, Vol. 34, No. 4, pp. 293-295, April, 1973. Original article submitted July 10, 1972.

$$C_{var,\,i} = pK_i + a_{AEP}K_i + C^{AEP}_{pers,i} + Q_T(\eta^* - \eta_i)\,\tau\varphi^e_{fix}, \tag{4}$$

and the variable part of the estimated cost of the basic version is

$$C^*_{var} = pK^* + a_{AEP}K^* + C^{AEP}_{pers}. \tag{5}$$

Here φ^e_{fix} gives the fixed charges for electric power; p is the standard efficiency of capital investment; and a_{AEP} is the total rate of amortization of deductions, expenditures for current maintenance, and other expenses for the AEP; C^{AEP}_{pers} and $C^{AEP}_{pers,\,i}$ are the yearly salaries for the AEP personnel for the basic version and the variant, respectively, determined by the number on the staff N^o_{AEP}, the average yearly salary of an AEP worker C^{AEP}_{sal}, and the installed power of the AEP $Q_T\eta^*$ and $Q_T\eta_i$.

The variant will have the same economic effect as the basic version if

$$C_{var,\,i} = C^*_{var}. \tag{6}$$

Assuming $C^{AEP}_{pers} = C^{AEP}_{pers,\,i}$ we find after some simple transformations of (6)

$$\Delta = \frac{Q_T(\eta_i - \eta^*)\,\varphi^e_{fix}\tau}{p + a_{AEP}}. \tag{7}$$

The changes in the installation will be economically expedient if for $\eta_i > \eta^*$ the extra cost does not exceed Δ, or if $\eta_i < \eta^*$ the decrease in capital investments is larger in absolute magnitude than Δ found from Eq. (7).

The economic efficiency of a given change in the system is

$$E = \frac{C^*_{var} - C_{var,\,i}}{C^*} \cdot 100\% \tag{8a}$$

or

$$E = \frac{Q_T(\eta_i - \eta^*)\,\tau \cdot \varphi^*_{fix} - \Delta(p - a_{AEP})}{C^*} \cdot 100\%, \tag{8}$$

where C* is the total estimated cost of the basic version of the system.

In more exact calculations the time for construction and shake down of the plant or unit before putting it into normal operation must be taken into account. Equation (8) then takes a somewhat more expanded form. Thus, for example, let us assume that the first unit of the AEP must be built in two years. In the first year n_1 is included for the cost of construction, and in the second year n_2; then in the third year, the year of shake down, the number of hours of use of installed power is τ_3, and in the fourth year under normal operation τ_4. We use the general formula for determining the estimated cost:

$$C = p\sum_{t=1}^{T_c} \frac{K_t}{(1+p_{red})^{t-1}} + \frac{U_N}{(1+p_{red})^{t-1}} \text{ rubles/yr},$$

where p is the standard efficiency of capital investment; p_{red} is the coefficient for reducing the costs in time (henceforth we assume $p = p_{red} = 0.12$); T_c is the construction period; K_t is the capital investment in year t in rubles/yr; t is the number of years from the start of construction; and U_N denotes the operating expenses in a year of normal operation. Then the economic effect, reduced to the year construction began, from a further capital investment Δ changing the efficiency of the AEP from η^* to η_i is

$$E = \frac{100}{C^*}\left\{Q_T(\eta_i - \eta^*)\,\varphi^e_{fix}\left[\frac{\tau_3}{(1+p)^2} + \frac{\tau_4}{(1+p)^3}\right] - \Delta\left[p\left(n_1 + \frac{n_2}{1+p}\right) + a_{AEP}\left(\frac{1}{(1+p)^2} + \frac{1}{(1+p)^3}\right)\right]\right\}. \tag{9}$$

Equations (7)-(9) enable us to determine the expediency of various changes in the thermal part of the system, such as the introduction of additional heaters, changing the temperature drives, etc., without performing complete design studies of the AEP. Only the change in the capital investment Δ and the efficiency of the installation need be estimated, and ordinarily this is not difficult to do.

As an example let us assume that the thermal power of a reactor is 2500 MW, $\eta^* = 0.35$, $C^* = 68 \cdot 10^6$ rubles, $\tau = 7000$ h/yr, $a_{AEP} = 0.0966$, $\Delta = 0.2 \cdot 10^6$ rubles, $\eta_i = 0.351$, and $\varphi^e_{fix} = 1.2$ kopecks/kWh. Then from (8) the economic effect is about 1%. However, an increase in the capital investment to $3.2 \cdot 10^6$ rubles for the same change in efficiency gives no saving in estimated cost. It should be noted that this procedure can be used only when the changes in the installation do not lead to a change in the conversion ratio or the cost of nuclear fuel, and involve admissible values of the parameters.

Thus the change in efficiency of an AEP operating in the base load band of the load curve leads to a change in the cost of replacement power and fuel inventory. In view of this the problem of increasing the efficiency of an AEP is no less important than the problem of increasing the efficiency of a TEP. The procedure presented permits a very simple estimate of the expediency of various changes from the basic version of a system and an AEP of a given type.

LITERATURE CITED

1. N. A. Dollezhal' and Yu. I. Koryakin, "Some problems of operating atomic electric plants in power systems," Atomnaya Energiya, 25, 387 (1968).
2. Yu. D. Arsen'ev, Similarity Theory in Engineering Economics Calculations [in Russian], Vysshaya Shkola, Moscow (1971).

COST OF IRRADIATION IN A RESEARCH REACTOR

A. S. Kochenov and P. Gitsesku

UDC 621.039.5.55

The great power of modern research reactors leads to a considerable nuclear fuel consumption. This explains the attention now being paid to the optimization of research reactor parameters [1-5]. The concept of the "productivity of a research reactor" was introduced in [4], this being defined as the quantity of usefully absorbed "excess" neutrons ("excess" with respect to a chain reaction). The concept of the "efficiency of a research reactor," or the proportion of usefully absorbed neutrons, was introduced in [5].

Naturally the cost of investigations will be lower, the more excess neutrons are used. However, in determining the cost of irradiating samples, allowance must be made, not only for the quantitative aspect (the number of absorbed neutrons), but also for the qualitative (the level of neutron flux, the level of background radiation, etc.).

In certain reactors the thermal neutron fluxes in different experimental channels differ by more than an order of magnitude from each other. If, in this case, we define the fuel constituent of the cost of the neutrons employed solely in accordance with the number of absorbed neutrons, the cost of irradiating the samples in an experimental channel with a large flux may be several times lower than this, because of the overestimated cost of irradiation in the channels with the low flux.

It is not hard to convince oneself that the cost of the neutrons employed depends on the magnitude of the flux. By way of example, let us consider the thermal neutron flux in the active zone.

Let us suppose that, in the absence of experimental samples from the reactor, the mean depth of burnup of the discharged fuel equals B_0, the neutron breeding factor in an infinite medium equals k_0, and the mean thermal neutron flux in the active zone for a power Q_0 equals Φ_0 (Φ being the mean neutron flux in the presence of the sample). On loading the experimental samples into the active zone the reactivity usually diminishes. In order to preserve the critical state, we may either reduce the depth of burnup, leaving the volume of the active zone intact, or reduce the volume of the active zone, without changing the burnup (of course we may also change both parameters at the same time). Let us consider the case in which only the critical volume changes on loading the samples (the reactor power remaining constant).

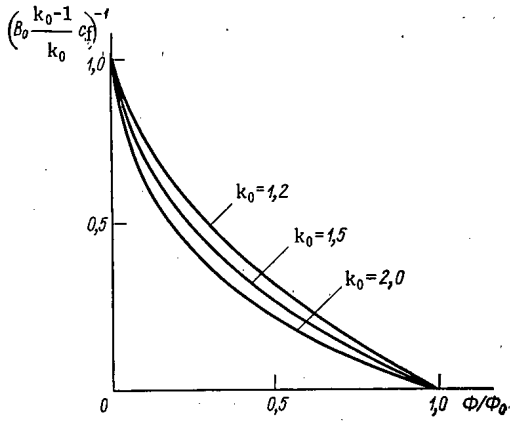

Fig. 1. Dependence of the fuel component of the cost of the neutrons on the neutron flux.

The productivity of the reactor with respect to excess neutrons per unit time equals

$$R_0=\frac{k_0-1}{k_0}\cdot\frac{Q_0}{E_f}\nu_f, \tag{1}$$

where ν_f is the number of secondary neutrons per fission; E_f is the energy per fission.

However, in carrying out experiments we use only some of the excess neutrons, a fraction εR_0 (here $\varepsilon = (R_0-R)/R_0 = 1-(k-1)/(k_0-1)\cdot k_0/k$; R and k are the corresponding parameters when samples occur in the active zone).

It is well known that the fuel expenses g_0 are proportional to the power and inversely proportional to the depth of burnup:

Translated from Atomnaya Énergiya, Vol. 34, No. 4, pp. 295-296, April, 1973. Original article submitted August 22, 1972.

$$g_0 \sim \frac{Q_0}{B_0}, \tag{2}$$

whence the fuel component of the cost of the neutrons c_f (in high-flux reactors this is the main component) referred to a single used neutron is given by

$$c_f \sim \frac{g_0}{\varepsilon R_0} \sim \frac{1}{B_0} \cdot \frac{k_0}{k_0 - 1} \cdot \frac{1}{1 - \frac{k-1}{k_0-1}\frac{k_0}{k}}. \tag{3}$$

If the influence of the experimental samples on the neutron migration length is negligibly small and the effective increment much smaller than the radius of the active zone, we have

$$\frac{\Phi}{\Phi_0} = \left(\frac{k-1}{k_0-1}\right)^{3/2}. \tag{4}$$

Using Eq. (4), we may rewrite Eq. (3) thus

$$c_f \sim \frac{1}{B_0} \cdot \frac{k_0}{k_0-1}\left[1 + k_0 \frac{(\Phi/\Phi_0)^{2/3}}{1-(\Phi/\Phi_0)^{2/3}}\right]. \tag{5}$$

The dependence of c_f on Φ/Φ_0 is shown in Fig. 1 for various k_0. It follows from this that, as the flux increases, so does the fuel component of the neutron cost. For $\Phi/\Phi_0 \ll 1$ the cost of a used neutron depends only slightly on the flux:

$$B_0 \frac{k_0-1}{k_0} c_f \sim 1 + k_0 (\Phi/\Phi_0)^{2/3}. \tag{6}$$

The dependence is stronger for $\Phi/\Phi_0 \approx 1$:

$$B_0 \frac{k_0-1}{k_0} c_f \sim \frac{k_0}{1-(\Phi/\Phi_0)^{2/3}}. \tag{7}$$

Naturally as $\Phi/\Phi_0 \to 1$, $c_f \to \infty$. This is because there are then no samples in the active zone and the excess neutrons are not used, although the reactor is working at nominal power.

The foregoing example shows that the cost of irradiation with thermal neutrons for any particular sample should be fixed, not by the total absorption of neutrons in the sample $\Sigma_c V\Phi$ (here Σ_c is the macroscopic absorption cross section of the sample, V is the sample volume, and Φ is the flux of thermal neutrons in which the sample is irradiated), but by the product $\Sigma_c V\Phi c_\Phi$, where c_Φ is the cost of a single excess neutron in the flux.

LITERATURE CITED

1. S. M. Feinberg et al., Second Geneva Conference (1958) [in Russian], Vol. 2, Atomizdat, Moscow (1959), p. 334.
2. V. A. Tsykanov, At. Energ., 14, 469 (1963).
3. A. S. Kochenov, ibid., 21, 97 (1966).
4. A. N. Erykalov and Yu. V. Petrov, ibid., 25, 52 (1968).
5. V. A. Tsykanov, ibid., 31, 15 (1971).

ESTIMATED ACTIVITY OF A THICK SPECIMEN IN A MULTIPLYING MEDIUM (CONJUGATE RANDOM WALK METHOD)

V. B. Polevoi

UDC 539.172.4

A formal transformation of the adjoint transfer equation useful in constructing a random-walk schema for Monte Carlo estimates of a point linear functional of the flux in a moderating medium with specified sources has been proposed [1].

We now take up application of that method to a procedure for solving one practical problem: estimating activation of a real specimen placed in a multiplying medium. The unknown functional is estimated as the mathematical expectation M of the random variable ξ^+:

$$J = \int \varphi(x) \sum(x)\, dx = \int \varphi^+(x)\, S(x)\, dx = M\xi^+;$$

$$\xi^+ = \sum_i S(x_i).$$

In the case of a reactor, the sources in the original equation are determined by the formula

$$S(x) = \int F(\mathbf{r}', \Omega, E) \exp[-\tau(\mathbf{r}, \mathbf{r}', E)] \times \delta\left(\Omega - \frac{\mathbf{r}-\mathbf{r}'}{|\mathbf{r}-\mathbf{r}'|}\right) \Big/ |\mathbf{r}-\mathbf{r}'|^2\, d\mathbf{r}',$$

where $F(\mathbf{r}', \Omega, E)$ is the distribution of fission neutrons:

$$F(\mathbf{r}', \Omega, E) = \frac{1}{4\pi} \int_{4\pi} d\Omega' \int_0^\infty \varphi(\mathbf{r}', \Omega', E')\, \nu\Sigma_f(\mathbf{r}', E')\, \chi(E)\, dE';$$

τ is the optical distance. The cross section $\Sigma(x)$ of the specimen serves as the source of the adjoint equation; x_i is the point or site of collision of the pseudoneutron, which is our term for a particle whose random walks are controlled by the kernel K^+ of the adjoint equation. The rest of the notation is conventional.

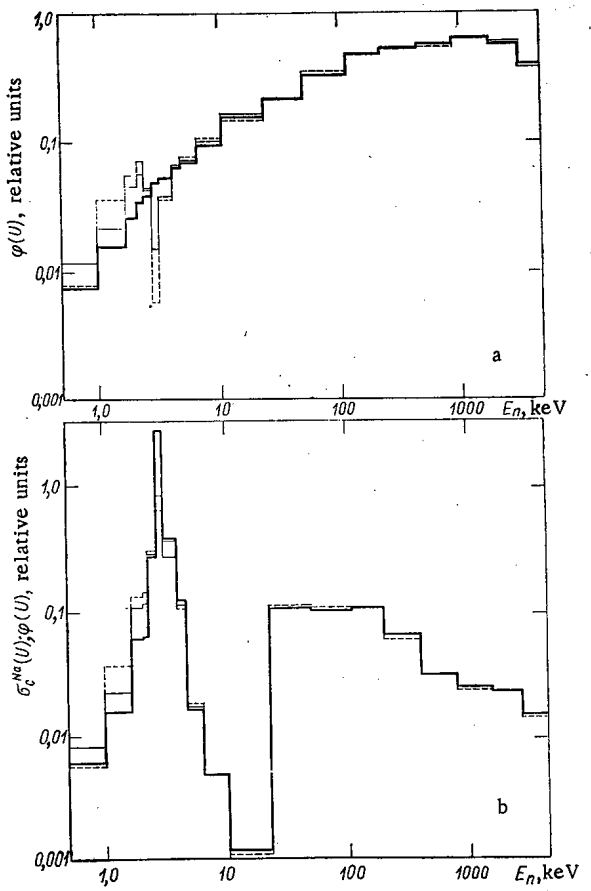

Fig. 1. Spectra of neutrons (a) and of capture events in sodium (b): – – – –) in central layer of thick indicator; ——) on surface of indicator; ▬▬) in medium placed remote from indicator.

The function F(x) can be considered known whenever computation of $S(x_i)$ at points of collision becomes unmanageably cumbersome. Consequently, in contrast to [1], here the schema of conjugate (adjoint) random walks is constructed such that the values of the function F(x) with certain weights assigned can be summed.

For practical realization of this conjugate random walk system, we have to normalize the kernel K^+ with respect to the finite transition states of the pseudoneutron. We can represent K^+ in the form of the product

Translated from Atomnaya Énergiya, Vol. 34, No. 4, pp. 296-298, April, 1973. Original article submitted August 22, 1972.

$$K^+ = T^+ C^+ G,$$

where G depends on the selection of T^+ and C^+. We define

$$T^+(\mathbf{r} \to \mathbf{r}') = \Sigma_t(\mathbf{r}', E) \exp[-\tau(\mathbf{r}, \mathbf{r}', E)]\, \delta\left(\Omega - \frac{\mathbf{r}-\mathbf{r}'}{|\mathbf{r}-\mathbf{r}'|}\right) \Big/ |\mathbf{r}-\mathbf{r}'|^2;$$

$$C^+(E \to E^+,\ \Omega \to \Omega') = \frac{1}{\Sigma^+(\mathbf{r}', E)} C(E' \to E,\ \Omega' \to \Omega) = \frac{1}{\Sigma^+(\mathbf{r}', E)} \sum_{A, i} \sigma_{A, i}(E')\, g_{A, i}(E',\ \Omega' \to E,\ \Omega)\, \rho_A;$$

A is the type of nucleus; i is the mode of scattering; T^+ is clearly normalized such that: $\int T^+(\mathbf{r} \to \mathbf{r}')d\mathbf{r}' = 1$. The constant Σ^+ is selected on the basis of the normalizing conditions $\int C^+ dE' d\Omega' = 1$:

$$\Sigma^+(\mathbf{r}', E) = \int C\, dE',\ d\Omega' = \sum_{A, i} \rho_A(\mathbf{r}')\, \sigma^+_{A, i}(E) \equiv \sum_A \Sigma^+_A,$$

where

$$\sigma^+_{A, i}(E) = \int_E^\infty \int_{4\pi} \sigma_{A, i}(E')\, g_{A, i}(E',\ \Omega' \to E,\ \Omega)\, dE'\, d\Omega'.$$

From the definition of T^+ and C^+ and from the identity $K^+(x \to x') \equiv K(x' \to x)$, we infer $G = \Sigma^+/\Sigma_t$. Accordingly, the possibility of drawing the history of the pseudoneutron can be arrived at by presenting the kernel of the adjoint equation in the form

$$K^+(x \to x') = G(r', E)\, T^+(\mathbf{r} \to \mathbf{r}') \sum_A B_A(\mathbf{r}', E) \sum_i R_{A, i}(\mathbf{r}', E)\, g^+_{A, i}(E,\ \Omega \to E',\ \Omega'),$$

where

$$B_A(\mathbf{r}', E) = \Sigma^+_A(\mathbf{r}', E)/\Sigma^+(\mathbf{r}', E)$$

can be viewed as the probability of scattering of the pseudoneutron on a nucleus of type A;

$$R_{A, i}(\mathbf{r}', E) = \rho_A(\mathbf{r}')\, \sigma^+_{A, i}(E)/\Sigma^+_A(\mathbf{r}, E)$$

is the probability that scattering of mode i will be experienced on the nucleus of type A;

$$g^+_{A, l}(E,\ \Omega \to E',\ \Omega') = \sigma_{A, i}(E')\, g_{A, i}(E',\ \Omega' \to \Omega,\ E)/\sigma^+_{A, i}(E)$$

is the probability density of the corresponding transition. These functions can be calculated beforehand for any E and any $\mathbf{r}$. The function T^+ can be computed with ease at any point. We can therefore arrive at the random walks according to normalized T^+, B, R, g^+ with weighted function G.

It can be shown with ease that, after tracing out N histories

$$J \approx \frac{1}{N} \sum_{l=1}^{M} F(\mathbf{r}_l,\ \Omega_{l-1},\ E_{l-1})\, W_l,$$

where M is the number of all collision points, and

$$W_l = W_{l-1} \Sigma^+(\mathbf{r}_{l-1},\ E_{l-2})/\Sigma_t(\mathbf{r}_l,\ E_{l-1});$$

$$W_1 = \int \Sigma(x)\, dx/\Sigma_t(\mathbf{r}_1,\ E_0).$$

Note that the pseudoneutron does not lose its energy in the collision. Nor can it end up absorbed either, since its trajectory through the infinite medium is likewise infinite. In practical calculations, the trajectory can break off in any one of three cases: 1) when the pseudoneutron escapes from the system entirely; 2) when the pseoduneutron attains the maximum energy E_{max} in the specific problem; 3) when the assigned weight is less than a certain value W_{min} needed for the specified accuracy in the result. This last condition is valid when the weight of the pseudoneutron decreases monotonically in successive collisions.

The conjugated cross sections and the functions g^+ appear, in the group treatment, in the form:

$$\sigma_{in}(k) = \sum_{i=1}^{k} \sigma^3_{in}(i \to k);$$

$$\sigma^+_{el}(k) = \sigma^3_{el}(k-1) + \sigma_{el}(k) - \sigma^3_{el}(k);$$

$$\sigma^+_t(k) = \begin{cases} \sigma^+_{el}(k) + \sigma^+_{in}(k) & \text{for } k \leqslant \Gamma; \\ \sigma^+_{el}(k) & \text{for } k > \Gamma; \end{cases}$$

$$g^+_{in}(k \to i) = \sigma^s_{in}(i \to k)/\sigma^+_{in}(k);$$

$$g^+_{el}(k \to k-1) = \sigma^s_{el}(k-1)/\sigma^+_{el}(k);$$

$$g^+_{el}(k \to k) = (\sigma_{el}(k) - \sigma^s_{el}(k))/\sigma^+_{el}(k),$$

where Γ is the boundary for inelastic collisions. In the subgroup treatment [2], the same functions become:

$$\sigma^+_{in}(l \in k) = \sigma^+_{in}(k)\, a^{l \in k};$$

$$\sigma_{el}(l \in k) = \sum_j \left(\sigma^{j \in k}_{el} a^{j \in k}\left(1 - \frac{\xi_k}{\Delta u_k}\right) + \sigma^{j \in k-1}_{el} a^{j \in k-1} \frac{\xi_{k-1}}{\Delta u_{k-1}}\right) a^{l \in k};$$

$$g^+_{el}(l \in k \to j \in k-1) = \sigma^{j \in k-1}_{el} a^{j \in k-1} \xi_{k-1} a^{l \in k}/\Delta u_{k-1} \sigma^+_{el}(l \in k);$$

$$g^+_{el}(l \in k \to j \in k) = \sigma^{j \in k}_{el} a^{j \in k}\left(1 - \frac{\xi_k}{\Delta u_k}\right) a^{l \in k}/\sigma^+_{el}(l \in k);$$

$$g^+_{in}(l \in k \to j \in i) = \sigma_{in}(i \to k)\, a^{j \in i}/\sigma^+_{in}(k).$$

On the basis of the proposed algorithm, the distribution of activation over a sodium indicator foil 0.68 cm thick and placed in a homogeneous medium consisting of a mixture of nuclei U^{238}, Pu^{239}, oxygen, and carbon (in the ratios 1 : 0.071 : 2.08 : 0.73) was calculated on an M-220 computer. It was assumed that flux depression near the indicator would have no effect on the distribution of fission events in the medium. The calculations were performed on the basis of constants cited in [3], in which groups 12-14 were broken down further into nine subgroups in order to facilitate a detailed description of the sodium resonance. The results obtained appear in Fig. 1. The effect of resonant self-screening is clearly in evidence. The activation density at the center of the indicator is 1.59 times lower, and on the surface 1.44 times lower, than the activation density in an infinitely thin specimen. The activation density is seriously affected by moderation of neutrons traversing the sodium.

The author takes this opportunity to express his heartfelt thanks to M. N. Nikolaev for the formulation of the problem, and for the kind assistance rendered in solving it, and also M. Yu. Orlov for invaluable discussions and counsel.

LITERATURE CITED

1. B. Eriksson et al., Nucl. Sci. and Engng., 37, 410 (1969).
2. M. N. Nikolaev et al., At. Energ., 29, 11 (1970); 30, 426 (1971).
3. L. P. Abagyan et al., Group Constants for Nuclear Reactor Calculations [in Russian], Atomizdat, Moscow (1964).

ENERGY DISTRIBUTION OVER THE CROSS SECTION OF THE TRACK OF CHARGED PARTICLES HAVING THE SAME LINEAR ENERGY TRANSFER

I. K. Kalugina, I. B. Keirim-Markus, A. K. Savinskii, and I. V. Filyushkin

UDC 539.12.08

In [1] we obtained the distribution of the energy transmitted to the medium in the radial cross section of the track of heavy charged particles. The data were represented in the form of a universal function of the maximal energy of δ electrons $E_{\delta max}$ and the distance r from the axis of the track expressed in fractions of the maximal length of the path of δ electrons $R_{max} = f(E_{\delta max})$.

Figure 1 shows the radial distribution, calculated according to the indicated function, of the energy over the cross section of the tracks of three particles having the same linear energy transfer in water

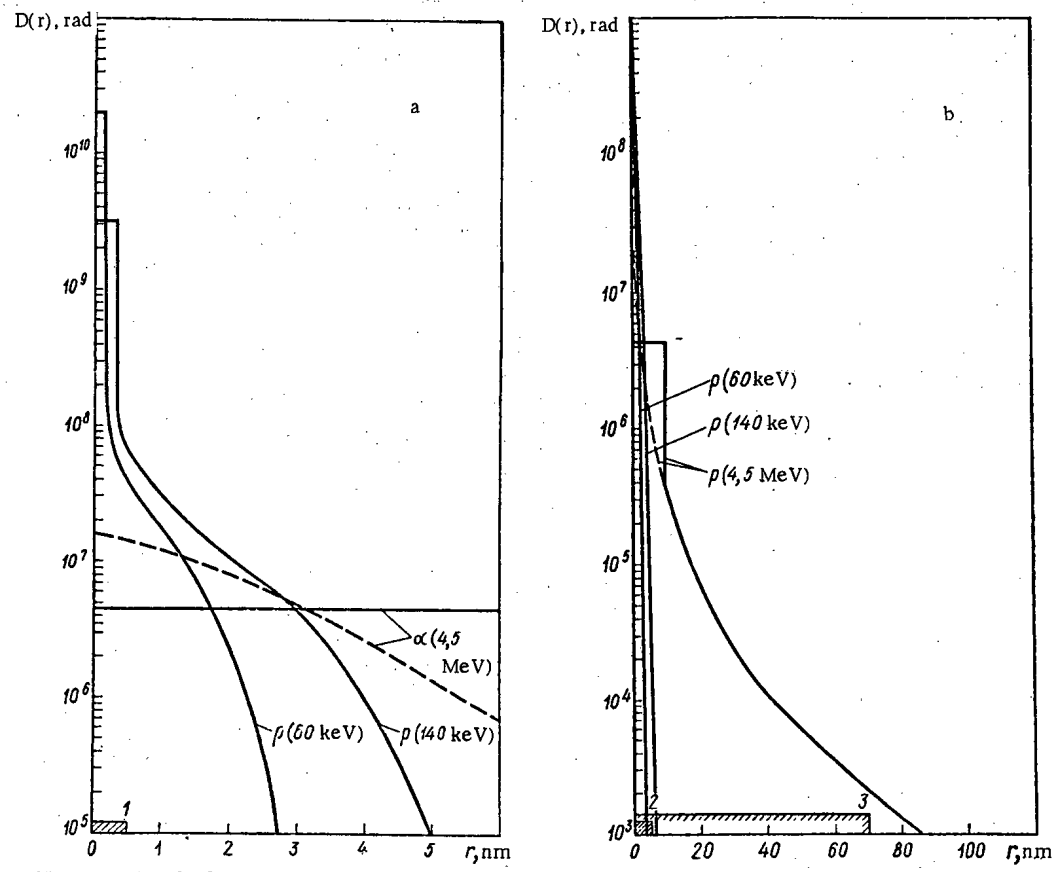

Fig. 1. Radial energy distribution over the cross section of tracks of protons with energy 60 and 140 keV and γ particles with energy 4.5 MeV having the same linear energy transfer in water (L_∞ = 90 keV/μ). For clarity two different scales are given in the figure (a and b).

Translated from Atomnaya Énergiya, Vol. 34, No. 4, pp. 298-299, April, 1973. Original article submitted September 27, 1972.

L_∞ = 90 keV/μ: protons with energies 60 and 140 keV and α particles with energy 4.5 MeV. In Fig. 1 we give dimensions of typical biological structures: the radius of a nitrous base or a nucleotide of DNA (1); the radius of a small virus (2); and the radius of a large virus (3).

It is known that the biological effect of radiation is related to L_∞, it being assumed that charged particles with the same L_∞ also have the same radiobiological effectiveness. On this basis the coefficient of quality of radiation OF that is used in radiation safety is unambiguously related to L_∞ [2].

As is seen from Fig. 1, the radial distribution of energy in the tracks of the three forms of particles with the same L_∞ varies considerably. Near the axis of the track of the protons the absorbed dose is so large that a large fraction of the atoms are ionized at a distance 2-5 Å, corresponding to the radius of a nitrogen base or a nucleotide of DNA. The transmission of α particles can cause the ionization of isolated atoms of the nucleotide. A similar effect will appear also with respect to other low-molecular groups of cells. With passage of charged particles through a small virus we can expect a local action of protons on part of the virus, while an α particle generates a comparatively uniform radiation. On comparatively large viruses, the action of α particles will be local, just as it is for protons.

Thus the calculations verify that L_∞ cannot sufficiently completely characterize the features of biological action of various forms of radiation.

LITERATURE CITED

1. I. K. Kalugina et al., Radiobiologiya, No. 4 (1973).
2. Norms of Radiation Safety (NRB-69) [in Russian], Atomizdat, Moscow (1971).

CHANGE IN OPTICAL PROPERTIES OF POLYETHYLENE TEREPHTHALATE FILM IRRADIATED WITH 25-150 keV PROTONS

S. P. Kapchigashev, V. P. Kovalev, V. A. Sokolov, and É. S. Barkhatov

UDC 541.15:539.125.4.02

Convenient dosimetric methods are needed for use with low-energy heavy charged particles in radiation chemistry and radiobiology. One such method is based on the use of thin organic films whose optical properties are affected by ionizing radiation. In addition these films have dosimetric characteristics (effective atomic number, electron density, mean excitation potential) similar to those of many media of interest in radiation chemistry and radiobiology [1].

We have investigated the characteristics of polyethylene terephthalate (PETPH) film 9.5 μ thick (without plasticizer) having a density of 1.4 g/cm^3. The film thickness was monitored in all experiments by the measurement of α-spectra.

PETPH is a linear polyester formed by the condensation of ethylene glycol and terephthalic acid [2]:

$$(-O-CH_2-CH_2-O-CO-C_6H_4-CO-)_n.$$

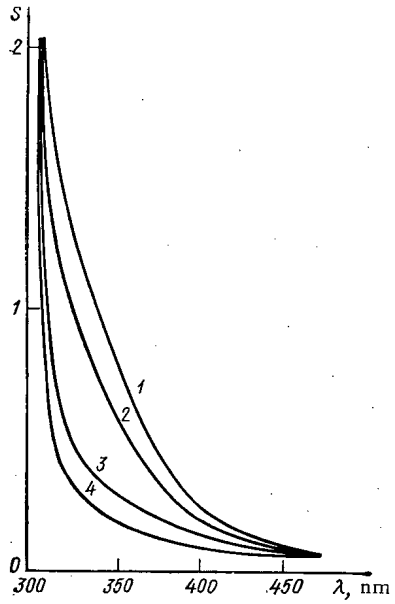

Fig. 1

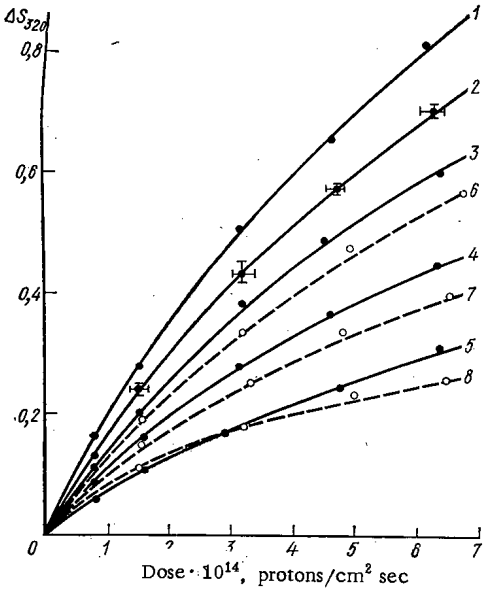

Fig. 2

Fig. 1. Change in the absorption spectrum of PETPH for various energies of the incident particles. Protons: 1) 100 keV; 2) 50 keV. Mixed beam: 3) 10 keV; 4) unirradiated film (control).

Fig. 2. ΔS as a function of the radiation dose. Protons: 1) 150 keV; 2) 100 keV; 3) 75 keV; 4) 50 keV; 5) 25 keV. Mixed beam: 6) 50 keV; 7) 25 keV; 8) 10 keV.

Translated from Atomnaya Énergiya, Vol. 34, No. 4, pp. 299-300, April, 1973. Original article submitted October 2, 1972.

Radiation damage results mainly in the breaking of the ester groups and intermolecular cross linking [3].

The dosimetric characteristics of PETPH were investigated by irradiating films with 25-150 keV protons. The protons were obtained from a modified NG-160 neutron generator. The protons could be separated from the heavier ions in the beam, H_2^+, H_3^+, and ions of impurity gases, by a magnetic separator at the generator exit. The uniformity of the proton current over the cross section of the beam was monitored by the method of interchangeable diaphragms and also by the uniformity of the optical absorption of films placed in various parts of the radiation field.

The change in the optical absorption of PETPH films characterizes the extent of the radiation damage (Fig. 1). The measurements were made with a wavelength of 320 mμ corresponding to the flat part of the absorption spectrum. The optical measurements were made with USV-1 (German) and SP-700 (British) spectrophotometers.

Figure 2 shows the change ΔS in optical density of PETPH films as a function of the radiation dose in the 25-150 keV energy range. Each curve is plotted from the results of from three to five series of irradiations. The maximum error in determining the dose does not exceed 10%. The dashed curves show similar relations for a nonseparated ion beam. In the energy range investigated the proton ranges are significantly less than the film thickness and therefore the change ΔS is uniquely determined by the product of the number of protons and their energy. To use the film as a dosimeter it is necessary to plot calibration curves or to use the linear initial parts of the curves (up to 10^{14} protons/cm^2) as proposed in [4].

The effect was independent of the dose rate in the range $1.5 \cdot 10^{11}$-$1.5 \cdot 10^{12}$ protons/cm$^2 \cdot$ sec. It was established that irradiated films stored in darkness at room temperature for two months did not fade.

LITERATURE CITED

1. A. M. Kabakchi, Ya. I. Lavrentovich, and V. V. Pen'kovskii, Chemical Dosimetry of Ionizing Radiations [in Russian], Izd-vo AN USSR, Kiev (1963), p. 151.
2. A. Charlesby, Atomic Radiation and Polymers, Pergamon Press, New York (1960).
3. R. Bolt and T. Carrol (editors), Radiation Effects on Organic Materials, Academic Press, New York–London (1963), p. 164.
4. J. Boag et al., Radiation Res., 9, 589 (1958).

EXPERIMENTAL STUDY OF CURRENT FORMATION IN DIRECT-CHARGE DETECTORS WITH A RHODIUM EMITTER

V. I. Mitin, V. F. Shikalov, and S. A. Tsimbalov

UDC 539.1.074.8

A study of the properties of direct-charge detectors [1-3] has shown that these instruments may successfully be used as neutron flux monitors when constructing systems of intrareactor control. However, increasing demands as to measuring accuracy, rapidity of action, and other parameters have necessitated a more detailed investigation into the mechanism of current formation in direct-charge detectors under the conditions of reactor irradiation. The aim of the present investigation is to study the influence of reactor γ-radiation on the readings of a direct-charge detector and to refine the kinetic parameters of detectors with rhodium emitters.

For this purpose we used DPZ-1P detectors with rhodium emitters made in the All-Union Scientific-Research Institute of Current Sources. The length of the detectors was 50 and 100 mm, the diameter of the emitter was 0.8 mm. The measurements were carried out in the displacer of the working channel of the MR reactor of the I. V. Kurchatov Institute of Atomic Energy [4]. A dry measuring channel of internal diameter 6 mm was placed in the displacer. The external diameter of the detectors with their stainless steel sheath was 4 mm. This construction enabled the detector to be moved rapidly over the height of the active zone.

For recording the currents of the direct-charge detector we used a measuring system consisting of semiconducting electrometric amplifiers of the PÉMU-3 type, a K-107 loop oscillograph, and a KSP-4

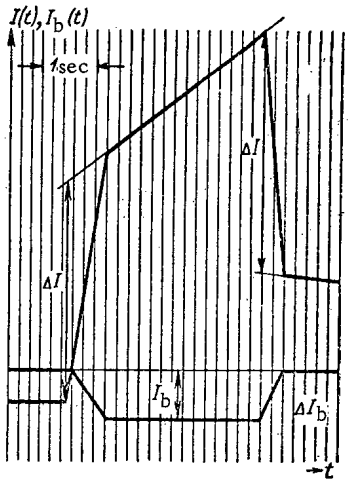

Fig. 1

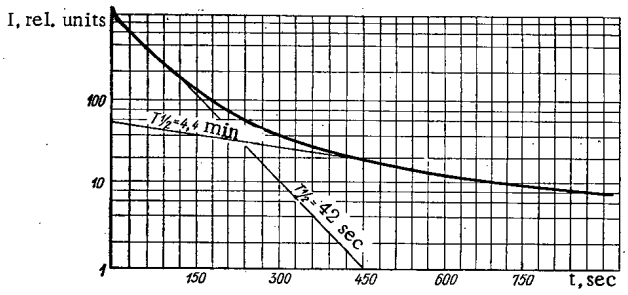

Fig. 2

Fig. 1. Current of the direct-charge detector and background current on introducing the detector into the active zone (oscillogram).

Fig. 2. Direct-charge detector current after rapid withdrawal from the active zone.

Translated from Atomnaya Énergiya, Vol. 34, No. 4, pp. 301-303, April, 1973. Original article submitted June 12, 1972.

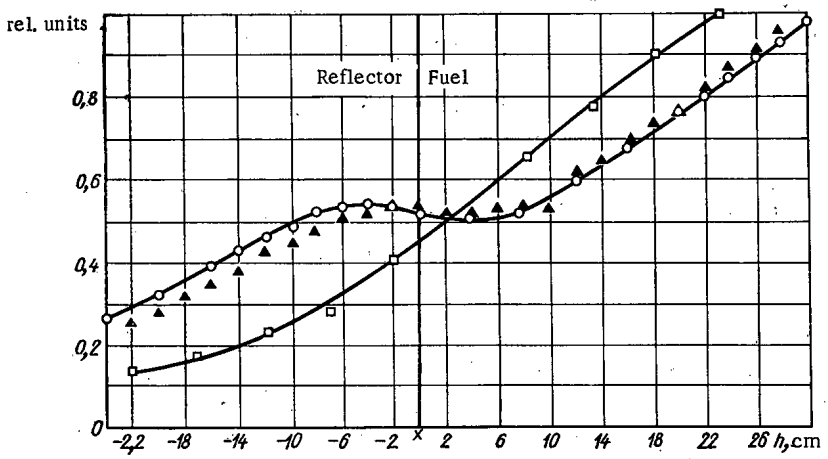

Fig. 3. Result of measurements at the active-zone/reflector boundary: □) current of the KNT-11 γ-chamber; ○) activation of the copper wire; ▲) current of the direct-charge detector (the instantaneous component coincides with the statistical measurement).

automatic-recording potentiometer. The detectors were coupled to the measuring system (16 m long) with a double-screen AVKE-1 cable.

Before starting the measurements the direct-charge detectors were placed in the channel at a distance of 50 cm above the upper edge of the active zone. When the start signal was given, the detector was let down in approximately 0.2 sec to a specific point in the active zone, held there for around 4 sec, then rapidly restored to its original position. The corresponding recordings of the detector current and the background current I_b are given in Fig. 1 (I is the current of the emitter and coupling line).

Dynamic Characteristics of the Direct-Charge Detector. The time dependence of the direct-charge detector current determined by the activation and β-decay of rhodium is described by the system of equations:

$$\left.\begin{aligned} &I(t)=k\lambda_1 N_1(t);\\ &\frac{dN_1(t)}{dt}=-\lambda_1 N_1(t)+\lambda_2 N_2(t)+\sigma_1 N\Phi(t);\\ &\frac{dN_2(t)}{dt}=-\lambda_2 N_2(t)+\sigma_2 N\Phi(t), \end{aligned}\right\} \qquad (1)$$

where λ_1 and λ_2 are decay constants; $N_1(t)$ and $N_2(t)$ are the number of nuclei; σ_1 and σ_2 are the cross sections of formation of the isotopes for Rh^{104} and Rh^{104m}, respectively; N is the number of Rh^{103} nuclei; and $\Phi(t)$ is the neutron flux.

By solving the system of equations in Eq. (1) we find that, when the detector is instantaneously withdrawn from the active zone after previously being held in a neutron flux until saturation has been achieved with respect to both isotopes Rh^{104} and Rh^{104m}, the time dependence of the current will take the form

$$I(t)=k\left[(\sigma_1+\sigma_2)N\Phi e^{-\lambda_1 t}+\frac{\lambda_1}{\lambda_1-\lambda_2}\sigma_2 N\Phi\left(e^{-\lambda_2 t}-e^{-\lambda_1 t}\right)\right],$$

while on instantaneously introducing the detector into a steady-state neutron flux with zero initial conditions it obeys

$$I(t)=k\left[(\sigma_1+\sigma_2)N\Phi\left(1-e^{-\lambda_1 t}\right)-\frac{\lambda_1}{\lambda_1-\lambda_2}\sigma_2 N\Phi\left(e^{-\lambda_2 t}-e^{-\lambda_1 t}\right)\right].$$

Figure 2 illustrates the changes taking place in the detector current on rapid withdrawal from the active zone and fairly prolonged cooling.

From the recordings of the transient processes (Figs. 1 and 2) we see that the detector current consists of instantaneous and retarded components, the time dependence of the latter component agreeing with the foregoing relationships. Repeated measurements at various points of the active zone with a small γ background showed that the instantaneous component equalled (7.3 ± 0.5)% of the total detector current.

Instantaneous Component of the Direct-Charge Detector Current in the Presence of a Rhodium Emitter. We devoted particular attention to determining the nature of the instantaneous current component in view of the fact that the literature contained insufficient information regarding this phenomenon. The phenomenon was explained in [2] by the "ejection of electrons from the emitter on account of the capture of γ-radiation in the silver" and in [3] by the effect of the reactor γ-radiation on the emitter material.

We ourselves considered it more likely that the instantaneous current from the direct-charge detector with the rhodium emitter involved two processes. Firstly, the first stage in the reaction

$$Rh^{103}(n\gamma)\begin{cases}Rh^{104m}\\Rh^{104}\end{cases},$$

in which the transition of the compound nucleus Rh^{103} + n into the state Rh^{104} or Rh^{104m} was accompanied by the emission of γ-quanta and conversion electrons of different energies [5]. The conversion electrons and also the electrons leaving the emitter as a result of interaction with the γ-quanta of the transition (Compton effect, photoeffect) create an instantaneous component of the detector current. Secondly, the γ-quanta of the fission reaction and the capture radiation of the materials surrounding the detector, interacting with the detector materials, create an instantaneous flux of charged particles which make their own contribution to the detector current. In order to discover which of the two mechanisms had the greater effect on the formation of the instantaneous component, we carried out a special experiment.

Keeping the state of the reactor active zone constant, we measured the distribution of the thermal neutron flux and the intensity of the γ-radiation over the height of the channel. The thermal neutron flux distribution was determined from the activation of a copper wire, and the intensity of the γ-radiation with a KNT-11 γ-chamber without any covering, the sensitive part being 50 mm high and 4 mm in diameter. Then we measured the current distribution of the rhodium detector over the height of the channel. The detector was held at the points of measurement for at least 15 min. At these same points we determined the instantaneous component of the detector current by withdrawing it sharply, and at the same time established the value of the background current. The results of the measurements are shown in Fig. 3. Particularly indicative are the results of the measurements in the region of the upper reflector, since here we have a sharp difference between the current of the γ-chamber and the activity of the copper wire. This is to be expected, since at the fuel/reflector boundary the flux of thermal neutrons increases on the reflector side while the intensity of the γ-radiation diminishes. The distribution of the saturation current of the detector with respect to height agrees closely with the distribution of the activity of the copper wire. A slight discrepancy in the region of the reflector and above may be explained by the different spectral sensitivity of copper and rhodium, the neutron spectrum becoming softer at this point of the reactor. Since the distribution of the instantaneous component of the detector current coincided with the distribution of the saturation current of the detector to within 1% (or better) at each measuring point, we may confidently assert that the first stage of the reaction $Rh^{103}(n\gamma)\begin{cases}Rh^{104m}\\Rh^{104}\end{cases}$ plays the main part in creating the instantaneous component of the rhodium detector current. The contribution of γ-radiation to the creation of this component is insignificant.

Thus at all measuring points the distribution of the instantaneous component of the detector current is proportional to the distribution of the saturation current of the detector, with an error of no greater than 1%. This indicates that the instantaneous or prompt component has a neutron origin, since in the region of the reflector, at which the neutron and γ-radiation fluxes have different distributions, the distribution of the instantaneous component is proportional to the neutron distribution and not the distribution of γ-radiation.

In addition to this, allowing for the fact that the coefficient of proportionality between the instantaneous component and the detector saturation current remains constant to within an error of ~1%, we may conclude that the contribution of the γ-radiation to the detector current is negligible.

We may thus consider that the detector current is due, on the one hand, to the β-particles of Rh^{104} formed as a result of the reaction $Rh^{103}(n\gamma)Rh^{104}$ and as a result of the γ-transition of Rh^{104m} into Rh^{104}. This component (which may be called the activation component) produces 92.7% of the direct-charge detector current. On the other hand, the electrons formed in the first ("instantaneous") stage of the capture of neutrons by rhodium make their own contribution to the current. The proportion of the instantaneous component relative to the whole detector current equals ~7.3%.

In conclusion, the authors are pleased to thank L. I. Firsov and V. V. Semak for help in preparing for and effecting the measurements, and also A. A. Voronin and E. N. Babulevich for constant cooperation and interest in the work.

LITERATURE CITED

1. N. D. Rozenblyum et al., At. Energ., 10, 72 (1961).
2. I. Ya. Emel'yanov et al., ibid., 27, 230 (1969).
3. I. Hilborn, Nucleonics, 22, No. 2, 69 (1964).
4. V. V. Goncharov et al., Third Geneva Conference (1971), Paper 323 (USSR).
5. G. A. Bartholomew et al., Collection of Measurements of Gamma Radiation Arising from the Capture of Thermal Neutrons, Part I (Z = 46) [Russian translation], Atomizdat, Moscow (1969).

THIRD ALL-UNION CONFERENCE ON CHARGED-PARTICLE ACCELERATORS

L. N. Sosenskii

In the beginning of October, 1972, in Moscow there took place the Third All-Union Conference on Charged-Particle Accelerators, attended by about 600 scientists and engineers from Soviet and foreign research institutions.

The work of the conference concentrated on the following basic areas: 1) high-energy and superhigh-energy accelerators; 2) colliding-beam apparatus; 3) meson factories; 4) use of superconductivity in accelerator technology; 5) computer control of accelerators; 6) new acceleration methods; 7) increasing the power of existing accelerators; 8) acceleration of heavy ions; 9) use of accelerators in related areas of physics and in medicine.

1. A group of scientists from the Institute of High-Energy Physics (IHEP, Serpukhov), the Scientific-Research Institute for Electrophysical Apparatus (SRIEA, Leningrad), and the Radiotechnical Institute (RTI) of the USSR Academy of Sciences (Moscow) proposed building an ~2 TeV accelerator-storage complex in which superconducting magnets would be used for the main proton–synchrotron ring and the IHEP accelerator with energy 76 GeV and beam intensity (after reconstruction) of $\sim 10^{13}$ protons/pulse would be used as the injector. Such a complex could also accelerate electrons to energies up to ~40 GeV. Such a complex would make possible studies of colliding beams of various types: proton–proton, proton–electron, and proton–antiproton.

The IHEP accelerator operates successfully at an energy of 76 GeV. The principal recent accomplishment of this accelerator was the introduction of a high-energy extraction system for the "Mirabel" liquid-hydrogen chamber, about which IHEP and CERN made a joint report. This system assures extraction in the energy range 30-76 GeV with efficiency ~98%, the feasibility of triple extraction in each accelerator cycle, high dimensional stability and hitting an external target with the beam. The introduction of the high-energy extraction system significantly increases the efficiency of the accelerator.

Work on perfecting the 6 GeV Erevan electron synchrotron is continuing. The vacuum system of the accelerator has been reconstructed: the metal epoxy chamber has been replaced by a ceramic one, metalized inside with a molybdenum–manganese alloy; the beam extraction system has been modernized.

There was no report at the conference on the start-up of the Batavia (USA) 200 GeV proton synchrotron. Nevertheless, this fact was at the participants' center of attention, since it heralds a new outstanding step in the development of accelerator technology.

CERN has begun construction of a several-hundred GeV proton synchrotron. The first stage for this accelerator (200 GeV) has been planned with a setup of omitted magnets, allowing significant increase in the energy in the future. Contracts have been let for the manufacture of ferrous magnet blocks. Two variants of the second stage have been considered: filling the entire ring with ferrous magnets (~400 GeV) and installing in the spaces superconducting magnets with fields of 4-5 tesla, not including the ferrous magnets (~500 GeV). The choice should be made by the end of 1973.

The report by the specialists from the Stanford accelerator center considered a new proposal for reconstructing the 25 GeV linear electron accelerator. The administration of the center rejected a plan for remaking the accelerator into a superconducting one (increasing the energy to 100 GeV) and stopped studies on using superconductivity in rf systems. It consists of introducing the electrons accelerated in

Translated from Atomnaya Énergiya, Vol. 34, No. 4, pp. 305-309, April, 1973.

the existing machine into a closed recirculator, where they circulate 120 times in the interval between pulses of the rf field of the main accelerator; then, the electrons are injected into the main accelerator and are accelerated by the next pulse to ~45 GeV. The recirculator contains two incomplete rings of 95 m radius at the ends of the main accelerator. The rings are connected by two long linear sections located in a tunnel of the main accelerator above them. The overall length of the recirculator is ~6.9 km. The authors of the project expect to receive by the end of 1974 the necessary funds (18 million dollars) and begin realizing the project.

2. Many nuclear and accelerator scientific centers give primary attention to colliding-beam apparatus.

At the Institute of Nuclear Physics, Siberian Branch of the Academy of Sciences of the USSR, there is being constructed a new electron–positron ring VEPP-2M for maximal energy of 670 MeV, in which it is expected to achieve in the first stage a luminosity of the order of $5 \cdot 10^{30}$ cm$^{-2} \cdot$ sec^{-1} at an energy of 500 MeV and beam currents of 40 A. Later, luminosity could be increased to ~10^{32} cm$^{-2} \cdot$ sec^{-1}. In July, 1972, electron capture in the synchrotron mode was achieved. On the VEPP-3 a system for controlling the beam dimension in a storage ring was studied.

CERN has operated for more than two years proton storage rings with beam energy of 25 GeV, in which there was observed the unexpected effect of beam loss due to pressure increase in the vacuum chamber. To control this phenomenon, the vacuum chamber is now heated before it is pumped out at 300°C over 24 h (instead of 200°C over 5 h). Besides this, the pumping rate of the pumps will be increased to 800 liter/sec and their number increased to 500. The first measure alone increased the current at which the pressure rise begins from 4 to 10 A. There are assurances that the completion of the planned program will increase the current to the projected level of 20 A.

Two electron–positron storage rings began operation in the USA in 1972: SPEAR at the Stanford accelerator center and the storage ring at the Cambridge Electron Accelerator. At Stanford, a luminosity of $2 \cdot 10^{30}$ cm$^{-2} \cdot$ sec^{-1} – the maximum obtained anywhere up to this time – was obtained at an energy of 2.3 GeV (maximum energy 2.8 GeV). The program for developing SPEAR, providing for increasing the maximum energy to 4.5 GeV with luminosity 10^{32} cm$^{-2} \cdot$ sec^{-1}, for which a new rf system is necessary, should be completed by July, 1974.

The reconstruction of the Cambridge electron synchrotron consisted of constructing magnetic bypass channels, including portions with small β. The maximal obtained luminosity at an energy of 2 GeV ($3 \cdot 10^{28}$ cm$^{-2} \cdot$ sec^{-1}) is still insufficient for the planned experiments, and work is now going on to increase it.

Three projects for new storage rings were presented. A combined Stanford–Berkeley group proposed constructing a complex allowing proton–electron–positron colliding beams (PEP) with electron energy 15 GeV, proton energy 72 GeV, and luminosity ~10^{32} cm$^{-2} \cdot$ sec^{-1}. The electron–positron and proton rings are to be located in a single tunnel, one over the other.

At Brookhaven National Laboratory (USA) the ISA project is being developed, which envisions the creation of two intersecting accelerator-storage units with superconducting magnets for proton–proton collisions at energy of 200 GeV. The protons are injected from a proton synchrotron at an energy of 30 GeV. After storage of currents of the order of 15 A, the protons are slowly accelerated to 200 GeV and then collide in special interaction regions with luminosity of the order of 10^{33} cm$^{-2} \cdot$ sec^{-1}.

In the DESY laboratory (Federal Republic of Germany) there is being built an electron–positron storage ring DORIS for 3.5 GeV with injection from an existing electron synchrotron. The system consists of two rings, one above the other. The projected luminosity is ~10^{32}–10^{33} cm$^{-2} \cdot$ sec^{-1}.

3. In the Soviet Union, RTI, AS USSR, and SRIEA have planned a meson factory for 600 MeV energy and 0.5 mA average proton current; the basis of the meson factory is a linear accelerator producing a proton beam with pulse duration 100 μsec and off-duty factor 1%. Simultaneously with protons in the linear accelerator, H^- ions with average current of 50 μA and polarized H^- ions are accelerated.

At the exit of the linear accelerator is a storage ring-extender using overcharged injection of H^- ions. Slow escape from the storage ring gives a continuous proton beam with a current of 50 μA; fast escape gives short pulses.

The Nuclear Problems Laboratory of the Joint Institute for Nuclear Research (JINR) has for several years studied the possibility of using ring accelerators (isochronous cyclotrons and high-current phasotrons) as meson factories. It has been shown that when $Q_z = 1.1-1.4$ proton beams can be accelerated with currents exceeding 100 mA. A new method for beam extraction has been worked out, based on widening the closed orbit in a limited range of radii, while preserving the beam emittance. This method will allow achieving a beam spacing in the extraction zone of 5 cm/cycle with an emittance of ~1 cm · rad. A project has been worked out for a phasotron with energy of 700 MeV and average current of 50 μA. Construction of the phasotron should be completed in 1975.

A large installation being constructed in Vancouver, Canada, is the TRIUMF meson factory based on a sector cyclotron weighing 4000 tons. The energy of the particles accelerated in the cyclotron can be varied smoothly from 160 to 520 MeV while one can extract simultaneously from the accelerator several beams with varying energies and off-duty factor 100%. The most intense extracted beam has a current of 100 μA. Start-up of the accelerator is planned for 1974.

A meson factory is being constructed by the Swiss Institute for Nuclear Research in Zurich with final energy of 590 MeV and current of 100 μA. The first experiments with the beam are expected toward the end of 1973.

4. In recent years, interest has risen sharply in the uses of superconductivity in accelerator technology.

Workers from RTI and SRIEA gave reports on work in the field of superconductivity. At RTI, systematic investigations of superconducting pulsed magnets have continued since 1969. In this time, solenoid and dipole magnet models have been constructed with maximum fields up to 6 tesla and cycle rise rates up to 4 tesla/sec. In the dipole magnet, a field uniformity of ~0.2% has been obtained. Presently, there are being constructed several superconducting dipoles with low parameter variation and also a dipole whose dimensions are close to natural.

Superconducting solenoids have been studied at SRIEA. Methods have been worked out for impregnating the windings so that the conductors are stationary.

In 1970, the Rutherford laboratory (Great Britain) and the scientific centers in Saclay (France) and Karlsruhe (FRG) created a commission (GESSS) to coordinate their efforts in creating pulsed superconducting magnets and applying them to accelerators. Encouraging data have been obtained. The GESSS laboratories have produced a series of models for magnets for a superconducting synchrotron. The magnets were tested in thousands of cycles of pulsed operation and gave satisfactory results in both the required field accuracy and reliability.

The next stage will be the creation of magnets suitable for mass production and testing their accuracy and reliability in millions of cycles.

Since the problem of pulsed magnets is close to solution, main attention in the near future will be directed at the system for liquefying and distributing helium over an object several kilometers in extent. A no less important system, whose production entails significant difficulty, is the power-supply system with stored energy of ~500 MJ.

The possible vacuum system variants for the ISA storage complex are being studied at the Brookhaven National Laboratory. A warm chamber is preferred, although use of a cold chamber could, in principle, lower the cost of the superconducting magnets through decreasing their aperture.

At the Argonne National Laboratory (USA) a project has been devised for a superconducting storage ring with a constant field for use as a beam extender in a zero-gradient proton synchrotron. The ring will double the average intensity and increase the off-duty factor of the extracted beam by a factor of 5. It is located in the main synchrotron tunnel.

At the Institute for Experimental Nuclear Physics in Karlsruhe (FRG) there has been constructed the first section with spiral retardation for a superconducting linear proton accelerator with projected energy 50 MeV and current 1 mA, which is a model for the projected superconducting accelerator with energy ~500 MeV. Superfluid helium at a temperature of 1.8°K is used for cooling. The first section operated stably for several hours at an intensity of 1.3 μA with accelerating field 1.3 MV/m.

5. At the present time methods of computer control of accelerators are being incorporated into most working installations, and the computer is an important part of all accelerators being built and planned.

At RTI, work is continuing on creating and perfecting methods for controlling closed orbits and for correcting multiple distortions of the magnetic field. With the participation of workers at IHEP, an ionization profilometer has been devised for measuring the transverse dimensions of the IHEP proton–synchrotron beam with spatial resolution of ~1 mm. Presently, apparatus is being designed for introducing information from the profilometer into a computer.

At the Institute of Theoretical and Experimental Physics (ITEP) a profilometer is also being devised for work under special conditions of the Institute's proton synchrotron at energies of 7 GeV, at which it is extremely difficult to screen the device from the stray field of the magnet. In 1970, the profilometer was tested experimentally on the accelerator and allowed measurement of the transverse dimensions of the beam with accuracy of 2 mm and time resolution of 50 $\mu \cdot$ sec.

At the Institute for Nuclear Physics, Siberian Branch AS USSR, since May, 1971, a system for the VEPP-3 storage unit has been in use which controls the magnet, the storage mode, and the equilibrium orbit. The system is used also for measuring the beam parameters, controlling the pulse system, and analyzing complex situations. A Minsk-22 computer is being used.

SRIEA has devised an automatic system of pulsed power supply of 95 drift tubes for the 38 MeV linear proton accelerator – the booster injector for the IHEP proton synchrotron. The system provides for remote programed control of the apparatus from a central console, and also interrogation and control of the current amplitudes.

Studies are continuing at the Erevan Physics Institute on a system for correcting the magnetic field of the electron synchrotron at high energies. This system decreased dynamic losses in the dipole and focusing magnets to $\sim 10^{-4}$ using self-compensating circuits which equalize the fields in all elements of the magnetic system.

The first complex system for controlling a large accelerator, planned as an integral part of the accelerator, has been introduced and used successfully: this is the control system of the meson factory in Los Alamos (USA). The entire start-up process of the meson factory (completed in June, 1972), from turn-on to the final adjustments, was accomplished with the help of the control system. The system has a modular structure: 8500 channels connected to sensors and control elements serve 64 modules which send information to the computer, which is located in the central control room, where there are two control panels. The system as a whole is organized around the computer, which works on-line, so that the meson factory can function only through the computer. With the help of this system, one can, in particular, find malfunctioning elements of the accelerator, and also diagnose the beam parameters and study its dynamics.

In contrast to the Los Alamos meson factory, where a single relatively large computer is used, the projected control system of the 200 GeV CERN accelerator is maximally decentralized. The use of secondary minicomputers for solving simple control problems reduces the load on the central computer. The decentralization of the synchrotron control system is taken to its logical end by the fact that even the central computer is a complex of medium-size computers, each of which carries out a strictly limited volume of functions. Control of the closed orbit allows decrease of the vertical magnet aperture exceeding a factor of 1.5. The correction algorithm for the closed orbit from information on the beam presumes two sources of orbital distortion: remanent fields and incorrect lens placement. The algorithm is a succession of iterations in each of which correction is accomplished by special dipoles on the injection level and translation of the basic quadrupoles on the high-energy level. The latter is accomplished when the accelerator is turned off according to results of closed-orbit measurements at high energy.

A complex control system is also being constructed at the TRIUMF meson factory, where six minicomputers combined into a single system are being used.

6. Reports about work on collective methods of acceleration show that in many laboratories in the USSR, USA, and FRG some successes have been achieved in the construction of such accelerators. However, up to the present, the difficulties arising during attempts to achieve high proton energies with these methods have not been overcome.

The idea of a linotron continues to attract the attention of physicists.

At SRIEA, the possibilities of using a linotron as a high-current accelerator are being studied. The limiting beam current at which the mode of acceleration with double recirculation is possible has been calculated.

The idea for a new accelerator, called the driftotron, arose at RTI. The driftotron is a cyclic accelerator in which the particles are accelerated by the rf field during their motion (drift) along the spiral equilibrium orbit in the axially symmetric field, which builds up along the axis of symmetry. The rf field is created by the accelerating gaps and the magnetic field is produced by a nonferrous magnet.

The recently organized interuniversity laboratory LIRF (Italy) devised a project for a 500 MeV linotron which should become the main accelerator at this laboratory.

7. The problem of increasing the power of existing accelerators and the associated problem of high-efficiency extraction of intense beams from ring accelerators attracts, as previously, the close attention of specialists. At present, the problem of achieving intensities greater than 10^{13} protons/pulse confronts proton synchrotrons with energies of several tens of GeV.

Great interest was given to reports of the proposed fundamental reconstruction of the IHEP proton synchrotron for an energy of 7 GeV. Three stages are planned: 1) reconstruction of the magnet system to create long linear gaps; 2) creation of high-efficiency, low-energy extraction with transport of the beam into a special "proton" building; 3) increasing the beam intensity to $\sim 10^{13}$ protons/pulse by increasing the injection energy to 300-400 MeV. A detailed plan for the first stage has been worked out.

As a preparation for the second stage, SRIEA and IHEP are studying measures to improve the magnetic field, in particular, measures to lower the field-pulsation coefficient to 10^{-6}/f and decrease the field instability to 10^{-4}. Similar measures must be applied for extraction at low energy from the IHEP accelerator.

Interesting studies of methods for decreasing the transverse beam instability in linear electron accelerators were conducted in 1969-1971 at the Physics Institute of the Academy of Sciences of the Ukrainian SSR. The basis of these studies was the devising and testing of an accelerating sector with a high critical current (theoretical value 3 A), at which a beam was obtained with a current of 700 mA in a pulse of 15 μsec long at an energy of 15 MeV with no signs of the instability effect. Studies of the dependence of the critical current of a multisegment 2 GeV accelerator on various factors showed that significantly increasing the critical current (to 100 mA) can be accomplished only through replacing the working sectors by sectors with a high critical current.

At the High-Energy Laboratory of JINR a system was devised for resonance high-efficiency beam extraction from a synchrophasotron operating at a radial betatron oscillation frequency of 2/3. At the beginning of the summer of 1972, the beam was extracted from the accelerator chamber and introduced into the experimental building. The extraction efficiency is no less than 90%. At the Leningrad Institute for Nuclear Physics there was devised an integrated system for low-energy extraction and single-cycle discharge of the beam onto an internal target. The efficiency of the low-energy extraction reaches 75%.

Adjustment of the system for single-cycle extraction of the electron beam with energy 1.35 GeV from the VEPP-3 storage unit has begun at the Institute for Nuclear Physics, Siberian Branch, AS USSR.

An important step in solving the problem of increasing intensity has been made at CERN, where adjustment of the 800 MeV booster is being made very quickly. By the end of September, 1972, CERN achieved multicycle (15 revolutions) injection into the booster, acceleration to 800 MeV, and extraction of the beam from four rings with its subsequent reconstruction and introduction into the main synchrotron. At present, half of the projected intensity has been achieved at the 800 MeV level.

8. The most significant results in accelerating heavy ions have been achieved at the Bevatron (USA), where there is now a whole series of extracted beams of various ions in the energy range from 250 MeV /nucleon to 2.1 GeV/nucleon, with the following particle intensities in the pulse: 10^{12} for protons, $2 \cdot 10^{11}$ for deuterons, $2 \cdot 10^{10}$ for α-particles, 10^{8} for carbon, 10^{7} for nitrogen, $1.5 \cdot 10^{7}$ for oxygen, and 10^{5} for neon. The emplacement of a new injector is envisioned, which would further increase the intensity. In the past year, 20% of the Bevatron's working time has been devoted to the use of heavy ions.

Work is continuing on increasing the efficiency of using the LVE synchrophasotron at JINR for accelerating heavy ions, where the acceleration proceeds in two stages with recapture. At present, 95% deuteron-recapture efficiency has been achieved.

Xenon ions with energy ~7 MeV/nucleon and intensity $2 \cdot 10^{10}$ particles/sec have been obtained by the accelerator system of the Nuclear Reactions Laboratory at JINR. The system consists of a classical cyclotron with radius 310 cm and an isochronous cyclotron with radius 200 cm.

In March, 1972, the isochronous cyclotron at the Nuclear Physics Institute of the Academy of Sciences of the Kazakh SSR was started up with regulated energy 7-30 MeV for protons, 14.5-25 MeV for deuterons, and 29-50 MeV for α-particles. The extracted-beam current is 30 μA for protons and 12 μA for α-particles.

9. A special session of the conference was devoted to questions of the use of accelerators in medicine, industry, and related areas of physics.

In medicine, accelerators are used mainly in treating cancers. Proton beams with energy less than 200 MeV and π-meson beams with energy ~500 MeV are especially valuable for radiation therapy because, when they are used, the dose at a subsurface focus may exceed by a factor of 10 the dose at the surface of the irradiated body. Besides this, bremsstrahlung from electron accelerators with energy ~20 MeV, and also electron beams with energy ~40 MeV are used for radiation therapy. Experimental high-energy proton beams for medical uses have been created at the synchrocyclotron at the Nuclear Problems Laboratory of JINR and at the IHEP proton synchrotron. Beams with regulated energy of 100-120 MeV have been used. At the present time, there are being worked out a project for a multichannel proton complex for massive irradiation of patients, based on the IHEP proton synchrotron, and also medical specifications for the construction of a clinical base using π-meson beams of the LYaP synchrocyclotron at JINR.

The use of accelerators in related scientific areas is connected at present with the use of synchrotron radiation whose spectral region 1000-1 Å (10 eV-10 keV) attracts the most attention, since it has the fewest efficient radiation sources. The sharply expressed directionality of the high degree of polarization of the synchrotron radiation and great energy density (tens of watts per cm^2) open up qualitatively new possibilities for experimental studies in solid-state spectroscopy, molecular biology, photochemistry, extra-atmospheric astronomy, etc.

Now, besides using existing electron synchrotrons, special machines (accelerators and storage units) are being created for this purpose. A project for such a storage unit has been devised at the Institute for Physical Problems, AS USSR. A 20 MeV microtron is used as the injector. The electron energy is increased to 1 GeV in the storage ring. The beam current is 100 mA; the lifetime is several hours. The beam gives 4.4 kW synchrotron radiation with wavelength at the spectral maximum of 4.7 Å. The use of special radiative magnets (superconducting with 7.5 tesla field) produces a wavelength of ~1 Å.

The 1.3 GeV electron synchrotron under construction in Krasnaya Pakhra by the P. N. Lebedev Institute of Physics, AS USSR, will be widely used as a source of synchrotron radiation. In the storage mode with local orbit distortion this synchrotron will give a high level of radiation in the range 0.5-100 Å.

The conference was very successful. This was in no small degree due to the excellent work done by the Organizational Committee headed by its chairman, Academician A. L. Mints.

XVIth INTERNATIONAL CONFERENCE ON HIGH ENERGY PHYSICS

S. A. Bunyatov

The XVIth biennial International Conference on High Energy Physics was held in the USA (Chicago and Batavia) on September 6-13, 1972. More than 800 physicists from 45 countries took part. Approximately 1000 reports were presented including 110 reports from the Soviet Union and OIYaI. The following main topics were discussed: strong interactions at high energy, weak interactions, electromagnetic interactions, and research methods in high energy physics.

1. The most interesting, accurate, and complete experimental results relating to strong interactions were presented, in the main, by the IFVE, OIYaI, ITEF, FIAN SSSR, and Erevan Institute of Physics Laboratories using the 70 GeV IFVE (USSR) accelerator and by the laboratories of CERN and its member nations where experiments were performed on the 28 GeV accelerator and 2 × 25 GeV colliding rings. The first results from the American National Laboratory at Batavia (USA) were of a preliminary nature due to large errors.

Total Cross Sections. Experiments performed at the IFVE accelerators studied the energy dependence to 65 GeV of the difference between particle and antiparticle total cross sections for particles belonging to the same isomultiplet. A series of experiments by Yu. D. Prokoshkina et al., shows that all total cross section differences decrease with increasing momentum, thus verifying the Pomeranchuk theorem. The first results on total pp-cross sections from the Batavia accelerator (100-300 GeV) and the CERN colliding rings (equivalent energy up to 1500 GeV) do not contradict the constancy of the pp total cross sections at the energies measured. However, these results are for the moment characterized by large errors (1.5 mb).

In the last several years, the energy dependence of the total hadronic cross section for γ-rays has been measured at SLAC (USA) up to an energy of 18 GeV. New results at higher energies from the electron beam at the IFVE accelerator (Erevan Institute of Physics, FIAN SSSR, IFVE) were presented to the conference. These showed that the total hadronic cross section for γ-proton interactions is constant at energies higher than 20 GeV. This is in qualitative agreement with the vector dominance model.

Elastic Scattering of Hadrons. New data on the ratio of real to imaginary parts of the forward proton–proton elastic scattering amplitude at an energy of 270 GeV was obtained at the CERN colliding rings. The magnitude of this ratio $(-1 \pm 7)\%$ is in agreement with the energy dependence found earlier at the IFVE accelerator by V. A. Nikitina at energies up to 70 GeV for both pp and pn collisions.

Measurements of elastic pp scattering in the region of the diffractive peak for four-momentum transfers of 0.01-0.5 $(\mathrm{GeV}/c)^2$ at the CERN colliding rings show the existence of a break in the differential cross section at a four-momentum transfer value of 0.1 $(\mathrm{GeV}/c)^2$. New data from Batavia and CERN on the slope parameter for elastic pp-scattering show that the slope of the pp-scattering peak continues to grow with increasing energy.

The first results on elastic scattering of pions, kaons, and antiprotons on protons at energies higher than 20 GeV were presented by two groups working at the IFVE accelerator: the IFVE–CERN collaboration (L. G. Landsberg, V. Kinzl) and S. B. Hurushev's group (IFVE). In the momentum transfer region 0.1-0.4 $(\mathrm{GeV}/c)^2$ the slope parameter is practically independent of energy for π^-- and K^--mesons with momenta up to 50 GeV/c. In the case of $\bar{p}p$-scattering, as energy increases, the slope parameter approaches the value of the pp-scattering slope parameter.

Translated from Atomnaya Énergiya, Vol. 34, No. 4, pp. 309-311, April, 1973.

New data from the CERN colliding rings exists on elastic pp-scattering in the region of large momentum transfer (greater than 0.5 $(GeV/c)^2$) at energies up to 1500 GeV. The differential cross section here has a simple diffractive structure.

Charge Exchange Scattering of Pions and Kaons. Results of a series of experiments by IFVE (Yu. D. Prokoshkin's group) on π^-- and K^--charge exchange scattering at energies greater than 20 GeV were presented at the conference. These experiments determined the differential cross sections of π^-p-charge exchange at zero degrees which is directly related to the π^-p- and π^+-total cross section difference.

The K^--charge exchange cross section on protons was measured at the IFVE accelerator and the Brookhaven accelerator at lower energies. It decreases with increasing energy much faster than predicted by the Regge pole model. Significant deviations from quark model predictions of π^-- and K^--charge exchange scattering are found at energies greater than 20 GeV.

Coherent Regeneration of K^0-Mesons. The study of the coherent regeneration amplitude energy dependence for K^0-mesons on protons allows a direct check of the Pomeranchuk theorem for kaon and antikaon interactions with nuclei from measurements of both the modulus and phase of the amplitude. The results obtained at the IFVE accelerator by the LVE OIYaI group (A. I. Savin et al.) show that the Pomeranchuk theorem holds. The modulus of the regeneration amplitude decreases with increasing energy while its phase remains constant (about $-130°$) up to 50 GeV/c. As a result of these measurements the energy dependence of the $K^{\pm}$-neutron total cross section difference has been determined. The data is in good agreement with the independent measurements at IFVE using a $K^{\pm}$-meson beam and confirm the growth of $K^{\pm}$-neutron total cross sections.

High Energy Production Processes. Many-particle production processes are becoming more and more important in the study of strong interactions. This is due to the fact that, first, many-particle states with multiplicities of up to 30 and total center of mass energy of up to 55 GeV have become available for study at the new accelerators (IFVE, CERN, Batavia Laboratory), and, second, because of new experimental verification of fundamental laws of scale invariance discovered in these processes. Furthermore, the possibility of effectively utilizing Regge pole ideas in constructing theoretical models that describe many-particle processes has been demonstrated. These trends stood out quite strikingly at the conference.

A group of theoreticians from IFVE (A. A. Logunov et al.) began studying processes with one secondary particle singled out as early as 1967 (these later acquired the name "inclusive"). Scale invariance in the formation of π^-- and K^--mesons and antiprotons on aluminum nuclei in the proton energy range of 20-70 GeV was discovered in an experiment by an IFVE–CERN collaboration (Yu. D. Prokoshkin and G. Allabi).

The first results on multiparticle production from the CERN colliding beams and from the hydrogen bubble chamber at Batavia have confirmed the existence of scale invariance up to the highest accessible energies. It has been possible to explain a number of observed regularities by using the generalized optical theorem in conjunction with ideas about Regge poles. The tendency for a widening exploration of multiparticle production processes will doubtless continue in the next several years.

In the field of strong interaction theory (F. Low, USA) no new approaches were discussed. The importance of calculating the effect of cuts was particularly stressed. In connection with this, the calculation of the Reggeon–Baryon scattering cross section presented by K. A. Ter-Martirosyan (ITEF) was mentioned.

2. In the field of weak interactions particular attention was devoted to discussion of the CP-invariance violation problem in K^0-meson decays. A large part of K. Rubbia's rapporteur's talk was devoted to a discussion of new results concerning the lifetime of the neutral shortlived kaons: $(0.8958 \pm 0.0045) \cdot 10^{-10}$ sec; $(0.899 \pm 0.005) \cdot 10^{-10}$ sec which are quite different from the preconference accepted values $(0.862 \pm 0.006) \cdot 10^{-10}$ sec.

The new data lead to a significant change in the parameters that characterize CP-invariance violation in the decay of neutral kaons.

The greatest interest was aroused by the discussion of the $K_L^0 \rightarrow 2\mu$ problem. The problem consists of the fact that A. Clark et al. have experimentally determined an upper limit to the branching ratio for this decay of $1.8 \cdot 10^{-9}$ while the theoretical lower bound, which follows from the unitarity condition is $6 \cdot 10^{-9}$. A report from a group of physicists from Brookhaven who have begun a new experiment searching for the two-muon decay of the long-lived kaon was presented. They have found four to six cases of such a decay which gives a branching ratio for two-muon decay of $1 \pm 0.45 \cdot 10^{-8}$. This value is in strong contradiction to the result of A. Clark et al.

Several models have been proposed in 1971-1972 to explain the $K_{L_0}^0 \rightarrow 2\mu$ decay. The most interesting one can be reduced to the assumption of CP-invariance violation in $K_L^0 \rightarrow 2\gamma$ decays. As a result of this assumption the existence of a two-muon decay for the short-lived kaon is theoretically predicted with a branching ratio of $\sim 10^{-6}$.

According to reports from CERN groups the decay $K_S^0 \rightarrow 2\mu$ has not been seen at a level of $4 \cdot 10^{-7}$.

The theory of weak interactions was discussed at a plenary session in a report by B. Lee (USA). Particularly great progress has occurred in the field of constructing models of weak interactions based on spontaneously broken chiral symmetries. This is connected with the proof of renormalizability of such models. The possibility has appeared of creating as complete a theory of weak interactions as, for instance, quantum electrodynamics for the electromagnetic interactions of leptons. The new theory unifies weak and electromagnetic interactions. The new models of weak interactions demand the existence of heavy leptons (particles with the same quantum numbers as electrons and muons but with considerably greater mass) which have not yet been seen experimentally. In connection with this much attention was given at the conference to the phenomenology of heavy leptons whose possible existence was first examined in the papers of E. M. Lipmanov (USSR).

3. In the field of electromagnetic interactions interest has shifted to many-particle photo- and electroproduction. Particularly interesting are studies of the dependence of many-particle production cross sections on the square of the mass of the virtual photon. It has been discovered at Stanford that with increasing virtual photon mass not only does the mean multiplicity not increase (as was predicted by some popular models) but it even shows a tendency to decrease. The study of these regularities is very much in the forefront in connection with intensive experimentation using fast cycling hydrogen chambers and streamer chambers with liquid hydrogen targets in the working volume.

Much experimental data has been accumulated on two-body electromagnetic reactions. Some of these regularities have turned out to be difficult to interpret in a simple and unique theoretical manner.

Considerable progress has been achieved in the field of study of electron–positron interactions (Orsay, Frascatti, Novosibirsk, Cambridge). Significant new results have been obtained on the production of hadrons in electron–positron collisions. A new vector meson, the ρ'-meson, with a mass of ~1600 MeV and a width of ~350 MeV, decaying into four charged pions, has been discovered in these collisions as well as the production of proton–antiproton pairs. The study of multiparticle production has begun using colliding beams and it has been shown that (contrary to theorists' expectations) the total cross section for hadron formation is three times larger at 4 GeV center of mass energy than the cross section for muon pair production. This field will grow rapidly in the next several years due to the completion of new colliding beam accelerators (USSR, USA, FGR).

From the theoretical side, attempts at explaining scaling in deep inelastic scattering from the point of view of field theory were most interesting. It has been shown (N. N. Bogolyubov, V. S. Vladimirov, A. N. Tavkhelidze, SSSR) that the scaling hypothesis does not contradict the basic postulates of field theory and, furthermore, that scaling is quite probable from the point of view of finite charge renormalization (A. V. Efremov, SSSR).

4. A special section chaired by L. Alvarez was set aside in the conference program to discuss the newest achievements in apparatus for experiments at modern accelerators. Invited talks concerning the most important new directions of experimental technology and a small number of original reports on the most interesting recent developments were presented.

The most significant recent accomplishments in the detection of transition radiation in the x-ray frequency region have come from the Soviet Union (Erevan Institute of Physics). In connection with this, A. Ts. Amatuni's report in which he presented the results of A. I. Alikhan'yan et al. on detecting transition radiation and pointed out future possibilities of using transition radiation in experiments at very high energy accelerators was interesting. This methodology is now being investigated at a number of laboratories and could become quite practicable with particle beams of 1 TeV (1000 GeV) energies.

Interesting news in the field of coordinate detectors was presented in a report by V. P. Dzhelepova (OIYaI) on the development of a solid argon wire detector. The possibility of creating such a detector has been demonstrated (A. F. Pisarev et al.), its characteristics have been studied, and a proposal has been made to use it to develop coordinate detectors.

Results of research on total absorption detectors performed in Hofstater's laboratory at Stanford were presented. Unique cylindrical sodium-iodide crystals 60 cm in diameter and up to 40 cm thick have a resolution of up to 2% for 16 GeV electron energies.

At the present time many laboratories are equipped with streamer chambers. As a rule, these are one or two meter streamer chambers with a liquid hydrogen target within the working volume. A new development in the creation of streamer chambers which are also gas targets was presented in a special report of Yu. Scherbakov (OIYaI). It has been shown possible for the first time to create a high pressure He^3 streamer chamber. Chambers of this type are a quite promising tool for high energy physics experiments that require a visible interaction vertex and the detection of short range tracks (as in the case of coherent production). The importance of the development of streamer chamber technology was underlined by the fact that immediately after the Batavia conference a special international conference on streamer chambers was held at the Argonne National Laboratory.

The main trends in the development of large liquid hydrogen bubble chambers are: the change to a multiexpansion regime per beam spill; the triggering of the photographic system of the chamber by a trigger system which selects a given reaction type, thus reducing the number of photographs to be scanned and increasing the statistics of good events.

In the field of new experimental technology used at accelerators, the system of cylindrical wire spark chambers with magnetostrictive readout built in Stanford for experiments with colliding beams should be mentioned. The system consists of a solenoidal magnet with a 3 m inner diameter. Four concentric cylindrical wire chambers subtending scattering angles in the range 45-135° are placed inside the magnet.

Special note should be made of the rapid expansion of the role of computers in high energy physics. Expenses on the development of computing centers at large laboratories constitute about 10% of the yearly budget. All large laboratories are equipped with powerful computing centers using IBM 360/91, CDC-7600, or several CDC-6600 machines. Most of the electronic experiments are performed directly with a digital computer. These are usually small machines of the PDP-11 type or similar machines produced by the firm of Hewlett–Packard. All digital computers are equipped with a multitude of external attachments (displays, teletypes, plotters, magnetic disk memories, photomemories).

Participants at the conference had the possibility of visiting Argonne National Laboratory where a 13 GeV proton synchrotron is in operation. After the conference, trips were arranged to other major accelerator centers in the USA: the Brookhaven National Laboratory, equipped with a 33 GeV proton synchrotron; the Lawrence Laboratory in Berkeley where experiments are performed on a 6.3 GeV proton synchrotron and a 740 MeV synchrocyclotron; the Stanford SLAC Laboratory, with a 20 GeV linear electron accelerator; the Los Alamos Anderson Meson Factory equipped with a 800 MeV linear proton accelerator with a projected mean current of up to 1000 mA.

INTERNATIONAL SYMPOSIUM ON THE PHYSICS OF HIGH ENERGIES AND ELEMENTARY PARTICLES

S. M. Bilen'kii and V. M. Sidorov

The symposium was organized by the Combined Institute for Nuclear Research and the Institute of Experimental Physics of the Slovak Academy of Sciences and took place on October 2-9, 1972, in Czechoslovakia (Strba Lake, High Tatra).

Physicists from the USSR, Czechoslovakia, the German Democratic Republic, Hungary, Poland, Bulgaria, Mongolia, Rumania, and Austria took part in the symposium. Forty-five reports were delivered. The results of recent experimental and theoretical research concerning a wide range of problems of the physics of strong, electromagnetic, and weak interactions were reported. Several reports were devoted to new methodological studies in the field of high-energy physics.

New concrete data obtained at the Dubna, Serpukhov, and CERN accelerators were presented.

A review of data on p–p and p–d scattering through small angles, obtained at the accelerator of the Institute of High-Energy Physics (IHEP), in the energy range 10-70 GeV was presented by M. G. Shafronova (Joint Institute for Nuclear Research). These studies allow us to verify the basic theoretical conceptions about the behavior of scattering amplitude at high energies.

Explanation of the anomaly in the decay $K_L \to \mu^+\mu^-$ is one of the important problems of recent years. In connection with this anomaly, a hypothesis was expressed concerning the possibility of a relatively high probability of the decay $K_S \to 2\gamma$. V. A. Shabanov reported on searches for this decay. Analysis of ~500,000 photographs showed that $\Gamma(K_S \to 2\gamma)/\Gamma(K_S) < 5 \cdot 10^{-4}$. In connection with the problem $K_L \to \mu^+\mu^-$ hypotheses were also expressed concerning the possibility that there exists a light boson which decays into μ^+ and μ^-. J. Gladky (Czechoslovakia) presented results of searches for this particle from the IHEP accelerator. No such boson was observed.

M. Novak (Czechoslovakia) told of studies of K_S meson regeneration with hydrogen and carbon, which was accomplished using the IHEP accelerator. These experiments give information on the amplitude difference of elastic scattering of K^0 and $\bar{K}^0$ mesons. Ya. Ruzhechka (JINR) presented preliminary results of searches for the Dirac monopole at the IHEP accelerator at proton energies of 70 GeV. An attempt was made to observe Cerenkov radiation which could be caused by the monopole. It was shown that the creation cross section of the monopole–antimonopole pair by protons at nuclei is less than $8 \cdot 10^{-40}$ cm^2 on condition that the monopole mass is ~5 GeV.

Great attention was given to experiments which studied single-particle processes. In experiments on the 2 m JINR propane chamber, reported by R. Sosnowski (Poland), data were obtained on multiplicity in interaction processes between π mesons and protons and neutrons. It was shown that in a wide energy range the equality $n_{charge} = 2n_{\pi^0}$ holds. The inclusive spectra which were found are in agreement with scale invariance.

Several reports concerned results obtained using the JINR 1 m hydrogen chamber irradiated by π mesons with pulse of 5 GeV/sec.

I. M. Gramenitskii reported on the results of the first experiments using a deuteron beam accelerated in the JINR synchrophasotron. This work studied various interaction processes of deuterons whose momentum was 3 GeV/sec with protons. A. Mihul (Rumania) reported on interesting ideas concerning new

Translated from Atomnaya Energiya, Vol. 34, No. 4, pp. 312-313, April, 1973.

means of presenting and analyzing experimental data. V. A. Shakhbazyan (JINR) reported on results of searches for resonance in many-baryon systems.

Reports were made on studies of low-energy processes. V. M. Sidorov (JINR) told of results of studies of the capture reaction of π^- mesons by nuclei of carbon, nitrogen, and oxygen. The probability of forming B^8 through the capture of π^- mesons by nitrogen nuclei was measured. V. S. Roganov (JINR) reported on a wide-ranging program of study of chemical compounds using μ mesons. The depolarization of μ^+ was measured in various media. The dependence of the μ^- depolarization on the length of the carbon chain in alcohols and chloralkides allowed determination of the radius of the chemical-interaction zone for mesonic atoms.

The theoretical reports were mainly devoted to the following questions:

1) devising methods for analyzing experimental data which would completely take into account analytical properties of elements of the S matrix;

2) the use of dispersion relations for studying strong interactions;

3) electromagnetic interactions and scale invariance;

4) studies of inelastic processes based on the Regge and Veneziano model;

5) weak interactions and the physics of K mesons;

6) devising methods for determining resonance spin and parity.

The review report by P. Preshnaider dealt in detail with a new statistical method for presenting experimental data through analytical functions, which was developed by theoreticians in Czechoslovakia. A. Nogova and J. Pisut used this method to determine the parameters of 3.3 resonance in a $\pi-N$ system. The values obtained differ from those accepted earlier ($M = 1204$ MeV and $\Gamma = 73$ MeV). P. Lichard reported on results of applying the statistical method for determining the pion–nucleon coupling constant. It was found that $f^2 = 0.794 \pm 0.0020$. On the basis of dispersion relations, taking two-particle unitarity into account, M. Blazhek has constructed a model for describing hadron-scattering processes at low and moderate energies.

The work of V. I. Zhuravlev and V. A. Meshcheryakov (JINR) is devoted to a detailed analysis of the dispersion equations of Chu and Low. New solutions to these equations have been found. S. Dubnichka (JINR) used dispersion relations to calculate the real part of the amplitude for elastic scattering of ions by He^4. S. M. Bilen'kii (JINR) presented the results of analysis of all available data on elastic e–p scattering and extremely inelastic scattering of electrons by protons. M. Petras (Czechslovakia) has constructed a model of nonlocal electromagnetic interactions. All physical consequences of the Petras model coincide with those of ordinary electrodynamics. M. Nog (Czechoslovakia) examined several consequences of scale invariance. The author showed that at the limit $f_\pi \to 0$ and $m_\pi \to 0$ the Pomeranchuk theorem follows from scale invariance. A. B. Kaidalov et al. (USSR) constructed a multiperipheral model with Regge pion, which allows one with one parameter to describe a large collection of experimental data. The results of calculating the inclusive spectra on the basis of the dual B_6 model in the Mellor theorem were presented by K. Bilbo et al. (GDR). There is good agreement with experiment. General limits on the quasipotential parameters were obtained by S. V. Goloskokov and V. A. Matveev (JINR). S. M. Bilen'kii in his review report presented the Vainberg theories of weak and electromagnetic interaction. Analysis of the possible effects related to weak second-order current was reflected in the paper by G. Pichman (Austria). M. Lokajcek (Czechoslovakia) gave a detailed analysis of the interrelations of unitarity for the S matrix. It was shown that a consistent formulation of field theory is possible without the principle of superposition and unitarity relation. J. Votrub et al. (Czechoslovakia) offered a new method for testing the SRT theorem. V. Novak (GDR) told of phenomenological methods he developed for determining the spin and parity of a system of three pions. The report by M. Bendar (Czechoslovakia) was devoted to methods for determining spin and parity for three-particle baryon resonances. A. V. Tarasov and L. G. Tkachev (JINR) examined coherent and incoherent interactions between high-energy particles and nuclei.

The above indicates the multiplicity of problems discussed at the symposium. We should mention the work of the organizational committee headed by the director of the Institute for Experimental Physics of the Slovak Academy of Sciences, Professor I. Dubinski. The close scientific ties and the unconstrained

atmosphere allowed the symposium participants to discuss in detail experimental and theoretical research on the physics of high energies which is being conducted in the socialist countries.

The symposium papers will be published by the Joint Institute for Nuclear Research in 1973.

INTERNATIONAL CONFERENCE ON THE INTERACTION OF LASER RADIATION WITH MATTER

P. P. Pashinin

The conference took place on October 9-13, 1972, in Marly-le-Roi (France). It was organized by the French Commissariat on Atomic Energy and the research center in Limeil and was devoted to one of the present trends in modern physics, namely, obtaining a high-temperature plasma using lasers and thus solving the problem of controlled thermonuclear reactions.

The conference is similar to the Gordon conferences, to which only a limited number of specialists most active at a given time in the field are admitted, and only by invitation from the conference organizing committee.

The main purpose of the conference is the operational exchange of information concerning the latest experimental results, new promising means of solving problems, new types of equipment, and programs of work at basic-research centers for the near future. About 110 people took part in the conference (of them, 50 were French scientists, mainly from the Limeil and Saclay centers). The foreign scientists represented practically all major world scientific centers at which such work is conducted. The Soviet delegation included Academician N. G. Basov, O. N. Krokhin, T. G. Kryukov, and P. P. Pashinin. Fifty-five reports were delivered. The conference materials will not be published.

One can conclude from the reports that no significant successes have been achieved recently in heating a dense plasma by using lasers. Several laboratories, following the lead of French scientists, obtained a stable neutron output of $\sim 2 \cdot 10^4$ neutrons/pulse based on nanosecond neodymium-glass lasers with energies up to 100 J and using solid targets of deuterium or deuterized polyethylene. The record remains $\sim 10^6$ neutrons/pulse achieved upon irradiation of a target at the 10 channel laser installation at the P. N. Lebedev Institute of Physics, AS USSR. Apparently, the most important results in this field are the determination of the strong dependence of neutron output on focusing conditions (research center at Limeil) and also the observation of a strong decrease in neutron output when using a yttrium–aluminum–garnet laser as the master oscillator in the laser system (Institute of Plasma Physics, Nagoya, Japan). The latter result is still difficult to explain even in qualitative terms.

Several theoretical reports were made on the mechanisms of energy transfer from the laser to the plasma. They analyzed various types of instabilities in a plasma in a strong field and their possible role in increasing the efficiency of the energy portion, including the role of the forced Brillouin scattering type of instabilities and parametric and beam instabilities, etc. Experimental work in this field is, as before, in its infancy, and new results are purely qualitative. Changes in the type of radiation reflection from the plasma dependent on the growth of flux density of the laser radiation, and also the appearance of fast neutrons, hard x-rays, and fast ions were observed. It is significant that in theoretical work the leading laboratories (Los Alamos, Livermore, etc.) have gone over to broad application of modern computers for designing numerical experiments. This allows more accurate evaluation of the relative role of various nonlinear interaction mechanisms between laser radiation and the plasma, and clearer presentation of the physical picture of instability in both time and space.

Notable progress has been achieved in devising methods for laser–plasma diagnostics. A diagnostic technique has been worked out for fast ions with simultaneous determination of the absolute output of fast particles and the energy distribution of the particles. It was shown that a significant portion of the hard x-radiation in laser experiments is caused by radiation arising at the chamber walls when fast particles

Translated from Atomnaya Énergiya, Vol. 34, No. 4, pp. 313-314, April, 1973.

hit them. This complicates plasma diagnostics using continuous-spectrum x-rays. Developed in more detail were methods of studying plasma parameters using absorption and radiation in the spectral lines of heavy multicharged ions. This method is very promising, since it allows one to move into the field of very high plasma densities, where the application of other methods is limited. Especially interesting was the report by P. Jeglay (France) on theoretical and experimental studies of nonequilibrium distributions of the state populations of highly excited ions. These results are important not only from the point of view of devising correct laser–plasma diagnostic techniques using spectral lines in the x-ray region. The authors, essentially for the first time, proved experimentally the possibility of obtaining highly unstable states, which allows us to expect that x-ray lasers will be produced. In general, perfecting of spectral measurements in the x-ray region, together with perfecting methods for measuring the distribution function of fast ions, apparently, will serve in the near future as the basis for laser–plasma diagnostics, especially for plasmas with very high densities.

Work on laser systems for obtaining high-temperature plasmas can be divided into two tendencies. The goal of the first tendency is devising the next generation of 10^3-10^4 J nanosecond and picosecond lasers. This apparatus is mainly for conducting experiments to determine fusion-energy output, electron and ion temperatures, the role of instabilities, and the efficiency of the energy contribution from the laser energy and power and also from the type of laser target. Main attention, as previously, is given to neodymium-glass lasers. The Livermore Laboratory, Los Alamos, Rochester University, and the Naval Research Laboratory (USA) propose to begin work in 1973 with ~10^3 J lasers. The Livermore Laboratory and the laboratory of KMS Industries (USA) plan ~10^4 J lasers. The Institute of Plasma Physics (Garching, FRG) is now working on creating a 1-2 GW laser with pulse length 10 nanoseconds based on photodissociation of CF_3I (or C_3F_7I) with wavelength 1.316 μ. A 10^3 J system is now being devised.

The goal of the second tendency is the more long-range prospect of solving the problem of controlled thermonuclear fusion. In this case, increasing the laser system efficiency and the feasibility of working in various spectral ranges are necessary. Electric-discharge lasers at the CO_2 molecule vibrational transitions with wavelengths 10.6 μ are promising. The Los Alamos Laboratory is now devising such a laser system with energy of the order of 10^3 J, with the prospect of further increasing it to 10^4 J. The National Research Council in Canada has produced a 300 J CO_2 laser with pulse length 60 nsec.

Attempts are now being made to efficiently transform infrared laser radiation into the visible and, possibly, ultraviolet spectra using nonlinear optics methods and induced effects.

The main burden of work on controlled thermonuclear fusion using lasers has changed to the analysis of proposals for realizing superhigh compression and heating of the spherical solid D–T target to densities 10^3-10^4 times the initial density. Qualitative examination has been made of the stability of compression and various aspects of the interaction of the laser radiation with the target and the surrounding plasma corona. Plasma instabilities in the region of strong laser radiation and their role in the efficiency of energy transport from the laser beam to the plasma, forced Brillouin and Compton scattering, and parametric, two-stream, and relativistic instabilities have been analyzed. Special attention was given to the possible influence of non-Maxwellian electron distribution arising through these effects on the heating of the compressed central target nucleus. This may greatly decrease the achievable compression.

There were new results concerning calculations of the compression of the D–T spherical shell. In the range of low laser energies this model gives less optimistic results than the solid spherical target. However, it is attractive because, in principle, it allows one to use long laser pulses and decreases the extreme demand for laser-beam focusing. Calculations show that at laser energy of 0.8 MJ one can obtain an energy amplification factor of the order of 100.

An interesting model for a thermonuclear target, in which the D–T fuel is compressed by a heavy spherical liner, was analyzed by S. Kalizski (Poland). Two cases were examined: ignition of the sphere using an explosion at the surface, and ignition using laser radiation. The given plan is advantageous since, because of the great system inertia, ignition can occur more slowly (and, consequently, the laser pulse duration can be greater, the power lower, and the role of instabilities less) and the D–T combustion conditions are improved.

In conclusion, we may note that in the most advanced countries recently, intensive work is being conducted on theoretical analysis and the creation of unique laser systems for testing the prospects for laser-induced thermonuclear fusion.

THIRD INTERNATIONAL CONFERENCE ON MEDICAL PHYSICS

V. S. Khoroshkov

The Third International Conference on Medical Physics took place in Göteborg, Sweden, from July 30 through August 4, 1972. It was organized by the International Organization for Medical Physics with the cooperation of the Swedish National Committee on Medical Physics and the Göteborg Center for Medical Technology. About 320 reports were given at 29 sessions. Many of the sessions show at a glance the broad range of physics and engineering trends which were reflected in the work of the conference. A series of reports of interest from the point of view of atomic physics (radiation sources, including heavy-charged-particle accelerators, dosimetry, and the production and use of isotopes, etc.) was also rather extensive.

About 20 reports were devoted to accelerators and their beams. More than half of these reports concerned proton, heavy-ion, and π-meson beams. Basic physical research in radiation medicine and biology is devoted to beams of heavy-charged particles. The two most complete review reports (M. Raju, USA, and B. Larsson, Sweden) reflect the situation in this field. Comparative analysis of the physical properties of beams of various heavy-charged particles are being conducted and the fields in which they can be applied in biology and clinical practice are being elucidated. It is known that beams of heavy-charged particles, due to the physical properties of their interactions with matter, allow one to produce a more sharply defined dose field than the dose fields associated with x-ray, γ-ray, and electron beams. They have a higher relative biological efficiency, and the radiation effect depends less strongly on the oxygen content in the irradiated tissue. This allows one to produce a better ratio of the dose at the focus to the dose which acts on surrounding tissues and the organism as a whole.

At the world's largest accelerators, a close interrelationship is being effected between oncological and radiological centers which conduct both research and clinical activities. An interesting report was given by L. Skaggs (USA), which was devoted to the prospects for developing medical and biological research at the world's largest proton synchrotron in Batavia. The use of three types of radiation is proposed: a 66-200 MeV linear-accelerator proton beam; a π^--beam generated by the proton beam from a booster synchrotron; fast neutrons generated at Be and D targets by a 37-66 MeV proton beam from a linear accelerator. The report included the expected radiation parameters, which are evidence of their usefulness both in biological research and in clinical practice. The Los Alamos scientific laboratory of the University of California (A. Landy et al., USA) plans to begin biological research using a meson beam as early as the middle of 1973. The expected beam intensity assures a dose rate up to 35 rad/min, which, in general, is sufficient for clinical use.

At the Bevatron of the Donner Laboratory of the University of California (H. Maccabee et al., USA) research is being conducted on a 200 MeV/nucleon oxygen-ion beam. A depth-distribution curve for the dose was obtained which takes into account the contribution from secondary particles; the ratio of the dose at the Bragg peak to the dose at the plateau is ~6 with peak width 3 mm. After the introduction of a new injector in 1973, the beam intensity will reach 10^9 ions/pulse, which is also sufficient for clinical use.

There is great interest in the report by E. Hall et al. (USA) on studies of a 3.9 GeV nitrogen-ion beam. The beam was produced at the Princeton proton accelerator (Columbia University), which was reconstructed in 1971 as a heavy-ion accelerator. Studies were made not only of the depth distribution of the dose (the depth of the peak in water is about 15 cm, the ratio of the dose at the peak to that at the plateau is ~4, and the peak half-width is several millimeters); in a series of biological tests, the relative biological

Translated from Atomnaya Énergiya, Vol. 34, No. 4, pp. 315-316, April, 1973.

efficiency (1.5 at the plateau and 6 at the Bragg peak) and the oxygen effect (2.5-3.0 at the plateau and 1.25-1.4 at the Bragg peak) were also measured.

The report by B. Winston (USA) was devoted to continuing biological research with the π^--meson beam of the Nimrod 7 GeV proton synchrotron. Clinical work in neurosurgery using α-particles is being developed in Berkeley (J. Lyman et al., USA). In the Soviet Union, medical and biological research and clinical work using proton beams are being conducted at the synchrophasotron of the Nuclear Problems Laboratory of the Joint Institute for Nuclear Research (Dubna) and at the synchrotron at the Institute for Theoretical and Experimental Physics (Moscow). L. L. Gol'din et al. (USSR) presented the main results of medical application of the 70-200 MeV variable proton beam of the ITEP synchrotron. One hundred and sixty three patients have undergone a course of radiation therapy using this beam since 1969.

Several reports dealt with applications of electron beams in radiology. There was interest in a survey of the history and present development of linear medical accelerators given by K. Karsmark and N. Perin (USA). The Swedish firm Instrument AB Skanditroniks presented a report on a new microtron (electron energy 10 MeV). The apparatus includes, besides the accelerator, a system for distributing and expanding the beam, attachments allowing the use of both electrons and bremsstrahlung, and, finally, irradiation stands.

We should note that reports were presented which confirm the great effectiveness of the physical approach to explaining biological mechanisms. The results of original research given in the report by E. L. Andronikashvili (USSR) are very interesting. Comparative activation analysis of microelements in cell nucleus and nucleic acid molecules of malignant tumors and healthy tissue reveals ways to explain a series of chemical and biological processes which occur in tumors. This allows one to establish hypothetical mechanisms for some radiation reactions which are important during the use of heavy-charged particles (especially the oxygen effect), but which have never had a single accurate explanation.

New methods in dosimetry for various types of radiation were presented along with the development of familiar dosimetric methods (ionization chambers, TLD, photodensitometry, etc.). The report by N. Ramsey (England) presents data on the variation of conductivity of an irradiated polystyrol due to temperature. The mechanism of conductivity variation is similar to the leaking effect in thermoluminescent dosimeters, but the recording technique (measurement of the conduction current) is definitely simpler. Interesting results on the variation of the resistance of water under irradiation were presented in the report by J. MacDonald and K. Short (England).

Also examined were problems concerning the production and use of isotopes in biological experiments and clinical practice. Short-lived isotopes were discussed at a separate session. The advantages and capabilities of C^{11}, O^{15}, N^{13}, and F^{18} in diagnostic use were shown clearly in reports by T. Jones (England), M. Ter-Pogossian (USA), and J. Laughlin et al. (USA).

A special session and a series of models at a technical exhibit were devoted to the use of computers in medicine (diagnostics, monitoring organism functions, planning treatment, etc.). An interesting report by J. Cunningham and J. Niderer (Canada) showed the feasibility of studying biological mechanisms through the use of mathematical models.

The conference demonstrated the wide inculcation of atomic physics in medicine and confirmed the urgent necessity and promise of close contact between these two sciences and the effectiveness of using physical methods in biological and clinical research. The conference was well organized. Abstracts of the reports are to be published in the journal Physics in Medicine and Biology (England).

SYMPOSIUM ON HANDLING WASTES FROM REPROCESSING SPENT NUCLEAR FUEL

N. V. Krylova and A. N. Kondrat'ev

A symposium on handling of wastes from reprocessing of spent nuclear fuels was held in Paris from November 27 through December 1, 1972. This symposium was organized under joint IAEA and Euratom auspices. Participating were about 250 specialists from 27 countries and 11 international agencies. Possible methods for handling high-level radioactive wastes forming in solvent-extraction reprocessing of spent fuel were discussed: storage of liquid wastes in tanks, burial of wastes in underground strata and in artificial voids, formed by nuclear explosions, immobilization of wastes by vitrification and bituminization. Other reports were heard on handling wastes resulting from nonaqueous techniques of reprocessing spent nuclear fuel, separations of the transuranium elements, and also reports on estimates of radiation hazards accompanying venting of radioactive iodine, krypton, and tritium to the atmosphere.

Some of the USA reports dealt with new methods of wastes disposal: transmutation of long-lived fission fragments, launching of high-level wastes into outer space, and disposal of solid high-level wastes in Antarctic ice masses by burial.

In dealing with problems of how to handle radioactive gases, the contributing authors reached the unanimous opinion that venting radioactive krypton to the atmosphere would not bring the radiokrypton level near critical tolerance limits in the air before the year 2000, but that krypton would have to be trapped in all countries in order to prevent local pollution of the atmosphere. The krypton trapping technology has already been developed and meets cost requirements. After krypton has been extracted from the wastes stream, it is to be stored in tanks or dumped at sea to depths of 4000 to 5000 meters down, in leaktight containers ($p = 150$ atm). But in that case there is still danger of gas leakage from the storage container, and danger of entrainment by bottom strata of water saturated with krypton to the surface of the sea via convective processes.

Methods for concentrating tritium by selective ion exchange and fractional distillation are expensive and practically inapplicable in the case of large volumes. These difficulties lend added emphasis to the earlier preference for two methods of tritium removal: by venting to the atmosphere with vapor and by dumping sufficiently diluted condensates into rivers. But burial of liquid wastes containing tritium in naturally-formed underground strata is a more reliable alternative.

The most reliable method for storing liquid radioactive wastes, as experience acquired in the USSR, USA, Britain, and France has demonstrated, is storage in stainless steel doubly shielded and cooled tanks with the aid of a flow coil for removal of heat generated in the radioactive decay process. The tanks are to be blown with air in order to dilute the hydrogen given off in radiolysis of the solutions.

In other countries, in contrast to the Soviet Union with its practice of wastes disposal by underground burial, feed of pulsed-flow or bubbling-flow air is envisaged as a means of mixing the solutions in order to keep precipitates from settling and accumulating on the tank bottom, and also in order to blow out gases formed in radiolysis. The cost of storing high-level solutions is estimated at one to two dollars per liter. Storage of liquid high-level wastes in deep-lying geological formations is now looked at skeptically (USA, West Germany, Italy). The degree of risk inherent in this method is now being determined.

A report by USA representatives analyzed the possible use of underground cavities dug out by nuclear explosions as suitable sites for disposal of high-level wastes by underground burial. When acted upon by

Translated from Atomnaya Énergiya, Vol. 34, No. 4, pp. 316-317, April, 1973.

heat generated in radioactive decay, the solutions heat up to the boiling point, vapor is given off, and the dry residue heats to the melting point, so that the surrounding silicate host rock also melts to form a vitrified mass which cools down within 90 years to form a monolith. The danger lodged in this method is that the void may become filled with water. Moreover, the structures of the wastes reprocessing plant must be capable of withstanding an underground explosion.

Solidification of high-level wastes was in the spotlight at the convention. Reports submitted by representatives of the USA, Britain, France, and West Germany cited results from the work of pilot plants and scaled-up semi-industrial plants in this line of work. For example, three distinct methods of vitrification (a two-stage technique with calcination in a spray dryer and subsequent meltdown in a crucible, a single-stage process involving vitrification in a crucible, and a continuous process by which phosphate glasses are produced) were put through experimental paces at the WSEP pilot plant at Hanford (USA), in order to secure information needed in selecting the appropriate method in the designing and servicing of a wastes solidification plant. This plant has been in service for four years: as a result, calcination and subsequent meltdown of the glass in a melting pot of refractory steel is considered the optimum variant at this stage of the game. But despite the promulgation of a law in the USA stipulating that plants reprocessing nuclear fuel are obliged to solidify liquid radioactive wastes over a five-year period, and to transport solidified high-level wastes to a Federal storage site for permanent storage over a ten-year period, industrial implementation of wastes solidification processes is being put off to 1980, and the wastes storage site will be ready for service only by 1986.

A fluidized-bed wastes calcination plant with a throughput of 250 liters liquid wastes per hour has been in service in Idaho (USA) since 1963, and has been producing 45 liters calcinate per hour. The calcinate powder is stored in air-cooled pressuretight tanks. The plant costs, including storage costs, is 1.25 dollar/liter. But the general assumption is that the powder will have to be vitrified sometime in the future.

Pilot plants designed for vitrification of real high-level wastes, with plant capacities ~20 liters/h, are also in service in Britain and France. The technical possibility of realizing the process both from the standpoint of producing glasses with sufficient stability to both radiation and chemical attack (borosilicate glasses for the most part) and from the standpoint of cleanup of the off-gases, has been demonstrated. We should note here that industrial implementation of wastes solidification plans in Britain is scheduled for not earlier than the Nineties, while French plans call for earlier implementation in the coming years.

Experiments on solidification of high-level wastes, carried out in West Germany, did not go beyond the framework of scaled-up laboratory facilities working on simulated wastes. For example, the possibility of converting wastes to borosilicate glasses is being verified at the facility, and the development of a thermite process of wastes solidification utilizing the heat from chemical reactions (specifically, mixtures of MnO_2 and Al), under laboratory conditions has commenced. The assumption is that industrial implementation of wastes vitrification processes in West Germany will become a reality not sooner than 30 years off.

Bituminization of wastes with specific activities to 10 Ci/liter is being carried out at the Eurochemik plant (at Mol, Belgium). Temporary storage and long-term vitrification is envisaged for high-level wastes. A low-temperature process for vitrification of liquid wastes, involving transformation of the wastes into alumophosphate ceramics (the Lotes program) is undergoing development. The resulting product exhibits excellent thermal conductivity and high chemical stability. The low temperature of the process (300°C) eliminates the materials selection problem, but the technology of the process is far from completely worked out.

Specialists discussing techniques for storage of vitrified waste products reached the conclusion that the storage site should be built in the vicinity of the wastes reprocessing plant, as a rule. Air cooling or water cooling of the burial grounds is viewed as mandatory.

Disposal of solid wastes by burial in salt mines is still on the agenda in the USA and in West Germany, but these countries have not yet made final decisions on organizing full-scale storage of wastes in abandoned salt mines and pits, since this involves a great risk and no agreement has been reached yet on the storage times required (300 to 600 years).

Investigations on reprocessing of high-level wastes accumulated in nonaqueous processes of nuclear fuel regeneration were reported on only by the USSR and France. Conversion of wastes to solid monolithic

preparations (phosphate glasses, cryolite structures) appears promising. A report by USSR representatives elicited great interest, particularly on the part of French scientists.

Reports submitted by USA specialists provided estimates and assessments of such problematic topics in the handling of high-level wastes as transmutation of long-lived fission-fragment isotopes, launching of high-level wastes into outer space, burial of solid wastes in the Antarctic ice masses, and so forth. But all of these techniques are in the initial stage of development and still far from practical implementation, while the costs of removing wastes by those methods are still far higher than generally acknowledged.

A lively discussion was provoked by reports presented by Soviet specialists on vitrification, bituminization, and underground burial of high-level liquid wastes. In contrast to scientists representing other countries, the Soviet scientists showed that the vitrification method is not only more reliable, in terms of technology, but also cheaper than other methods for storage of liquid wastes. The reason is that long-term storage of liquid wastes calls for constant rebuilding of new storage facilities to replace those that are no longer serviceable (over a span of 20 to 25 years).

Soviet specialists also demonstrated and provided costs estimates for the possibility of pumping high-level wastes with specific activities of 10 to 30 Ci/liter into underground strata. Work on studying bituminization of wastes with specific activities as high as 100 Ci/liter is now under way.

In conclusion, results of the symposium were discussed with answers solicited from experts on general topics. These experts included specialists from the USSR, USA, France, Britain, West Germany, and India.

The reports, and the concluding discussion, showed that the countries now leading in nuclear power development have accumulated vast experience in handling high-level wastes.

The proceedings of the symposium are to be published in the first half of 1973.

VISIT BY USSR STATE COMMISSION FOR THE USE OF ATOMIC ENERGY DELEGATION TO BELGIUM AND THE NETHERLANDS

O. A. Voinalovich

On October 2-16, 1972, in accordance with the agreement on cooperation, a delegation from the USSR State Commission for the Use of Atomic Energy visited the Netherlands and Belgium. The delegation familiarized itself with accelerator installations at research centers and universities in these countries, and also electrophysical apparatus and automatic systems and devices which provide for control of accelerators and conducting physical experiments.

In the Netherlands, the Soviet specialists became acquainted with the reactor in Petten, with the 12 MeV tandem accelerator at Utrecht University, and with the 30 MeV proton cyclotrons at the Free University of Amsterdam and at Groningen University.

An interesting project for a 500 MeV linear electron accelerator with off-duty factor up to 10% has been devised at the Institute for Nuclear Research in Amsterdam. Permission has been obtained for construction and until financing begins various subassemblies of the accelerator, in particular the modulators, are being perfected in mock-ups. Construction of the accelerator should take 5-6 years.

At Groningen University a modern three-sector isochronous cyclotron has been put into use. It was devised by the Philips company with the following beam parameters:

Particles	Energy, MeV	Current
Protons	5-70	25
Deuterons	10-80	25
He^3	15-165	10
He^4	20-160	10

A 60 kV electrostatic deflector assures extraction of protons with energy 50 MeV and beam emittance 25 mm · rad. At the end of an ion tube 30 m long and 46 mm in diameter, the beam dimensions are 5 × 10 mm. Physicists can already use the machine, but there is still an insufficiency of experimental apparatus.

In Belgium, besides several standard electrostatic generators, the University at Ottignies is operating a four-sector isochronous cyclotron produced by the French firm CSF Thomson, with the following beam parameters:

Particles	Energy, MeV
Protons	10-80
Deuterons	10-40
He^3	20-120
He^4	20-80

The internal current of accelerated protons and α-particles is 100 μA, and that of the extracted beam is 20 μA.

The delegation visited the nuclear center at Euratom, located in Geel (near Mol) where they were familiarized with the 70 MeV linear electron accelerator delivered by the French firm CSF Thomson in

Translated from Atomnaya Énergiya, Vol. 34, No. 4, p. 318, April, 1973.

1965. With pulse duration of 10 nsec, the current amplitude is 5 A, which assures obtaining $>1 \cdot 10^{18}$ neutrons/sec at a uranium target and produces good conditions for experimenting with neutrons when using transit-time methods.

The physics centers of Belgium and the Netherlands are well supplied with computer technology and measurement apparatus.

In the Netherlands, at the Institute on Applications of Atomic Energy in Agriculture, our delegation was shown two irradiation devices, one using isotopes and one using a 3 MeV electrostatic accelerator. Both installations were produced for experiments as well as industrial applications in a single building, but their load is insufficient. The Institute devised several processes for radiation treatment of food products in order to preserve them longer, but the Institute specialists believe that the consumer is not now prepared psychologically to use irradiated food products.

An important place at the installations is given to working out rules for irradiating medical preparations and instruments. The rules will then be instituted at the industrial γ-installation which our delegation also visited. The "Gammaster" installation was constructed by a consortium of pharmaceutical firms. It is located in a separate building. According to an official announcement, it is unique in the country, it works without losses, and is designed for a 1 MCi Co^{60} source. The initial loading was 160 kCi. The source and equipment were delivered by the Canadian firm AECL. The installation works 24 hours a day. Besides the director, an operator and a workman work one shift. The rest of the time, the installation building is closed and a conveyer works automatically with a 25 min exposure for a 2.5 Mrad dose. The daily output is 12 m^3 of various products with average density 0.1 g/cm^3.

The design of a similar installation has been completed in Belgium. Construction is expected to be completed in 1975.

BRIEF COMMUNICATIONS

A conference of Soviet and Czechoslovak specialists on 1973 scientific and technical collaboration between the State Atomic Energy Commission of the USSR (GKAE SSSR) and the Czechoslovak Atomic Energy Commission (KJE CSSR) was held in Prague from July 31 through August 4, 1972.

Information on the progress of work in planning 1972 collaborative efforts and information on plans for collaboration during 1973 was made available.

On August 4, 1972, the representative of the KJE CSSR, J. Neumann, signed a working draft, which was co-signed on August 7 in Moscow by the GKAE SSSR representative A. M. Petros'yants, of the 1973 plan of scientific and technical collaboration, stipulating details of joint work and joint research to be pursued and continued in the following avenues: fast sodium-cooled reactors; water-cooled water-moderated power reactors; nuclear chemistry and nuclear technology; materials science and testing; nuclear physics, solid state physics, plasma physics; radioactive isotopes.

The collaboration incorporates a huge volume of work in the field of the peaceful uses of atomic energy, and in particular the development of special types of equipment for nuclear power stations, as well as comprehensive research on structural materials. A broad range of scientists and specialists is to be tapped by the GKAE SSSR and KJE CSSR in order to carry out these plans.

A USA national conference on linear proton accelerators was held in Los Alamos (New Mexico), October 10-13, 1972. The conference attracted an audience of 160 scientists representing 35 scientific institutions in eight countries. The most numerous were the delegations from the USA, West Germany, Canada, and France. Also participating in this conference was a delegation of Soviet specialists (six persons from four distinct organizations).

Of the 64 papers presented at the conference, 38 were read from the floor, including eight papers combining several submitted contributions, and seven invited tutorial review reports on various aspects of accelerator science and engineering. The remainder of the papers will be published.

Linear proton accelerators were the subject matter of 27 papers, including nine submitted by colleagues of the Los Alamos meson factory installation, which is now in the mop-up stage of preliminary and adjustment operations. The initial portion of the Alvarez structure 100 MeV accelerator is completely in operation; a maximum pulsed current of 3 mA has been attained. The beam has already been passed through the entire accelerator, but particle losses are still considerable in the last portion of the tract. The conference demonstrated that almost all linear injector accelerators for proton synchrotrons are also being employed in research in other areas of science, notably medicine and biology.

Heavy ion accelerators were the subject of another six papers, and electron accelerators were discussed in five other papers.

Reports by D. Bohne and T. Niwednitschanski (Darmstadt, West Germany) covered the Unilac accelerator project, which will be capable of accelerating nuclei of all elements from hydrogen to uranium with design intensities of 10^{14}, $3 \cdot 10^{13}$, $2 \cdot 10^{12}$ particles/sec, for respective masses to 70, 164, and 238.

According to a communication by B. Panowsky, pulsed currents were successfully increased from 20 to 80 mA at the Stanford linear electron accelerator, after work had been done on suppressing transverse instability in the accelerating sections, and partial replacement of the 20 MW pulsed klystron amplifiers by 30 MW tubes made it possible to raise the output energy to 23 GeV. Complete replacement of the klystrons made it possible to attain energies of 25 GeV.

Klystrons designed for as much as 60 MW pulsed output power are being developed. Design work on a beam recirculation system capable of increased electron energies from 25 to 45 GeV through double beam transits through the accelerating structure has now been completed.

Translated from Atomnaya Énergiya, Vol. 34, No. 4, p. 319, April, 1973.

Eleven reports dealt with applications of superconductivity in accelerator engineering. An invited review report by W. Matthias stressing shortcomings in the study of superconductivity to date, which hold up the applications of the phenomenon in resonant type linear accelerators, provoked a lively discussion on the floor.

Of the four reports forthcoming from the Soviet Union, three were read out at the conference, and the fourth will appear in the printed proceedings of the conference. These reports dealt with a project involving building a meson factory, increasing currents in an existing linear proton accelerator, multipurpose utilization of linear accelerators, and several special topics in high-power radio electronics. The reports stimulated interest and a lively discussion.

A conference of IAEA experts on the dosimetry of fast neutrons was held in Vienna, November 20-24, 1972. This conference discussed the use of neutron radiation in radiobiological research and in radiation therapy (radiation shielding and radiation protection were not discussed). The need for such a conference was prompted by the undeniable complexity and specific features of neutron dosimetry in the study of biological objects, and by the low level of development of special procedures in this area.

Experts from Austria, Great Britain, Hungary, India, the Netherlands, the USSR, USA, France, and West Germany, as well as an IAEA representative, a total of twenty specialists, participated in the conference. Requirements applicable in dosimetry in radiobiological and radiotherapeutic uses of neutrons, and neutron dosimetry in particular, plus topics concerning mutual intercomparisons of dosimetric data, were discussed in the eleven papers presented. The neutron dosimetry procedures touched upon contrasted rather interestingly: ionization detectors, thermoluminescent detectors, chemical detectors, and threshold detectors are currently in use in this work (the threshold detectors involve recording of both induced activity and tracks of instantaneously emitted heavy ions).

The conference participants came to agreement on the need to work out an international system of standards covering irradiation of biomedical objects by neutrons. The recommendations forwarded to IAEA include a proposal for intercomparisons of absorbed-dose measurements and separate determinations of neutron components and γ-components. The standard dosimeters recommended in this work are ionization type condenser chambers with tissue-equivalent walls and detectors designed to record γ-radiation primarily. The insistent need for work geared toward securing information on radiation quality in neutron irradiations, particularly under clinical conditions, was also concluded in the deliberations.

BIBLIOGRAPHY

NEW ITEMS PUBLISHED BY ATOMIZDAT (FIRST QUARTER 1973)

A. A. Makarenya, N. G. Karpilo, and I. N. Filimonova (compilers), D. I. Mendeleev, in Reminiscences of His Contemporaries*

This book is a collection of reminiscences of the life and works of D. I. Mendeleev written down by contemporaries of his. The latter sketch a picture of Mendeleev as an original and independent-thinking scientist, and a patriot of old Russia. The authors of these reminiscences are scientists and public activists spanning two generations. Among them are some of Mendeleev's co-thinkers (I. M. Sechenov, K. A. Timiryazev, V. V. Stasov, I. E. Repin, and others) and Mendeleev's disciples (V. E. Tishchenko, D. P. Konovalov, G. G. Gustavson, and others), as well as prominent Russian and Soviet scientists (Academicians A. P. Karpinskii, V. L. Komarov, N. S. Kurnakov, V. A. Kistyakovskii). Reminiscences of relatives of D. I. Mendeleev, of his wife and children, are also included.

The first edition was dedicated to the 100th anniversary of the publication of D. I. Mendeleev's periodic table of the elements. The second edition of the book is supplemented by reminiscences from the pen of F. M. Dostoevskii, A. Blok, T. Torpe, and others.

The book is written for a broad audience.

ATOMIC AND NUCLEAR PHYSICS

V. M. Baier, V. M. Katkov, and V. S. Fadin, Radiation of Relativistic Electrons†

This book is devoted to a systematic presentation of the theory of bremsstrahlung and pair production in the passage of a high-energy particle through an external field, or in collisions of high-energy charged particles with polarization effects and spin effects taken into consideration. The special features of electromagnetic processes at high energies which tend to simplify their radiation appreciably are singled out for attention. This book is the first monograph to shed detailed light on this domain of electromagnetic phenomena.

The book is written for specialists working in the field of high-energy physics and the physics of elementary particles, and concerned with design and use of accelerators and storage rings, and may also prove useful to instructors, and to graduate and senior undergraduate students specializing in physics.

* * *

B. M. Smirnov, Asymptotic Methods in the Theory of Atomic Collisions‡

This book discusses processes involving collisions between atomic particles. Attention is centered on resonance processes occurring with large cross sections, and playing the major role in phenomena

* Atomizdat, Moscow, 1973, 2nd Edition.
† Atomizdat, Moscow, 1973.
‡ Atomizdat, Moscow, 1973.

Translated from Atomnaya Energiya, Vol. 34, No. 4, pp. 321-326, April, 1973.

taking place in gases and in plasma. The first part of the book deals with investigations of the interaction potentials of atomic particles separated by large distances. The second part of the book makes use of those interaction potentials in order to find the cross sections of resonance processes, and in studying the mechanisms underlying the transitions discussed. The presentation of these problems from a unified point of view relies on the asymptotic method, which is far superior to other theoretical methods of relevance in its potentialities for this range of scientific problems. Results of experimental research on these problems are presented. Problems drawn from different fields of physics and engineering, where these processes are of some practical importance, are presented to the reader.

The book is written for senior majors in physics and engineering departments, and also for research scientists whose object of investigation is plasma or gas (e.g., gas lasers, shock tubes, thermonuclear facilities and high-temperature facilities, the upper atmosphere, astrophysics, plasma generators).

* * *

E. Storm and H. Israel, Studies of γ-Radiation Interactions (for energies from 0.001 to 100 MeV and elements from 1 through 100)*

This is a handbook providing tabulated reference material on interactions of γ-radiation with matter in the case of elements from 1 through 100, and also for air, water, concrete, and sodium iodide, over the range of γ-photon energies from 0.001 to 100 MeV. The data obtained take into account results of recent experimental and theoretical investigations, and differ substantially from the values of cross sections in common use at the present time.

The book is written for physicists, engineers, research scientists working in research institutes and at design and planning institutes and laboratories, and for graduate and undergraduate students. It can also be useful to persons working with radioactive materials and with sources of ionizing radiations.

ELECTRON PHYSICS EQUIPMENT

V. P. Volodin, B. A. Korotin, and E. A. Ryabova, Operation and Upkeep of Equipment for Measurement of Ionizing Radiations. No. 3, Dosimeters†

Reference data on the characteristics of the basic types of ionizing radiations and their interaction with matter, the basic concepts of the dosimetry of ionizing radiations, terms, formulas, and relationships linking the characteristics of ionizing radiations and dosage levels, specific requirements imposed on dose-measuring devices and devices designed to measure the dose rate of ionizing radiations, are cited. Conditions and regulations regarding the operation of dosimeters of ionizing radiations, how they are to be checked out and calibrated, and verification of the basic parameters under the operating conditions of repair shops, are described. Detailed information is made available for each type of dosimeter, on rules governing adjustments, maintenance, and repair, and the monitoring and measuring equipment to be employed in their upkeep and calibration.

The book is written for dosimetry service equipment personnel, and also for specialists whose work involves radiation measurements.

NUCLEAR POWER

G. M. Kuzovlev, Special-Purpose Hydraulic Engineering Installations at Nuclear Enterprises‡

The first edition of this book (1966) was met with interest by specialists, and received a positive assessment in the periodical literature as the first publication in practice to provide comprehensive coverage

* Atomizdat, Moscow, 1973. Handbook, translated from English.
† Atomizdat, Moscow, 1973.
‡ Atomizdat, Moscow, 1973.

of the specific topics in the design and construction of hydraulic engineering facilities for performing technological process operations with fluids other than ordinary water, and with solutions of radioactive materials at hazardous concentration levels. In the second edition, amply supplemented with new data and reworked with due attention given to the latest achievements in this area, the author lays bare topics in the design of installations intended for storage and transport of liquid radioactive materials at atomic industry plants. In the elucidation of migration of radioactive isotopes, descriptions are given of the principal physicochemical processes affecting the flow of contaminants.

The book is writen for engineers and technicians engaged in the design and construction of special-purpose hydraulic engineering installations for atomic plants.

* * *

B. I. Taratorin, Simulation of Stresses in Nuclear Reactor Structures*

The book is a first experiment in a consistent presentation of the theory and practical methods of simulation and polarization-optical investigation of stresses in the structural members of nuclear reactors. Some original results on methods in the production of optically sensitive polymeric materials, on the theory of simulation and on practical techniques for stress simulation in inelastic strains and inhomogeneous temperature fields, are cited in the text. The theory and methods are illustrated by examples of polarization-optical stress studies relevant to structural members of nuclear reactors.

The book is written for research scientists, design engineers, and graduate students specializing in research and stress calculations in the design of nuclear reactors. This text may also prove useful to students and instructors in technical colleges in "dynamics and strength of machines" courses.

CHEMICAL ENGINEERING. RADIOCHEMISTRY. RADIATION CHEMISTRY

R. V. Dzhgatspanyan and M. T. Filippov, Radiation Chemistry of Halogenated Organic Compounds†

This book discusses radiochemical halogenation processes from the standpoint of their utilization in chemical engineering. Radiolysis of organic halogen-containing compounds, radiation chlorination and sulfochlorination of organic compounds, telomerization of olefins with halogen-containing compounds, hydrobromination of ethylene, etc., appear among the topics described. Current processes of radiation halogenation and processes of possible technological interest in the immediate future, are also described. Extensive bibliographies are appended to most of the sections in the text.

The book is written for research scientists interested in radiation chemistry and radiation technology, for chemical engineers interested in radiation technology, and for seniors majoring in related topics at college level. It would also be of interest to research scientists and chemical engineers concerned with chemical kinetics, photochemistry, chemical engineering, and petroleum chemistry.

* * *

S. V. Elinson, Spectrophotometry of Niobium and Tantalum‡

The book outlines spectrophotometric techniques in niobium and tantalum determinations, which are of great importance in quality control in the production of structural materials used in the nuclear power industry. The complexity of the chemistry of niobium and tantalum includes the proclivity of compounds of those elements to undergo hydrolysis, polymerization, and copolymerization with elements of neighboring groups in the periodic table of the elements, the readiness with which they form colloidal solutions and complex compounds, and is responsible for the widespread reliance on spectrophotometric methods using

* Atomizdat, Moscow, 1973.
† Atomizdat, Moscow, 1973.
‡ Atomizdat, Moscow, 1973.

organic reagents suitable for obtaining color-sensitive reactions with niobium and tantalum. Reliable methods for determinations of niobium and tantalum in ore materials, in concentrates, metals, alloys, and in numerous products incorporating those elements, are described in generous detail.

The monograph can constitute a useful manual for analytical chemists working at enterprises of the nonferrous metallurgy industry and ferrous metallurgy industry, and at scientific research institutes.

* * *

Vikt. I. Spitsyn and V. V. Gromov, Physicochemical Properties of Radioactive Solids*

This book discusses topics in the radiation chemistry and radiochemistry of solids – one of the most urgent and newest topics in modern physical chemistry. Special attention is reserved for changes in the physicochemical properties of radioactive preparations in response to their own radiation, as compared to similar effects occurring in response to external ionizing radiation, a topic which is of importance both in nuclear technology and in applications of radioisotopes in scientific research.

The book is for the most part the fruit of the labors of the two authors, who have been engaged in research, over the course of the past 10-12 years, on regularities in changes in the properties of highly radioactive solids (catalytic activity, surface structure, adsorptivity, contamination, etc.) in response to self-irradiation.

The book is written for research scientists, engineers, graduate students and senior undergraduates majoring in the radiochemistry and radiation chemistry of solids.

NUCLEAR MATERIALS SCIENCE AND MATERIALS TESTING

O. Week (editor), Plutonium†

This handbook consists of four major sections: plutonium chemistry, chemical engineering (Vol. 1, Atomizdat, Moscow, 1971); and plutonium metal science, nuclear fuel (Vol. 2).

The book is written for specialists on research and production of nuclear materials and fuel elements. It will also be of considerable interest to engineers and research scientists in various fields: chemists, physicists, metallurgists working with other rare metals.

* * *

V. Muller, G. Blacklidge, and J. Liebowitz (editors), Metal Hydrides‡

Up-to-date information on hydrides of the transition metals are reviewed in this book written by prominent American specialists. Physicochemical, mechanical, structural, and heat transfer properties of metal–hydrogen compounds are cited; the fabrication technology of hydride materials is described, as well as quality control measures, and information is presented on various aspects of applications of metal hydrides in nuclear industry. The translation is embellished by commentaries and supplements. An extensive bibliography, a survey of a multiplicity of experimental and theoretical information on hydrides, combines to render this text a valuable handbook for engineers, production experts, designers, and research scientists specializing either in nuclear materials science and testing or in powder metallurgy, chemical engineering, aerospace, solid state physics, theory of chemical bonds, etc.

* Atomizdat, Moscow, 1973.

† Atomizdat, Moscow, 1973. Handbook, Vol. 2, translated from English under editorship of N. T. Chebotarev.

‡ Atomizdat, Moscow, 1973. Translated from English under editorship of R. A. Andrievskii and K. G. Tkach.

N. S. Kostyukov, F. Ya. Kharitonov, and N. P. Antonova, Radiation Stability and Corrosion Stability of Electrical Ceramics*

This book is devoted to a current problem concerning applications of ceramic materials in the nuclear power industry, in radio electronics, and in other branches of industry. Experimental data on testing of ceramic materials in corrosive media (water and steam, vapors of special fuels and oils, melts and vapors of alkali metals, etc.), are cited. The effect of ionizing radiation on ceramics and on ceramic-to-metal bonds, the effect of chemical composition and structure on the corrosion stability and radiation stability of ceramic materials, are discussed, and the principal fields of applications of electrical ceramics in modern industry are analyzed.

This book is intended for research scientists, engineers, and technicians engaged in production and research work on structural materials for nuclear industry.

SOLID STATE PHYSICS. CRYSTALLOGRAPHY

A. A. Predvoditelev and O. Troitskii, Dislocations and Point Defects in Hexagonal Metals†

This book discusses the nature and properties of imperfections in the crystal structure of hexagonal metals. Various methods are presented for experimental studies of imperfections, and an assessment is given of their potentialities and the basic findings obtained through their use. Dislocation mechanisms in plastic flow, and in the movement, interaction, and locking of dislocations are discussed. A critical review is given of competing theories on strain hardening in hexagonal metals. Data derived from experimental studies of point imperfections, specifically those of radiation origin, and on the interaction between imperfections in the crystal structure and electrons in the metal, are analyzed.

The book is written for research scientists, graduate students, and engineers specializing in solid state physics.

* * *

M. Steel and E. Veural, Interaction between Waves in a Solid State Plasma‡

This book presents the properties of solid state plasma and wave interaction in a solid state plasma from a unified vantage point. The book is in two parts. The first part discusses interaction between waves. The presentation is done in the language of quasiparticles. The derivation of the macroscopic hydrodynamical model is done on the basis of fundamental microscopic models. In the second part of the book, the macroscopic model is utilized in a discussion of the interaction between electrokinetic waves, and also their interaction with other collective excitations in the solid. The book contains an extensive bibliography of both theoretical and experimental papers.

This text is intended for engineers and physicists interested in solid state plasma, and also for students majoring in this and related subjects.

APPLICATIONS OF ISOTOPES AND RADIATIONS

V. A. Vorob'ev, V. I. Gorbunov, and A. V. Pokrovskii, Betatrons in Nondestructive Testing**

This book discusses practical applications of sources of high-energy bremsstrahlung from betatrons for quality control of products in the manufacture of power machinery. The physical fundamentals of the

* Atomizdat, Moscow, 1973.
† Atomizdat, Moscow, 1973.
‡ Atomizdat, Moscow, 1973. Translated from English.
** Atomizdat, Moscow, 1973.

method are outlined in brief, and the advantages of the method are discussed. Radiographic and radiometric methods of recording radiations and their applications in industrial nondestructive testing work are described. Radiometric flaw detection instruments incorporated in various systems for high-speed automated quality control under plant conditions are discussed, as well as their design, allocation, and controls.

The book is written for engineers and technicians in industrial plants concerned with nondestructive flaw detection in materials and products.

* * *

N. V. Churaev and N. I. Il'in, Radiotracer Techniques for Studying the Flow of Underground Waters*

The book discusses the theoretical fundamentals of applications of radioactive tracers in the study of moisture transport processes in porous media, and the flow of underground waters. The accuracy of radiotracer methods is evaluated, and results of experimental verification are cited. A special section of the book is devoted to procedures for carrying out radiotracer measurements in field work. A review of the present state of the art in application of radiotracer techniques in hydrogeology, hydrology, and hydraulic engineering is also included. Descriptions of research done by the authors personally takes up much of the space. The first edition appeared in 1967 and was soon exhausted in sales.

The book is intended for research scientists, engineers, and technicians concerned with the study and implementation of tracer methods in the investigation of flow of underground waters.

DOSIMETRY AND RADIATION SHIELDING

D. L. Broder, L. N. Zaitsev, M. M. Komochkov, V. V. Mal'kov, and B. S. Sychev; D. L. Broder (editor), Concrete in Shielding of Nuclear Installations†

The text outlines the basic tenets of design and calculations of biological shielding for nuclear reactors and elementary-particle accelerators developed as a result of analysis of theoretical and experimental investigations on shielding of nuclear facilities. Information on cost estimates of concrete shielding for reactors and accelerators is provided; optimized selection of materials, particularly concretes, from the standpoint of minimum cost of the shielding and of the installation as a whole, is discussed. A large array of reference material needed in shielding thickness calculations and in determining engineering costs of shielding structures is reviewed.

The book is written for engineers and technicians engaged in the design and building of nuclear installations. It will also prove useful to students in engineering and physics colleges and civil engineering colleges.

* * *

I. A. Arshinov, G. A. Vasil'ev, Yu. A. Egorov, et al.; Yu. A. Egorov (editor), Serpentinite in Nuclear Reactor Shielding‡

The book describes the physicomechanical, heat transfer, thermal, vibrational, shielding, and other properties of serpentinite concrete. With its excellent shielding properties, serpentinite concrete is becoming increasingly popular in reactor construction applications. Constants are cited, as well as procedures for design calculations of serpentinite shielding. Fabrication, preparation, and laying of concrete in the construction of shielding are discussed.

The book can be a useful handbook for engineers and designers concerned with shielding of nuclear reactors.

* * *

* Atomizdat, Moscow, 1973, 2nd Edition.
† Atomizdat, Moscow, 1973, 2nd Edition.
‡ Atomizdat, Moscow, 1973.

N. D. Ponikarov and V. I. Chumakov, Shielding Structures in Underground Workings*

This brochure provides validation for the possibility and feasibility of using underground shelters to protect people from the effects of nuclear weapons blasts.

Special features of the effect of striking factors of a nuclear explosion on underground cavities are outlined. The characteristics of underground structures are discussed from the standpoint of the protection they afford to people inside. Basic requirements for correctly adapted underground structures are cited, and recommendations are given on the design of underground shelter installations.

The brochure is written for specialists in mining work and in civil defense concerned with the utilization of mining type structures for the protection of the population.

* * *

S. M. Gorodinskii, Personnel Protection Means in Work with Radioactive Materials†

The book presents basic Soviet and foreign materials on protection of personnel working with radioactive substances. The basic designs of equipment for protection of breathing organs and skin of personnel in different sets of production conditions are described. Special attention is given to work under conditions typical of repair and accident situations. Close attention is given to techniques for evaluating the effectiveness of personnel protection means, to their correct performance and use, and to repair and deactivation. The first edition of the book came out in 1967. This second edition is greatly revised and supplemented with information secured in recent years. The second edition goes into much greater detail on general questions of theory and method in radiation protection of personnel.

The book is intended for research scientists, physicians, and engineers working in the field of radiation safety.

* * *

M. Frank and V. Stolz; I. B. Keirim-Markus (editor), Solid State Dosimetry of Ionizing Radiation‡

This book, written by specialists of the German Democratic Republic, is devoted to a trend in the field of dosimetry of ionizing radiations which is current and promising from both theoretical and practical vantage points: dosimetry using inorganic and organic solids. Here for the first time we find assembled ample material on research in this field completed to date in all countries around the world. Considerable attention is given to description of designs and to practice in the use of solid-state dosimeters. Integrating solid-state dosimeters, scintillation dosimeters, semiconducting and thermoluminescent dosimeters, get their share of attention. Numerous diagrams, photographs, and tables of data are provided.

The book will be of interest to research workers and practical workers. It can also be recommended as a helpful text for instructors and students in colleges with courses specialized in this area.

RADIOBIOLOGY

L. A. Pertsov, Ionizing Radiations in the Biosphere**

This book discusses the basic regularities in the formation of natural radiation loads, within the sphere of influence of which the life activities of all plant and animal organisms take place. The reasons

* Atomizdat, Moscow, 1973.
† Atomizdat, Moscow, 1973, 2nd Edition.
‡ Atomizdat, Moscow, 1973. Translated from German.
** Atomizdat, Moscow, 1973.

for oscillations of those loads are pointed out. The effect of modern technical progress and of intense urbanization on shifts in components of the radiation field in the biosphere and sociosphere are discussed. Indices of radioactivity of components of the environment, in tissues of plants, animals, and humans, are cited. Detailed descriptions are provided of the properties of various radionuclides, their distribution and migration through the troposphere, atmosphere, hydrosphere, and pedosphere as a function of the physical and chemical properties of the radionuclides, with attention given to features of the landscape and terrain, climate, meteorological conditions, and so forth. Quantitative and qualitative estimates of the degree of hazard in probable uncontrolled access of radioactive mixtures to the environment are advanced.

The book is written for instructors at college level, for research scientists, health physicists, public health personnel, and engineers.

COMPUTERS

Engineering Mathematics Techniques in Physics and in Cybernetics. Collection of Articles No. 2*

This collection of articles cites results on the development and utilization of engineering mathematics techniques in theoretical and experimental physics, cybernetics, and computer work. Methods of description, numerical analysis, and simulation of complex processes and systems are reported. Some computer calculations are presented.

The book is written for research scientists, engineering physicists, and students majoring in computer work and in cybernetics.

* Atomizdat, Moscow, 1973.

I. L. Karol'

RADIATION ACTIVE ISOTOPES AND GLOBAL TRANSPORT THROUGH THE ATMOSPHERE*

Reviewed by B. A. Nelepo

This book by I. L. Karol', a leading specialist in the field of tracer investigations of atmospheric processes, is most timely. Methods for determining the global propagation of radioactive isotopes would come in very handy at the present time in the solution of problems involving overall contamination of the atmosphere. We now have the opportunity of applying the methods of nuclear physics to allied branches of science and engineering.

The first chapter (there are eight chapters in all in the book) surveys the experimental data providing a picture of the fields of concentration of radioactive isotopes in the atmosphere and of variations in the characteristics of those fields in space and in time. Results of research on radioisotopes of different origin are also surveyed; the text offers a review of data on the disperse composition of radioactive aerosols in the atmosphere.

The text proceeds further into a discussion of a model of global transport of impurities through the troposphere and lower stratosphere; it derives the basic equation and the boundary conditions; a correct estimate is given for the terms of the equation for different groups of isotopes.

A special chapter (the third) is devoted to vertical transport and to removal of radioactive aerosols present in the troposphere. The author attempts an analysis of these little-studied processes that affect removal of radioactive aerosols, for which a few quantitative models relating those processes to the physical characteristics of the troposphere are investigated.

The next chapter generalizes upon traditional concepts on the distribution of medium-zone parameters of transport in the troposphere and lower stratosphere.

The fifth chapter presents a procedure for numerical solution of the boundary problems for the equations of global transport of atmospheric impurities.

Analysis of the special features of propagation of radioactive contaminants present in the aerosol state and the vapor state enabled the author to arrive at some adequate solutions. That is demonstrated through the example of the formation of fields of radon concentration, as well as radioactive products of a series of powerful nuclear weapons explosions (this is covered in the sixth and seventh chapters).

The last chapter in the book discusses some interesting problems concerning the shaping of fields of cosmogenic isotopes.

The author thereby clearly formulates principles of tracer investigations of global transport of impurities. Optimum time averaging scales (one month), height averaging scales (1 km), and horizontal averaging scales (10 degree zonal belt in latitude) are determined, so that it becomes possible to distinguish ordered and macroturbulent transport through the planetary atmosphere.

The solution of numerical problems corresponding to the models constructed made it possible to analyze the fields of concentrations in the atmosphere up to 25 km, and fields of fallout for the following radioactive isotopes: Rn^{222}, Pb^{210}, Bi^{210}, Po^{210}, and Na^{22}, Be^{7}, P^{32}, P^{33}.

* Gidrometeoizdat, Leningrad, 1972.

Translated from Atomnaya Energiya, Vol. 34, No. 4, p. 325, April, 1973.

Planetary distributions of artificial and naturally occurring radioisotopes were calculated, and confirmed by results of experimental research. That makes it possible to utilize the methods developed by the author both in order to forecast the radiation situation and in order to solve problems involving transport of various pollutants through the atmosphere.

There is every reason for assuming that this monograph by I. L. Karol' will meet with great interest on the part of specialists, and that it will prove useful in the solution of many problems in nuclear meteorology and nuclear hydrophysics.

P. Quittner

γ-RAY SPECTROSCOPY*

Reviewed by L. V. Groshev

Applications of electronic computers to modern γ-ray spectroscopy, using scintillation detectors and semiconductor detectors, are discussed. The basis of this book is the author's work in nuclear physics laboratories and nuclear chemistry laboratories of the Central Physics Institute in Budapest and in various laboratories in the USA.

Literature appearing up to the end of 1964 is covered. Results of several more recent papers appearing while the book was being written are also covered.

There are ten chapters. The first chapter (a brief introduction) takes note of the need to use computers in processing the very large amount of information obtained in modern γ-ray spectroscopy with the aid of scintillation detectors and semiconductor detectors.

The second chapter deals with statistical fluctuations and smoothing of spectra. Measurements of intensities are also discussed in this chapter, and the concept of mean value and dispersion are introduced. The spectrum smoothing process is discussed in quite some detail. Numerical examples are cited as illustrations.

The third chapter discusses the determination of the shape of the detector line (response function). Basic mechanisms active in the interaction between γ-radiation and the material comprising the radiation counter are cited, and the shape of the expected line is given for the case of monochromatic γ-photons. A table of sources of γ-radiation should be useful for calibrating counters. The shape of the total-energy peak is analyzed, then relationships between the parameters of this peak are discussed. Shapes of lines outside the total-energy peak are also described in this chapter. The results are illustrated by a number of concrete examples.

Total-energy peaks contain the most valuable information in γ-ray spectroscopy. The position of the peaks determines the energy of the corresponding γ-photons, while the area under the peaks determines the line intensities. The fourth chapter is devoted to determinations of the position of the peak by a variety of methods: by searching for maxima in the distribution to be analyzed, by the method of smoothing the first derivative, and by the method of generalized second differences.

In the largest chapter, the fifth, we find a treatment of determination of the area under the peaks, i.e., of the intensity of γ-radiation. The relationship between intensities in the case of the total-energy peak and a peak with both annihilation photons taken into account is discussed. The latter is, of course, the higher-intensity peak at energies in excess of several mega electron volts. Relative and absolute measurements of γ-radiation intensity, calibration of detector efficiency, and various related difficulties, are covered here also. Methods for determining the area under a peak when the contribution by background is taken into account are described, and a method for selecting the end channels of the analyzer for determining extrapolation of background is also described. A program is put forth for computer work, one used by the author in determining the position of peaks and the areas under the peaks in the case of a Ge(Li)-detector.

Modern computers are capable of analyzing complex γ-ray spectra with great facility, by utilizing the method of weighted least squares. The sixth chapter is devoted to this method. The author notes that the

* Akademiai Kiado, Budapest, 1972.

Translated from Atomnaya Energiya, Vol. 34, No. 4, pp. 325-326, April, 1973.

exposition in this chapter is restricted to the basic assumptions and principal mathematical concepts of the method, and refers to other sources for more detailed specific information. Three basic assumptions are pointed out as underlying the method: 1) the spectrum to be analyzed is due to a mixture of known nuclides, and the exact shape of the standard spectra of those nuclides is either known from direct measurements or is subject to calculations; 2) the activities of the individual components add up linearly and the shape of the line in the detecting system is independent of line intensity; 3) each component of the complex spectrum possesses a different spectrum, and all of them are linearly independent. In practice this condition is even stronger, because of statistical fluctuations and the instability of the electronic circuitry, so that the spectra must differ substantially. How these assumptions are likely to be met under different sets of conditions is also discussed. The equation of least squares is derived and the validity of the results obtained by this method is discussed; a method for compensating gain is also pointed out, etc. The selection of weighting factors is described, a method for bringing out discarded components in the calculations is analyzed, determination of intensities by measuring the area under a peak and by the method of least squares is compared. Numerical examples are advanced.

A method of graphical expansion of a complex spectrum into its components, starting with the upper edge, is presented later on in the text. This method is admittedly of restricted application.

The eighth chapter discusses various applications. Decay curves are analyzed, different methods for solving this problem are discussed, particularly the method of maximum likelihood, which is described in brief; optimization of programs is analyzed, and programs for activation analysis are discussed, and so on.

The ninth chapter deals with special-purpose measuring equipment (anti-Compton spectrometers, pair spectrometers), coincidence techniques, and the summing method.

The brief last chapter discusses possible experimental errors in the measurement of γ-ray spectra.

The book is provided with a generous list of related literature.

This publication thus covers a broad range of topics related to the use of scintillation detectors and semiconductor detectors, and up-to-date techniques for processing data acquired with that equipment, to record γ-radiation.

breaking the language barrier

WITH COVER-TO-COVER ENGLISH TRANSLATIONS OF SOVIET JOURNALS

in physics

Title	# of Issues	Subscription Price
Astrophysics *Astrofizika*	4	$100.00
Fluid Dynamics *Izvestiya Akademii Nauk SSSR mekhanika zhidkósti i gaza*	6	$160.00
High-Energy Chemistry *Khimiya vysokikh énergii*	6	$155.00
High Temperature *Teplofizika vysokikh temperatur*	6	$125.00
Journal of Applied Mechanics and Technical Physics *Zhurnal prikladnoi mekhaniki i tekhnicheskoi fiziki*	6	$150.00
Journal of Engineering Physics *Inzhenerno-fizicheskii zhurnal*	12 (2 vols./yr. 6 issues ea.)	$150.00
Magnetohydrodynamics *Magnitnaya gidrodinamika*	4	$100.00
Mathematical Notes *Matematicheskie zametki*	12 (2 vols./yr. 6 issues ea.)	$185.00
Polymer Mechanics *Mekhanika polimerov*	6	$120.00
Radiophysics and Quantum Electronics (Formerly Soviet Radiophysics) *Izvestiya VUZ. radiofizika*	12	$160.00
Solar System Research *Astronomicheskii vestnik*	4	$ 95.00
Soviet Applied Mechanics *Prikladnaya mekhanika*	12	$160.00
Soviet Atomic Energy *Atomnaya énergiya*	12 (2 vols./yr. 6 issues ea.)	$160.00
Soviet Physics Journal *Izvestiya VUZ. fizika*	12	$160.00
Soviet Radiochemistry *Radiokhimiya*	6	$155.00
Theoretical and Mathematical Physics *Teoreticheskaya i matematicheskaya fizika*	12 (4 vols./yr. 3 issues ea.)	$145.00

Back volumes are available. For further information, please contact the Publishers.

SEND FOR YOUR FREE EXAMINATION COPIES

PLENUM PUBLISHING CORPORATION
227 WEST 17th STREET
NEW YORK, N. Y. 10011
Plenum Press • Consultants Bureau
• IFI/Plenum Data Corporation

In United Kingdom
Plenum Publishing Co. Ltd., Davis House (4th Floor)
8 Scrubs Lane, Harlesden, NW10 6SE, England